

STATISTICAL ALGORITHMS FOR LOW-FREQUENCY DIFFUSION DATA: A PDE APPROACH

BY MATTEO GIORDANO^{1,a} AND SVEN WANG^{2,b}

¹*ESOMAS Department, University of Turin, matteo.giordano@unito.it*

²*Department of Mathematics, Humboldt University Berlin, sven.wang@hu-berlin.de*

We consider the problem of making nonparametric inference in multi-dimensional diffusion models from low-frequency data. Statistical analysis in this setting is notoriously challenging due to the intractability of the likelihood and its gradient, and computational methods have thus far largely resorted to expensive simulation-based techniques. In this article, we propose a new computational approach which is motivated by PDE theory and is built around the characterisation of the transition densities as solutions of the associated heat (Fokker-Planck) equation. Employing optimal regularity results from the theory of parabolic PDEs, we prove a novel characterisation for the gradient of the likelihood. Using these developments, for the nonlinear inverse problem of recovering the diffusivity (in divergence form models), we then show that the numerical evaluation of the likelihood and its gradient can be reduced to standard elliptic eigenvalue problems, solvable by powerful finite element methods. This enables the efficient implementation of a large class of statistical algorithms, including (i) preconditioned Crank-Nicolson and Langevin-type methods for posterior sampling, and (ii) gradient-based descent optimisation schemes to compute maximum likelihood and maximum-a-posteriori estimates. We showcase the effectiveness of these methods via extensive simulation studies in a nonparametric Bayesian model with Gaussian process priors. Interestingly, the optimisation schemes provided satisfactory numerical recovery while exhibiting rapid convergence towards stationary points despite the problem nonlinearity; thus our approach may lead to significant computational speed-ups. The reproducible code is available online at <https://github.com/MattGiord/LF-Diffusion>.

CONTENTS

1	Introduction	2
2	Likelihood and gradient computation via PDEs	5
3	Applications to statistical algorithms	11
4	Numerical experiments	15
5	Summary and further discussion	18
6	Proofs of Theorem 2.2, Corollary 2.3 and Proposition 3.2	19
	Acknowledgments	22
	Funding	22
	References	23
A	Proof of Theorem 2.1	26
B	Auxiliary technical results on parabolic equations and heat kernels	35
C	Further numerical results	43

MSC2020 subject classifications: Primary 62M15; secondary 62F15, 62G05.

Keywords and phrases: nonparametric Bayesian inference, Gaussian prior, Markov chain Monte Carlo, MAP estimator, maximum likelihood estimator, gradient descent, numerical methods for PDEs.

1. Introduction. ‘Diffusions’ are mathematical models used ubiquitously across the sciences and in applications. They describe the stochastic time-evolution of a large variety of phenomena, including heat conduction [9], chemical reactions [61], cellular dynamics [19] and financial markets [68]. See the monograph [5] for further examples and references. In many situations, the ‘drift’ and ‘diffusivity’ parameters of a stochastic process $(X_t, t \geq 0)$ are not precisely known, and have to be estimated from discrete-time observations of a particle trajectory

$$(1.1) \quad X^{(n)} := (X_0, X_D, X_{2D}, \dots, X_{nD}),$$

for some ‘observation distance’ $D > 0$. This is the central inferential problem considered in the present article. Due to their unorthodox likelihood structure, which is implicitly determined by the transition probabilities of $(X_t, t \geq 0)$, discrete diffusion data have posed formidable difficulties for statistical analysis. While remarkable progresses have recently been made in deriving theoretical recovery guarantees, devising efficient computational algorithms remains a significant challenge – see below for more discussion.

Here, we shall study these issues in a representative nonparametric model for diffusion inside a bounded, insulated, and inhomogeneous medium; possible extensions will be discussed below. Taking, throughout, the diffusion domain to be a subset $\mathcal{O} \subset \mathbb{R}^d$, $d \in \mathbb{N}$, such a system is *macroscopically* described by the (Fokker-Planck) parabolic partial differential equation (PDE), which we shall refer to as the ‘heat equation’,

$$(1.2) \quad \begin{cases} \partial_t u - \nabla \cdot (f \nabla u) = 0, & \text{on } (0, \infty) \times \mathcal{O}, \\ \partial_\nu u = 0, & \text{on } (0, \infty) \times \partial\mathcal{O}, \end{cases}$$

encapsulating the changes over time in the substance density $u(t, x)$ at each location $x \in \mathcal{O}$ [34, Chapter 11]. Above, $\nabla \cdot$ and ∇ denote, respectively, the divergence and gradient operators, ν is the inward-pointing unit normal vector with associated normal derivative ∂_ν , and $f : \mathcal{O} \rightarrow (0, \infty)$ is a ‘conductivity’ function modelling the spatially-varying intensity at which diffusion occurs throughout the inhomogeneous medium. At the *microscopic* level, the discretely trajectory $(X_t, t \geq 0)$ of a diffusing particle, started inside \mathcal{O} , evolves according to the associated stochastic differential equation (SDE),

$$(1.3) \quad dX_t = \nabla f(X_t)dt + \sqrt{2f(X_t)}dW_t + \nu(X_t)dL_t, \quad t \geq 0,$$

where $(W_t, t \geq 0)$ is a standard d -dimensional Brownian motion and the term $\nu(X_t)dL_t$ models reflection of the particle at the boundary $\partial\mathcal{O}$ via the local time process $(L_t, t \geq 0)$; see [71] for details. The connection between the SDE (1.3) and the PDE (1.2) will play a key role throughout this paper.

The statistical reconstruction task consists of determining nonparametrically (i.e. within some infinite-dimensional function class) f from the discrete measurements (1.1) separated by a (fixed) time lag $D > 0$. Often times, because of the characteristics of the data collection process, D cannot be reduced under a certain non-zero threshold – in the statistical literature, this is referred to as the ‘low-frequency’ regime, which is the main setting our PDE techniques will be targeted at. An illustration of the problem with synthetic data is provided in Figure 1. For example, [50, Chapter 1] describes a filtering problem in weather forecasting where measurements are inputted in a large scale dynamical system every few hours; see also [42] for a similar situation in system biology. Other possible approaches based on stochastic analysis which are typically only available with ‘high-frequency’ or continuous-time measurements of $(X_t, t \geq 0)$ will not be pursued here; more discussion can be found below.

Related ‘parameter identification’ problems for the conductivity in diffusion equations have been widely studied in the inverse problem literature, largely in applications where

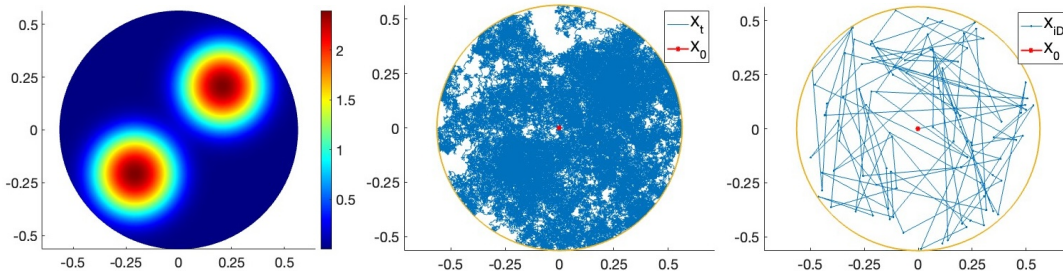


FIG 1. *Left: a (reparametrised) conductivity function, modelling two areas of more intense diffusion around the points $(.2, .2)$ and $(-.2, -.2)$. Centre: the (unobserved) continuous trajectory $(X_t, 0 \leq t \leq T)$, initialised at the origin and run until time $T = 5$. Right: low-frequency observations $X^{(100)} = (X_0, X_D, \dots, X_{100D})$ of the continuous trajectory, sampled with time lag $D = .05$.*

observations of a steady-state system are available in the form of (possibly noisy) point evaluations of the solution of a time-independent elliptic PDE. Among the many contributions, we refer to [1, 20, 46, 51, 75] for models with boundary measurements in the context of the famous ‘Caldéron problem’, and to [32, 37, 57, 64, 70] for interior measurements schemes connected to the ‘Darcy’s flow’ model.

1.1. *Challenges.* In the present setting, the invariant distribution of the diffusion process $(X_t, t \geq 0)$ in (1.3) can be shown to coincide with the uniform distribution $\text{vol}(\mathcal{O})^{-1}dx$ on \mathcal{O} [10, Chapter 1.11.3], and therefore to be non-informative about the conductivity f . Similarly, in the low-frequency regime, many commonly used sample statistics (such as the ‘sample quadratic variation’) cannot be employed to validly estimate f [39, Section 1.2.3]. Instead, the problem must rather be approached using the information contained in the transition densities $p_{D,f}(x, y)$, $x, y \in \mathcal{O}$, namely the probability density functions of the conditional laws $\Pr(X_D \in dy | X_0 = x)$, and the resulting likelihood function

$$(1.4) \quad L_n(f) = \prod_{i=1}^n p_{D,f}(X_{(i-1)D}, X_{iD}).$$

However, apart from certain special cases, the transition densities of diffusion processes, including those of model (1.3), are generally not available in closed form, making the likelihood for low-frequency observations analytically intractable. This is the central issue posing a huge challenge to the design, implementation and theoretical analysis of statistical algorithms.

In such context, a large part of the existing parametric and nonparametric methods relies on computational strategies that involve sophisticated (and often computationally onerous) missing data techniques, whereby the unobserved continuous trajectory between the data points is treated as a latent variable and inputted via simulation schemes for diffusion bridges, enabling the approximation of the likelihood for low-frequency observations by the more tractable one relative to continuous-time measurements. This approach was first pioneered, in general diffusion models, by Pedersen [60] to construct simulated maximum likelihood estimators, and by Roberts and Stramer [65], Elerian et al. [31] and Eraker [33] to implement Bayesian inference with data-augmentation. See [13–15, 27, 30, 40, 47, 59, 67, 77] and the many references therein.

1.2. *Main contributions.* In this paper, we adopt a novel PDE perspective to address the computational challenges arising in the nonparametric diffusion statistical model (1.3) with low-frequency observations. Our main contributions are as follows.

- We derive theoretical PDE formulae for likelihoods and gradients which are concretely computable via standard finite element methods for elliptic PDEs.
- We formulate several novel algorithms for posterior sampling and optimisation.
- We implement and numerically demonstrate the efficacy of the algorithms for computing maximum-a-posteriori, maximum likelihood and posterior mean estimates, as well as for posterior sampling.

Let us briefly expand on these points. In Section 2, building on the characterisation of the transition densities $p_{D,f}$ appearing in (1.4) as the fundamental solutions of the heat equation (1.2), we first show how the computation of $p_{D,f}$ can be reduced to a corresponding time-independent eigenvalue problem for the elliptic (self-adjoint) infinitesimal generator. This will later lead to a simple likelihood evaluation routine, cf. (2.10), that does not require any data-augmentation step. Building on such PDE characterisation, the main theoretical result of this article, Theorem 2.1, is then derived. In particular, we prove a ‘closed-form’ expression for the gradient of the likelihood, by characterising the Fréchet derivatives of the maps $f \mapsto p_{D,f}(x, y)$, for $x, y \in \mathcal{O}$ fixed. These are obtained using perturbation arguments for parabolic PDEs and the so-called ‘variation-of-constants’ principle [49, Chapter 4], building on the regularisation step developed by Wang [81] to deal with the singular behavior of the transition densities relative to vanishing time instants. The full argument is fairly technical; it is presented in Appendix A. Again using the self-adjointness of the generator and numerical methods for elliptic PDEs, we then propose an efficient strategy to numerically evaluate the likelihood gradient, which can serve as the building block for the implementation of gradient-based statistical algorithms.

Section 3 details the statistical procedures which we derive from the above theoretical developments. Our results enable a large algorithmic toolbox of common likelihood-based computational techniques – in particular, we pursue both gradient-free (preconditioned Crank-Nicolson, pCN) and gradient-based (unadjusted Langevin, ULA) algorithms for posterior sampling, as well as gradient descent methods. These schemes allow to obtain numerical approximations for posterior mean and maximum a posteriori (MAP) estimates, posterior quantiles for uncertainty quantification, as well as (penalised) maximum likelihood type estimators. The detailed description of the algorithms can be found in Sections 3.2-3.4.

In several simulation studies, presented in Section 4, we apply the above methods to a representative nonparametric Bayesian model with truncated Gaussian series priors. In the large data limit $n \rightarrow \infty$, these priors have recently been shown by Nickl [53] to lead to consistent inference of the data-generating ‘ground truth’ conductivity f – but in principle, our numerical methods are also applicable to any other prior distribution, too. Interestingly, [53] undertook a similar PDE-based point of view to prove the injectivity of the nonlinear map $f \mapsto p_{D,f}$ from the conductivity to the transition densities, providing the first statistical guarantees for nonparametric Bayesian procedures with multi-dimensional low-frequency diffusion data.

Our work in principle also opens the door for the implementation of further Markov Chain Monte Carlo (MCMC) [12, 22, 23, 41, 69] and gradient-based optimisation methods, an important direction of future research.

1.3. Related literature and discussion. In the seminal paper [39] by Gobet et al., spectral methods (related to the ones pursued here) were used to obtain minimax-optimal nonparametric estimators in one-dimensional diffusion models. However, it seems challenging to apply their approach to the present multi-dimensional setting, where the elliptic generator defines a genuine PDE. Analogous ideas also underpin the parametric estimators built by Kessler and Sørensen [44] using certain spectral martingale estimating functions. We also mention the works by Aït-Sahalia [3, 4] which (in a parametric setting) derive closed-form likelihood

approximations via Hermite polynomials along with resulting approximate maximum likelihood estimators. In contrast to our work, calculations of gradients are not considered there; moreover, the expansions on the eigenbasis of the self-adjoint generator of (1.3) considered here lead to rapidly (i.e. exponentially) decaying remainders terms.

Let us briefly discuss future directions of research which may build on the present work. A first important avenue would be the extension of the developed methodology beyond the (divergence form) diffusion model (1.2)-(1.3). Natural generalisations would e.g. encompass anisotropic diffusions with matrix-valued conductivities, as well as models for diffusion in a ‘potential energy field’; see Section 5 for further discussion. Secondly, our calculations, combined with the results in [53], may also pave the way to proving ‘gradient stability’ properties in the sense of [58]; further see [17], [6] and [52, Chapter 3]. Using the program put forth in [58], a rigorous investigation of the complexity of the employed sampling and optimisation algorithms can then be carried out, with the goal of deriving bounds for the computational cost that scale polynomially with respect to the discretisation dimension and the sample size.

Another interesting question concerns the relationship between the observation time lag $D > 0$, the ‘numerical stability’ of the proposed methodology, and the ‘statistical information’ contained in the sample. While, algorithmically, lower frequency samples imply better spectral approximations of the likelihood and its gradient, higher sampling frequencies allow to capture finer characteristics of the observed process. For very-high frequency or continuous data, likelihood evaluations become tractable via Girsanov’s theorem. Understanding the more detailed ‘phase transitions’ between the different regimes will inform which methods to employ in practice. Recent work has shown that nonparametric Bayesian procedures based on Gaussian priors can achieve optimal statistical convergence rates in the model (1.3) with ‘high-frequency’ observations (where $D = D_n \approx n^{-\gamma} \rightarrow 0$ for some $\gamma > 0$) [43] and with continuous-time observations [38, 55, 62, 78, 80].

2. Likelihood and gradient computation via PDEs. Throughout, let $\mathcal{O} \subset \mathbb{R}^d$, $d \in \mathbb{N}$, be a non-empty, open, bounded and convex set with smooth boundary $\partial\mathcal{O}$. It is well-known that for any twice continuously differentiable and strictly positive $f \in C^2(\bar{\mathcal{O}})$, $\inf_{x \in \mathcal{O}} f(x) > 0$, and any given starting point $X_0 = x_0 \in \mathcal{O}$ the SDE (1.3) has a unique path-wise solution $(X_t, t \geq 0)$, constituting a continuous-time Markov diffusion process reflected at the boundary (since f and ∇f are Lipschitz); see [71]. In view of these regularity assumptions, for some $f_{\min} > 0$ we maintain

$$(2.1) \quad \mathcal{F} := \left\{ f \in C^2(\bar{\mathcal{O}}) : \inf_{x \in \mathcal{O}} f(x) \geq f_{\min} \right\}$$

as the parameter space. Recall the low-frequency observations $X^{(n)}$ from (1.1) with measurement distance $D > 0$, which we shall keep fixed throughout.

2.1. Parabolic PDE characterisations. The Markov property of $(X_t, t \geq 0)$ implies that the likelihood $L_n(f)$ of any $f \in \mathcal{F}$ factorises as a product of the (symmetric) transition densities $p_{t,f}(x, y) = p_{t,f}(y, x)$, $t \geq 0$, $x, y \in \mathcal{O}$; cf. (1.4). These characterise the conditional laws

$$(2.2) \quad \Pr(X_{s+t} \in A | X_s = x) = \int_A p_{t,f}(x, y) dy, \quad A \subseteq \mathcal{O} \text{ measurable}, \quad s \geq 0,$$

and more generally the transition operator

$$(2.3) \quad P_{t,f}[u](x) := \mathbb{E}[u(X_{s+t}) | X_s = x] = \int_{\mathcal{O}} p_{t,f}(x, y) u(y) dy, \quad s \geq 0,$$

acting on square-integrable test functions $u \in L^2(\mathcal{O})$. The semigroup $(P_{t,f}, t \geq 0)$ is known to play the role of the ‘solution operator’ for the heat equation (1.2); thus the transition densities $p_{t,f}$ also constitute the fundamental solution to (1.2). Informally, this means that for $y \in \mathcal{O}$ fixed, the map $(t, x) \mapsto p_{t,f}(y, x)$ solves (1.2) with Dirac initial condition,

$$(2.4) \quad \begin{cases} (\partial_t - \mathcal{L}_f)u = 0, & \text{on } (0, \infty) \times \mathcal{O}, \\ \partial_\nu u = 0, & \text{on } (0, \infty) \times \partial\mathcal{O}, \\ u(0, \cdot) = \delta_y(\cdot), & \text{on } \mathcal{O}. \end{cases}$$

Here, we denoted by \mathcal{L}_f the elliptic divergence form operator

$$\mathcal{L}_f u = \nabla \cdot (f \nabla u) = \sum_{l=1}^d \partial_{x_l} (f \partial_{x_l} u),$$

a notation that we will use throughout. The operator \mathcal{L}_f , with domain given by the set of functions in the Sobolev space $H^2(\mathcal{O})$ with zero Neumann boundary conditions,

$$H_N^2(\mathcal{O}) := \{u \in H^2(\mathcal{O}) : \partial_\nu u = 0 \text{ on } \partial\mathcal{O}\},$$

constitutes the infinitesimal generator of the process (1.3). While the transition density functions are not available in closed form, their characterisation through (2.4) implies a convenient spectral expansion in terms of the eigenpairs of the generator \mathcal{L}_f , cf. (2.9), which we will use below for evaluating the likelihood $L_n(f)$.

A more intricate question is whether the gradient of the likelihood function L_n also satisfies a PDE characterisation which can be exploited for computational purposes. The key challenge is thus to understand the perturbations of the nonlinear map $f \mapsto p_{t,f}$, which turns out to provide insight into the preceding question – this is the content of Theorem 2.1. To understand the intuition behind the theorem, let us fix some perturbation $h \in C^2(\bar{\mathcal{O}})$ such that $f + h \in \mathcal{F}$. Then, subtracting the PDE (2.4) for $f + h$ and for f yields immediately that the difference $w(t, x) := p_{t,f+h}(y, x) - p_{t,f}(y, x)$ solves (again, informally)

$$\begin{cases} (\partial_t - \mathcal{L}_f)w(t, x) = \nabla \cdot (h \nabla p_{t,f+h}(y, \cdot))(x), & \text{for } (t, x) \in (0, \infty) \times \mathcal{O}, \\ \partial_\nu w(t, x) = 0, & \text{for } (t, x) \in (0, \infty) \times \partial\mathcal{O}, \\ w(0, x) = 0, & \text{for } x \in \mathcal{O}, \end{cases}$$

which is another instance of the heat equation, now with an inhomogeneity and with zero initial conditions. A natural candidate for the linearisation (in h) of the right hand side is $\nabla \cdot (h \nabla p_{t,f+h}(y, \cdot)) \approx \nabla \cdot (h \nabla p_{t,f}(y, \cdot))$, and thus $(\partial_t - \mathcal{L}_f)^{-1}[\nabla \cdot (h \nabla p_{t,f}(y, \cdot))]$ in turn provides a natural candidate for the linearisation of the transition densities. Here, we have written $(\partial_t - \mathcal{L}_f)^{-1}$ to informally denote the linear ‘solution operator’ to an inhomogeneous heat equation with zero initial condition, which under suitable regularity conditions is given by the variation-of-constants formula $(\partial_t - \mathcal{L}_f)^{-1}[\nabla \cdot (h \nabla p_{t,f}(y, \cdot))] = \int_0^t P_{t-s,f}[\nabla \cdot (h \nabla p_{s,f}(y, \cdot))] ds$ – see e.g. Chapter 4 of [49].

Making the above argument rigorous is technically delicate due to the singularity of $\delta_y(\cdot)$ and of the source term $\nabla \cdot (h \nabla p_{t,f})$ for $t \rightarrow 0$, which makes the standard parabolic regularity theory (e.g. from [49]) not directly applicable. Thus, one needs to clarify in which sense the above PDEs hold, and whether existence and uniqueness can be guaranteed suitably for $(\partial_t - \mathcal{L}_f)^{-1}$ to be well-specified. Generalising a regularisation technique developed in [81] (in a related one-dimensional model), we accomplish this in the ensuing theorem for dimensions $d \leq 3$, proving a variation-of-constants representation for the linearisation of $f \mapsto p_{t,f}$. For $x, y \in \mathcal{O}$ and $D > 0$ fixed, define the operator

$$\Phi(f) \equiv \Phi_{D,x,y}(f) := p_{D,f}(x, y), \quad f \in \mathcal{F},$$

where \mathcal{F} is given by (2.1). Note that Φ depends nonlinearly on f .

THEOREM 2.1. *Suppose that $d \leq 3$, that $D > 0$ and fix any $x, y \in \mathcal{O}$. Then, the Fréchet derivate of Φ at $f \in \mathcal{F}$ is given by the following linear operator*

$$(2.5) \quad D\Phi_f : C^2(\bar{\mathcal{O}}) \rightarrow \mathbb{R}, \quad D\Phi_f[h] := \int_0^D P_{D-s,f} [\nabla \cdot (h \nabla p_{s,f}(x, \cdot))] (y) ds.$$

More specifically, for any $R > 0$ and $\kappa > 0$, there exist $\zeta > 0$ and $C > 0$ such that for any $h \in C^2(\bar{\mathcal{O}})$ with $f + h \in \mathcal{F}$ and $\max\{\|f\|_{C^{1+\kappa}}, \|f + h\|_{C^{1+\kappa}}\} \leq R$,

$$(2.6) \quad \frac{|\Phi(f + h) - \Phi(f) - D\Phi_f[h]|}{\|h\|_{C^1}} \leq C \|h\|_{C^1}^\zeta = o(\|h\|_{C^1}).$$

Here, $C \equiv C(\mathcal{O}, d, f_{\min}, \kappa, R, D)$ can be chosen independently of $x, y \in \mathcal{O}$ and f, h as above.

The preceding theorem states that the map Φ is Fréchet differentiable with respect to $\|\cdot\|_{C^1}$, with derivative at $f \in \mathcal{F}$ identified by the linear operator (2.5). In particular, this is implied by the remainder estimate (2.6), which holds uniformly for f and h in balls of the Hölder space $C^{1+\kappa}(\mathcal{O})$. The proof of the result can be found in Appendix A. Note that our derivative is obtained ‘pointwise’ in $x, y \in \mathcal{O}$, thus rigorously providing a gradient formula for $L_n(\theta)$ conditional on any data $X^{(n)}$ rather than just in ‘quadratic mean’, a weaker regularity condition in terms of which several key results from asymptotic frequentist statistical theory [79] are formulated. Differentiability in quadratic mean is, in particular, implied by Theorem 2.1.

In fact, by the same proof techniques that we employ for Theorem 2.1, one can show that the Fréchet derivative $D\Phi_f$ is Hölder continuous (with respect to the operator norm). Such regularity statements for gradients are essential for understanding the discretisation error incurred by the algorithms constructed below, and thus may be important for future work. The proof is presented in Section 6.1.

THEOREM 2.2. *Assume the setting of Theorem 2.1 and let $R > 0$, $\kappa \in (0, 1)$. Then, there is some $\zeta \in (0, 1)$ (independent of R, κ) and some $C > 0$ such that for all f, g, h with $f, f + g \in \mathcal{F}$, $h \in C^{1+\kappa}(\mathcal{O})$ as well as $\max\{\|f\|_{C^{1+\kappa}}, \|g\|_{C^{1+\kappa}}, \|h\|_{C^{1+\kappa}}\} \leq R$,*

$$|D\Phi_{f+g}[h] - D\Phi_f[h]| \leq C \|h\|_{C^1} \|g\|_{C^1}^\zeta.$$

2.2. Reduction to elliptic eigenvalue problems. By the divergence theorem, e.g. [26, p. 171], if $v, w \in H_N^2(\mathcal{O})$ then

$$\langle \mathcal{L}_f v, w \rangle_{L^2} = \int_{\mathcal{O}} \nabla \cdot (f \nabla v)(x) w(x) dx = - \int_{\mathcal{O}} f(x) \nabla v(x) \cdot \nabla w(x) dx = \langle v, \mathcal{L}_f w \rangle_{L^2},$$

which shows that \mathcal{L}_f is self-adjoint with respect to the inner product of $L^2(\mathcal{O})$. By a suitable application of the spectral theorem (e.g. [72, p. 582]), we deduce the existence of an orthonormal system of eigenfunctions $(e_{f,j}, j \geq 0) \subset L^2(\mathcal{O})$ and of associated (negative) eigenvalues $(\lambda_{f,j}, j \geq 0) \subset [0, \infty)$ such that

$$(2.7) \quad \begin{cases} \mathcal{L}_f e_{f,j} + \lambda_{f,j} e_{f,j} = 0, & \text{on } \mathcal{O}, \\ \partial_\nu e_{f,j} = 0, & \text{on } \partial\mathcal{O}, \end{cases} \quad j \geq 0.$$

We will take throughout the increasing ordering $\lambda_{f,j} \leq \lambda_{f,j'}, j \leq j'$. Then it holds that $e_{f,0} = \text{vol}(\mathcal{O})^{-1}$ is constant with corresponding eigenvalue $\lambda_{f,0} = 0$, independently of f . For notational convenience, we shall take $\text{vol}(\mathcal{O}) = 1$, so that $e_{f,0} = 1$. Also, by ellipticity, the first non-zero eigenvalue satisfies the ‘spectral gap’ estimate $\lambda_{f,1} \geq c$ for some constant

$c > 0$ only depending on \mathcal{O} and f_{\min} . The eigenvalues diverge following Weyl's asymptotics $\lambda_{f,j} = O(j^{2/d})$ as $j \rightarrow \infty$, with multiplicative constants only depending on \mathcal{O} , f_{\min} and $\|f\|_{L^\infty}$. These facts follow similarly to the arguments for the Neumann-Laplacian (here corresponding to the case $f = 1$) developed in [72, p. 403f], in view of the boundedness and the boundedness away from zero of f . For details, see [53, Section 3].

Using such a spectral analysis of the generator, we can represent the action of the transition operator $P_{t,f}[v]$ from (2.3) on any 'initial condition' $v \in L^2(\mathcal{O})$ by

$$(2.8) \quad P_{t,f}[v](x) = \langle v, 1 \rangle_{L^2} + \sum_{j=1}^{\infty} e^{-\lambda_{f,j}t} \langle v, e_{f,j} \rangle_{L^2} e_{f,j}(x), \quad t \geq 0, \quad x \in \mathcal{O}.$$

Accordingly, the transition densities (2.2), which form the integral kernels of $P_{t,f}$, satisfy

$$(2.9) \quad p_{t,f}(x, y) = 1 + \sum_{j=1}^{\infty} e^{-\lambda_{f,j}t} e_{f,j}(x) e_{f,j}(y), \quad t \geq 0, \quad x, y \in \mathcal{O}.$$

We conclude that for any $f \in \mathcal{F}$, if we have numerical access to the eigenpairs $(e_{f,j}, \lambda_{f,j})$, the likelihood $L_n(f)$ may be evaluated using the spectral formula

$$(2.10) \quad L_n(f) = \prod_{i=1}^n \left[1 + \sum_{j=1}^{\infty} e^{-\lambda_{f,j}D} e_{f,j}(X_{(i-1)D}) e_{f,j}(X_{iD}) \right], \quad f \in \mathcal{F}.$$

Upon closer inspection, we can also derive a spectral representation of the Frechét derivatives $D\Phi_f$ from Theorem 2.1. Indeed, since the transition density functions $p_{s,f}$ and the transition operators $P_{D-s,f}$ can be expanded with respect to the same eigenpairs $\{(e_{f,j}, \lambda_{f,j}), j \geq 0\}$ of \mathcal{L}_f , we obtain a convenient double series expansion of the integrand $P_{D-s,f}[\nabla \cdot (h \nabla p_{s,f}(x, \cdot))](y)$ in (2.5). This further allows to separate the spatial and time dependency, leading to a closed form expression for the integration in time, which avoids potential numerical instability caused by the singular behaviour of the integrand for $s \rightarrow 0$. In summary, the following spectral characterisation of the linear operator $D\Phi_f$ is obtained; see Section 6.2 for the proof.

COROLLARY 2.3. *For any $f \in C^2(\bar{\mathcal{O}})$ satisfying $\inf_{x \in \mathcal{O}} f(x) \geq f_{\min} > 0$, let $(e_{f,j}, j \geq 0) \subset L^2(\mathcal{O})$ be the orthonormal system of the eigenfunctions of the elliptic differential operator in divergence form $\mathcal{L}_f[\cdot] = \nabla \cdot (f \nabla[\cdot])$, with associated eigenvalues $(\lambda_{f,j}, j \geq 0) \subset [0, \infty)$, solving (2.7). Then, under the assumptions of Theorem 2.1,*

$$(2.11) \quad D\Phi_f[h] = \sum_{j,j'=1}^{\infty} C_{f,j,j'} \langle h, \nabla e_{f,j} \cdot \nabla e_{f,j'} \rangle_{L^2} e_{f,j'}(x) e_{f,j}(y),$$

$$C_{f,j,j'} := \begin{cases} -De^{-\lambda_{f,j}D}, & \lambda_{f,j} = \lambda_{f,j'} \\ (e^{-\lambda_{f,j}D} - e^{-\lambda_{f,j'}D}) / (\lambda_{f,j} - \lambda_{f,j'}), & \text{otherwise.} \end{cases}$$

2.3. Numerical PDE methods. While the eigenpairs $(e_{f,j}, \lambda_{f,j})$ are generally not available in closed form, the elliptic eigenvalue problem (2.7) has been widely investigated in the literature on numerical techniques for PDEs, with foundational work by Vainikko [76] and later landmark contributions in [7, 18, 21, 28, 45] among the others. We further refer to the monograph [8] and to the recent survey article [16] for overviews. Specifically, the problem can be tackled with efficient and reliable Galerkin methods (e.g., of finite element type), returning approximations $\{(e_{f,j}^{(\varepsilon)}, \lambda_{f,j}^{(\varepsilon)}), 1 \leq j \leq J\}$ of the first $J \in \mathbb{N}$ non-constant eigenfunctions; see Figure 2 for an illustration. The superscript (ε) is used as a proxy for

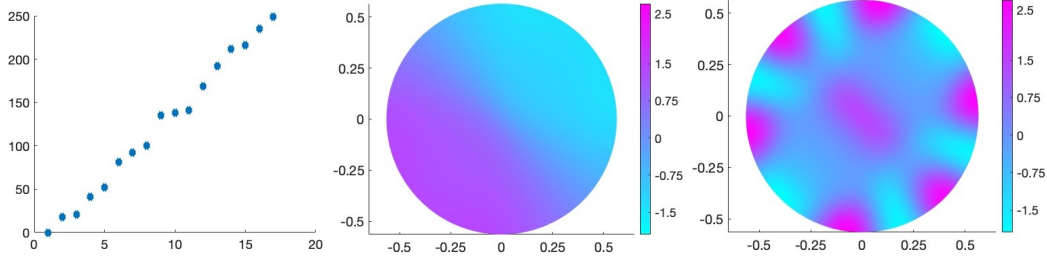


FIG 2. Left: numerical approximation of the eigenvalues $\lambda_{f,j}$ associated to the conductivity function displayed in Figure 1 (left). The eigenvalues exhibit a linear growth as expected from Weyl's asymptotics in two-dimensional domains. Centre and right, respectively: numerical approximations of the first and J^{th} non-constant eigenfunctions $e_{f,1}$ and $e_{f,J}$, with $J = 17$.

the parameter $\varepsilon > 0$ governing the reconstruction quality of the employed numerical method, in the sense that smaller values of ε yield smaller approximations errors, with convergence when $\varepsilon \rightarrow 0$ (cf. Remark 2.4 below). For example, in standard finite element methods based on piece-wise polynomial functions defined over a triangular mesh covering the domain, ε is typically chosen to be an upper bound for the side length of the mesh elements.

Based on such numerical techniques, the computation of the transition density functions and the likelihood via the spectral characterisations (2.9) and (2.10) respectively can be concretely performed by replacing the eigenpairs with their approximations, and by truncating the series at level J , resulting in the simple routines

$$(2.12) \quad p_{t,f}^{(\varepsilon)}(x, y) := 1 + \sum_{j=1}^J e^{-\lambda_{f,j}^{(\varepsilon)} t} e_{f,j}^{(\varepsilon)}(x) e_{f,j}^{(\varepsilon)}(y), \quad t \geq 0, \quad x, y \in \mathcal{O},$$

$$(2.13) \quad L_n^{(\varepsilon)}(f) := \prod_{i=1}^n p_{D,f}^{(\varepsilon)}(X_{(i-1)D}, X_{iD}), \quad f \in \mathcal{F}.$$

This is the likelihood approximation that we will employ in Section 3.2 for the implementation of posterior sampling via the pCN method [22].

Turning to the gradient, for any fixed direction h , the Fréchet derivative $D\Phi_f[h]$ can be efficiently computed according to the formula from Corollary 2.3, analogously truncating the double series at some level $J \in \mathbb{N}$, and replacing the eigenpairs with their numerical approximations. For a stable computation of the two internal series, since for eigenvalues with multiplicities finite element methods generally return distinct approximations that differ by small amounts, the conditions $\lambda_{f,j'} \neq \lambda_{f,j}$ and $\lambda_{f,j'} \neq \lambda_{f,j}$ should be replaced by the requirements $|\lambda_{f,j'}^{(\varepsilon)} - \lambda_{f,j}^{(\varepsilon)}| \leq \text{Tr}$ and $|\lambda_{f,j'}^{(\varepsilon)} - \lambda_{f,j}^{(\varepsilon)}| > \text{Tr}$, respectively, for a sufficiently small threshold $\text{Tr} > 0$ to be specified by the user. This results in the derivatives evaluation routine

$$(2.14) \quad D\Phi_f^{(\varepsilon)}[h] = \sum_{j,j'=1}^J C_{f,j,j'}^{(\varepsilon)} \langle h, \nabla e_{f,j}^{(\varepsilon)} \cdot \nabla e_{f,j'}^{(\varepsilon)} \rangle_{L^2} e_{f,j}^{(\varepsilon)}(x) e_{f,j'}^{(\varepsilon)}(y),$$

$$C_{f,j,j'}^{(\varepsilon)} := \begin{cases} -D e^{-\lambda_{f,j}^{(\varepsilon)} D}, & |\lambda_{f,j'}^{(\varepsilon)} - \lambda_{f,j}^{(\varepsilon)}| \leq \text{Tr} \\ (e^{-\lambda_{f,j}^{(\varepsilon)} D} - e^{-\lambda_{f,j'}^{(\varepsilon)} D}) / (\lambda_{f,j}^{(\varepsilon)} - \lambda_{f,j'}^{(\varepsilon)}), & \text{otherwise,} \end{cases}$$

which will serve as a basis for the implementation of gradient-based statistical algorithms. In particular, upon discretising the parameter space \mathcal{F} , the log-likelihood gradient can be derived from an application of the chain rule and the above derivative formulae, wherein

the directions are identified by the ‘coordinates’ in the chosen discretisation scheme – see Section 3.1 below for details.

REMARK 2.4 (Numerical approximation errors). The numerical routines (2.13) and (2.14) entails two sources of approximation errors, arising, respectively, from the numerical solution of the elliptic eigenvalue problem (2.7) and the truncation of the series appearing in (2.10) and (2.11). For the latter, explicit error bounds readily follow from Weyl’s asymptotics, the available estimates for the norm of the eigenfunctions, and since $D > 0$ is fixed. For instance, by Corollary 1 in [53], provided that f lies in a Sobolev space $H^s(\mathcal{O})$ of sufficient smoothness $s > d$, the j^{th} series term of the numerical likelihood formula (2.13) satisfies, for arbitrarily small $\eta > 0$ and for constants $c_1, c_2 > 0$ only depending on \mathcal{O}, d, f_{\min} , and $\|f\|_{H^s}$,

$$e^{-\lambda_{f,j}D} e_{f,j}(X_{(i-1)D}) e_{f,j}(X_{iD}) \leq c_1 e^{-c_2 D j^{2/d}} j^{1+\eta}$$

for all j large enough and all $i = 1, \dots, n$, whereupon the tails of the series in (2.10) are seen to decay exponentially. Thus, depending on the application at hand and the magnitude of the time lag D between consecutive observations, a relatively low truncation level J in (2.13) may be expected to yield the desired accuracy level.

Concerning the numerical solution of the elliptic eigenvalue problem (2.7), there is a wide literature developing error analyses for a variety of finite element methods; see [16] and references therein. Among these, well-known results for the widespread approach based on piece-wise polynomial approximating functions over a triangulation of the domain, combined with the norm estimates in Corollary 1 in [53], assuming again that $f \in H^s(\mathcal{O})$ for some $s > d$, yield the error bound for the eigenvalues

$$(2.15) \quad |\lambda_{f,j} - \lambda_{f,j}^{(\varepsilon)}| \leq c_3 j^{c_4} \varepsilon^{c_5}, \quad j = 1, \dots, J,$$

with constants $c_3, c_4, c_5 > 0$ only depending on \mathcal{O}, d, f_{\min} , and $\|f\|_{H^s}$, and where ε is the (user-specified) maximal side length for the elements in the triangular mesh, cf. [7, Section 10.3]. Analogous bounds also holds for the approximation errors in Sobolev norms of the eigenfunctions. Note that the estimate (2.15) deteriorates as the index j grows, due to the more pronounced oscillatory behaviour that the eigenfunctions tend to exhibit at higher frequencies. However, as observed earlier, in the presence of a fixed time lag D , only a small number J of eigenpairs are generally needed to approximate the series in (2.10) and (2.14) with high accuracy, so that we may expect the overall error resulting from the numerical solution of the eigenvalue problem (2.7) by finite element methods to be small even for a relatively coarse triangular mesh.

REMARK 2.5 (Computational cost). The numerical approximation of the eigenpairs underpinning the proposed computational approach can be performed via the off-the-shelf PDE solvers implemented in many mathematical and statistical software. Since, in light of Remark 2.4, only a small number of eigenpairs is needed in practice, such step is generally computationally inexpensive, at least for applications in low dimensional domains (including the relevant physical cases $d = 1, 2, 3$). For reference, the approximation of the first $J = 17$ eigenpairs associated to the conductivity function f displayed in Figure 1 (left) required around .1 seconds on a MacBook Pro with M1 processor, using the finite element method implemented in MATLAB R2023a Partial Differential Equation Toolbox, based on a discretisation of the domain with an unstructured triangular mesh comprising 1981 nodes. Since the routines (2.13) and (2.14) only require a single numerical solution of the eigenvalue problem (2.7), and only further involves exponentiation, products and sums, we then obtain an overall comparable computational cost, with no additional bottlenecks. In fact, for the numerical likelihood formula (2.13), since handling a larger number of observations only implies a linear growth in the number of product terms, the proposed approach results to be extremely scalable with respect to the sample size.

3. Applications to statistical algorithms. We now turn to the problem of estimating the conductivity function f from the low-frequency diffusion data $X^{(n)}$. Leveraging the novel approach developed in Section 2, we gain direct access to the large algorithmic toolbox of likelihood-based nonparametric statistical inference, overcoming the need of computationally expensive data-augmentation techniques [14, 59, 65, 67, 77]. For illustration, we shall consider below, within a representative Bayesian model, instances of:

- Gradient-free Metropolis-Hastings MCMC algorithms for posterior sampling;
- Gradient-based posterior sampling methods of Langevin type;
- Gradient-based optimisation techniques for the computation of the MAP estimates (i.e. penalised MLE).

3.1. *A nonparametric Bayesian approach with Gaussian priors.* We shall focus on nonparametric Bayesian procedures with prior distributions arising from Gaussian processes. These are among the most universally used priors on function spaces in applications, e.g. [52, 63, 70], [36, Chapter 7] and [35, Chapter 11], and in the estimation problem at hand they have recently been shown by Nickl [53] to lead to ‘asymptotically consistent’ posteriors that concentrate around the ground truth as the sample size increases. For concreteness, let us follow in this section the prior construction of [53]; more general classes will be considered in Appendix C.

3.1.1. *Parametrisation.* In order to incorporate the point-wise lower bound required in the definition (2.1) of the parameter space \mathcal{F} , we model any $f \in \mathcal{F}$ as

$$(3.1) \quad f(x) = (\phi \circ F)(x) \equiv \phi(F(x)), \quad x \in \mathcal{O},$$

for some real-valued $F \in C^2(\mathcal{O})$ and for some smooth and strictly increasing link function $\phi: \mathbb{R} \rightarrow [f_{\min}, \infty)$ (e.g. the standard choice $\phi(\cdot) = f_{\min} + \exp(\cdot)$). Under such bijective reparametrisation, we regard F as the unknown functional parameter to be estimated and discretise it by

$$(3.2) \quad F \equiv F_\theta := \theta_0 + \sum_{k=1}^K \theta_k e_k, \quad K \in \mathbb{N}, \quad \theta_0, \dots, \theta_K \in \mathbb{R},$$

where $e_k := e_{1,k}$, $k \in \mathbb{N}$, are the (smooth) non-constant eigenfunctions of the standard Neumann-Laplacian with associated (strictly positive) eigenvalues $\lambda_k := \lambda_{1,k}$, solving (2.7) with $f = 1$, cf. [72, p. 403f]. Correspondingly, we write $f_\theta := \phi \circ F_\theta$.

3.1.2. *Prior and posterior.* We assign to F in (3.1) a truncated Gaussian series prior by endowing the vector of Fourier coefficients $\theta := (\theta_0, \dots, \theta_K) \in \mathbb{R}^{K+1}$ in (3.2) with the diagonal multivariate Gaussian prior

$$(3.3) \quad \theta \sim N(0, \sigma^2 \Lambda_\alpha), \quad \Lambda_\alpha := \text{diag}(1, \lambda_1^{-\alpha}, \dots, \lambda_K^{-\alpha}) \in \mathbb{R}^{K+1, K+1}, \quad \alpha, \sigma^2 > 0.$$

In the following we will, in slight abuse of notation, interchangeably write $\Pi(\cdot)$ for the prior (3.3) on θ as well as for the resulting push-forward priors on F_θ and f_θ . By Bayes’ formula (e.g., [35, p. 7]), the posterior distribution $\Pi(\cdot | X^{(n)})$ of $\theta | X^{(n)}$ has probability density function (with respect to the Lebesgue measure of \mathbb{R}^{K+1})

$$(3.4) \quad \pi(\theta | X^{(n)}) \propto \exp\left(\ell_n(f_\theta) - \frac{1}{2} \theta^T \Lambda_\alpha^{-1} \theta\right), \quad \theta \in \mathbb{R}^{K+1},$$

where $\ell_n(f_\theta)$ is the log-likelihood of $f_\theta = \phi \circ F_\theta$, that is

$$(3.5) \quad \ell_n(f_\theta) := \log(L_n(f_\theta)) = \sum_{i=1}^n \log p_{D, f_\theta}(X_{(i-1)D}, X_{iD}).$$

REMARK 3.1 (α -regular Gaussian priors). For fixed $K \in \mathbb{N}$, the prior (3.3) induces a multivariate Gaussian distribution on the $(K + 1)$ -dimensional linear space spanned by the eigenfunctions $\{1, e_1, \dots, e_K\}$. For $K \rightarrow \infty$, the prior converges towards an infinite-dimensional ‘ α -regular’ Gaussian probability measure with RKHS included into the Sobolev space $H^\alpha(\mathcal{C})$, e.g. arguing as in the proof of Lemma 2.3 in [38], using Proposition 2 in [53] and the results in Section 11.4.5 of [35]. In fact, Theorem 10 in [53] gives a precise growth condition on K as a power of the sample size that leads, under certain additional regularity conditions, to rates of contraction for the associated posterior distribution.

3.1.3. *Gradients of log-posterior densities.* A careful application of Theorem 2.1 and of the chain rule to the maps $\theta \mapsto \log p_{D, f_\theta}(X_{(i-1)D}, X_{iD})$, $i = 1, \dots, n$, implies the differentiability of the posterior density (3.4) (and of its logarithm). We identify the resulting formula for the gradient in the next proposition.

PROPOSITION 3.2. *For fixed $K \in \mathbb{N}$ and a given smooth and strictly increasing function $\phi : \mathbb{R} \rightarrow [f_{\min}, \infty)$, let the posterior probability density function $\pi(\cdot | X^{(n)})$ be as in (3.4). Then, $\log \pi(\cdot | X^{(n)})$ is continuously differentiable on \mathbb{R}^{K+1} . In particular, $\nabla \log \pi(\cdot | X^{(n)}) = (\partial_{\theta_k} \log \pi(\cdot | X^{(n)}), k = 0, \dots, K)$, where*

$$(3.6) \quad \partial_{\theta_k} \log \pi(\theta | X^{(n)}) = \sum_{i=1}^n \partial_{\theta_k} \log p_{D, f_\theta}(X_{(i-1)D}, X_{iD}) - \lambda_k^\alpha \theta_k,$$

and where, denoting by $D\Phi_{f_\theta, i}$, $i = 1, \dots, n$, the linear operators defined as in (2.5) with $f = f_\theta$, $x = X_{(i-1)D}$ and $y = X_{iD}$,

$$\partial_{\theta_k} \log p_{D, f_\theta}(X_{(i-1)D}, X_{iD}) = \frac{D\Phi_{f_\theta, i}[(\phi' \circ F_\theta)e_k]}{p_{D, f_\theta}(X_{(i-1)D}, X_{iD})}.$$

In view of the developments presented in Section 2, the concrete implementation of the above characterisation of the partial derivatives can be approached by replacing the transition densities p_{D, f_θ} and the Fréchet derivatives $D\Phi_{f_\theta, i}$ with their numerical counterparts $p_{D, f_\theta}^{(\varepsilon)}$ and $D\Phi_{f_\theta, i}^{(\varepsilon)}$ defined as after (2.12) and (2.14) respectively. This results in the gradient evaluation routine $\nabla^{(\varepsilon)} \log \pi(\cdot | X^{(n)}) := (\partial_{\theta_k}^{(\varepsilon)} \log \pi(\cdot | X^{(n)}), k = 0, \dots, K)^T$, where

$$(3.7) \quad \partial_{\theta_k}^{(\varepsilon)} \log \pi(\theta | X^{(n)}) := \sum_{i=1}^n \frac{D\Phi_{f_\theta, i}^{(\varepsilon)}[(\phi' \circ F_\theta)e_k]}{p_{D, f_\theta}^{(\varepsilon)}(X_{(i-1)D}, X_{iD})} - \lambda_k^\alpha \theta_k.$$

For the latter, we note that a single solution via finite element methods of the elliptic eigenvalue problem (2.7) with $f = f_\theta$ is required across all the partial derivatives, whereupon the exponential coefficients $C_{f_\theta, j, j'}^{(\varepsilon)}$ appearing in (2.14) can also be calculated before the specification of the directions $h = (\phi' \circ F_\theta)e_k$. Thus, overall, the numerical gradient formula (3.7) is only marginally computationally more expensive than the efficient likelihood evaluation routine (2.13).

3.2. *Posterior inference via the pCN algorithm.* To perform inference based on the posterior density (3.4), we begin by considering the class of ‘zeroth-order’ Metropolis-Hasting MCMC sampling methods, whose implementation in the present setting is readily enabled by the numerical likelihood formula (2.13). We focus here on the widespread pCN algorithm [22]. Given the low-frequency diffusion data (1.1) and under the prior construction (3.3), the algorithm generates a \mathbb{R}^{K+1} -valued Markov chain $(\vartheta_m, m \geq 0)$ by repeating the following steps, given some initialisation point $\vartheta_0 \in \mathbb{R}^{K+1}$,

1. Draw a prior sample $\Psi \sim \Pi(\cdot)$ and for a given ‘stepsize’ $\delta > 0$ define the ‘proposal’ $p := \sqrt{1 - 2\delta}\vartheta_m + \sqrt{2\delta}\Psi$.
2. Set

$$(3.8) \quad \vartheta_{m+1} := \begin{cases} p, & \text{with probability } \min \left\{ 1, \frac{L_n(f_p)}{L_n(f_{\vartheta_m})} \right\}, \\ \vartheta_m, & \text{otherwise,} \end{cases}$$

where L_n is the likelihood function in (1.4).

The first step only involves the straightforward task of drawing a sample Ψ from the diagonal multivariate Gaussian prior $\Pi(\cdot)$. The second step requires the evaluation of the proposal likelihood $L_n(f_p)$, which is achieved through the routine (2.13). Apart from the latter, all the operations involved within the two steps are elementary; therefore the computational complexity of each pCN iteration is largely driven by the cost of evaluating the numerical likelihood formula (2.13). One can thus expect generally modest computation times, cf. Remark 2.5. An excellent scalability with respect to the sample size is also obtained.

The proposals and acceptance probabilities prescribed by the pCN algorithm are of Metropolis-Hastings type, e.g. Proposition 1.2.2 in [52], so that the generated Markov chain can be shown to be reversible and to have invariant probability measure equal to the posterior distribution $\Pi(\cdot|X^{(n)})$, cf. [73]. The posterior mean estimator $\bar{\theta}_n := E^\Pi[\theta|X^{(n)}]$ is then numerically evaluated through the Monte Carlo average $\bar{\vartheta}_M := (M + 1)^{-1} \sum_{m=0}^M \vartheta_m$ for some large $M \in \mathbb{N}$, typically after discarding an initial ‘burnin’ batch of iterates in order to account for the convergence from the initialisation point towards equilibrium. Similarly, the posterior quantiles can be approximated by the empirical quantiles of the MCMC samples. The corresponding posterior mean estimator $\bar{F}_n := E^\Pi[F|X^{(n)}]$ of the unknown functional parameter F is given by

$$(3.9) \quad F_{\bar{\vartheta}_M} = \bar{\vartheta}_{M,0} + \sum_{k=1}^K \bar{\vartheta}_{M,k} e_k.$$

As argued in [22], the pCN algorithm leads to well-defined MCMC methods in function spaces whose performance has certain robustness properties with respect to the discretisation dimension (here, the truncation level K), in that its acceptance probabilities do not deteriorate under a discretisation refinement.

3.3. Posterior inference via the unadjusted Langevin algorithm. In alternative to the pCN algorithm laid out above, the results of Section 2 can also be used to build a variety of gradient-based iterative methods, which, through the incorporation of the resulting geometric information on the likelihood surface, may achieve potentially significant improvements in the efficiency of exploration of the parameter space.

Here, we shall consider approximate sampling from the posterior density (3.4) via MCMC algorithms of Langevin type, arising from the discretisation of the Langevin SDE

$$(3.10) \quad d\vartheta_t = \frac{1}{2} \nabla \log \pi(\vartheta_t|X^{(n)}) dt + dB_t, \quad t \geq 0, \quad \vartheta_0 \in \mathbb{R}^{K+1},$$

where $(B_t, t \geq 0)$ is a standard $(K + 1)$ -dimensional Brownian motion, and $\nabla \log \pi(\cdot|X^{(n)})$ is as after (3.6). The solution $(\vartheta_t, t \geq 0)$ to (3.10) is well-known to have stationary distribution equal to the posterior $\Pi(\cdot|X^{(n)})$, as the latter can be shown to be invariant with respect to the associated infinitesimal generator, cf. p. 45-47 in [10].

Among the posterior sampling methods based on the SDE (3.10), let us focus on the unadjusted Langevin algorithm (ULA) which is obtained by an Euler-Maruyama discretisation. Specifically, for a stepsize $\delta > 0$, the ULA generates an \mathbb{R}^{K+1} -valued Markov chain

($\vartheta_m, m \geq 0$) via

$$(3.11) \quad \vartheta_{m+1} = \vartheta_m + \frac{\delta}{2} \nabla \log \pi(\vartheta_m | X^{(n)}) + \sqrt{\delta} B_m, \quad B_m \stackrel{\text{iid}}{\sim} N(0, I_{K+1}), \quad \vartheta_0 \in \mathbb{R}^{K+1},$$

whereby the characteristics of $\Pi(\cdot | X^{(n)})$ are approximated by their empirical analogues relative to a sufficiently high number of ULA samples (e.g. as in (3.9) for the posterior mean).

From (3.11), it is seen that the central operation underlying each step of the ULA is the computation of the gradient of the log-posterior density for the current state of the chain. In the problem at hand, this task can be efficiently (and scalably) performed in concrete via the evaluation routine (3.7).

Employing the proposed computational approach, further gradient-based MCMC methods can similarly be implemented. For example, in the popular Metropolis-adjusted Langevin Algorithm the ULA updates (3.11) are used to construct the proposals within a Metropolis-Hastings architecture, and are subject to an accept-reject step similar to the one specified for the pCN algorithm in (3.8), leading to similar dimension-robustness properties. We refer to [66, Section 1.4] and [22, Section 4.3] for more details and references.

3.4. MAP estimation via gradient descent. Lastly, it is also of interest to consider optimisation techniques. In particular, given the posterior density $\pi(\cdot | X^{(n)})$ in (3.4), the associated MAP estimator is defined as any element

$$(3.12) \quad \hat{\theta}_n \in \operatorname{argmax}_{\theta \in \mathbb{R}^{K+1}} \left\{ \log \pi(\theta | X^{(n)}) \right\} = \operatorname{argmax}_{\theta \in \mathbb{R}^{K+1}} \left\{ \ell_n(\theta) - \frac{1}{2} \theta^T \Lambda_\alpha^{-1} \theta \right\}.$$

In fact, identifying, through the parametrisation (3.2), conductivities $f = f_\theta \in \mathcal{F}$ with the corresponding coefficient vectors $\theta \in \mathbb{R}^{K+1}$, the MAP estimator $\hat{\theta}_n$ is seen to be a discretisation of the penalised MLE

$$\hat{f}_n \in \operatorname{argmax}_{f \in \mathcal{F}} \left\{ \log[L_n(f)] - \|f\|_{H^\alpha}^2 \right\},$$

where L_n is the likelihood in (1.4), and where the Sobolev norm penalty corresponds to the limit of the RKHS norm for the truncated Gaussian series prior (3.3) when $K \rightarrow \infty$, cf. Remark 3.1.

A standard approach to solve the optimisation problem (3.12) is the gradient-descent algorithm, prescribing the iteration of

$$(3.13) \quad \vartheta_{m+1} = \vartheta_m + \delta \nabla \log \pi(\vartheta_m | X^{(n)}), \quad \vartheta_0 \in \mathbb{R}^{K+1}, \quad \delta > 0.$$

The MAP estimator $\hat{\theta}_n$ is then concretely computed through the output ϑ_M of the M^{th} step, for some $M \in \mathbb{N}$ typically chosen according to a suitable convergence criterion. The associated MAP estimator \hat{F}_n of the reparametrised functional coefficient F is approximated by

$$F_{\vartheta_M} := \vartheta_{M,0} + \sum_{k=1}^K \vartheta_{M,k} e_k.$$

Similarly to the ULA for posterior sampling described in Section 3.3, the single gradient evaluation required at each iteration of the gradient descent algorithm (3.13) can be tackled via the efficient routine (3.7).

REMARK 3.3 (Multimodality of the posterior). In view of the nonlinear dependence of the transition densities $p_{D,f}$ on the conductivity function f , cf. (2.9), the log-likelihood and the log-posterior density are generally non-concave and potentially multimodal. This can indeed be seen in our numerical experiments; see Appendix C. Thus, while gradient-based

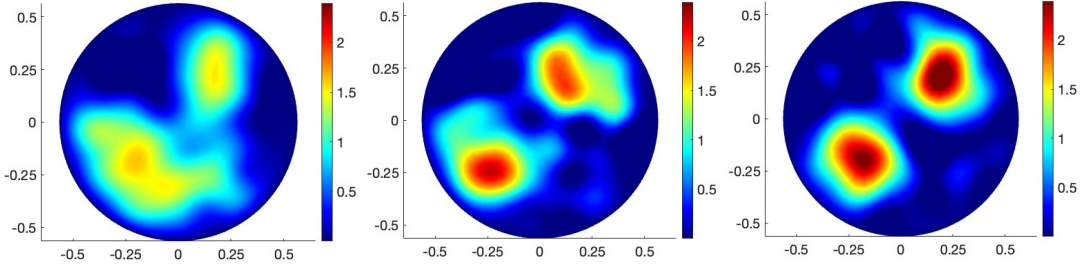


FIG 3. Left to right, top to bottom: posterior mean estimates \bar{F}_n for $n = 500, 2500, 50000$, obtained via the pCN algorithm, to be compared to the ground truth F_0 shown in Figure 1 (left). The computational times ranged between 55 and 59 minutes.

TABLE 1
 L^2 -estimation errors for the posterior mean estimates (obtained via the pCN algorithm)

n	500	1000	2500	5000	10000	50000
$\ F_0 - \bar{F}_n\ _2$.4846	.3953	.3532	.3343	.3188	.2097
$\ F_0 - \bar{F}_n\ _2 / \ F_0\ _2$	55.73%	45.29%	40.47%	38.30%	36.53%	24.02%

iterative schemes may be able to compute global maximisers under specific conditions and ‘warm starts’ (see e.g. [32, Chapter 11], [58]), in general one should only expect to reach convergence towards a local optimum. The global convergence behaviour of gradient-based schemes in SDE models is a highly challenging topic for future research.

On the other hand, compared to MCMC algorithms, optimisation methods are generally computationally attractive, in that they typically require only a small fraction of the number of iterations. In our simulation studies, the MAP estimates also yielded satisfactory reconstructions; see Section 4.5. We further note that, in the present setting, the latter could also be used in conjunction with the posterior samplers described in Section 3.2 and 3.3 as a fast-to-compute initialisation point, reducing the associated burnin times.

4. Numerical experiments. We tested the proposed computational approach in extensive simulation studies, using the ‘non-parametric’ Bayesian model introduced in Section 3.1. Here, we present part of the results, while deferring further examinations to Appendix C. All the numerical experiments were carried out on a MacBook Pro with M1 processor (and 8GB RAM), to which the reported computation times refer. All the required finite element computations for elliptic eigenvalue problems were performed using MATLAB Partial Differential Equation Toolbox (R2023a release), based on a triangulation of the domain \mathcal{O} comprising 1981 nodes (with maximal side length $\varepsilon = .05$).

4.1. *Data generation.* Throughout, we used the unit area disk $\mathcal{O} = \{(x_1, x_2) \in \mathbb{R}^2 : x_1^2 + x_2^2 \leq \pi^{-1}\}$ as the working domain, and took the true conductivity function to be $f_0(x_1, x_2) = 1.1 + 10e^{-(7.25x_1 - 1.5)^2 - (7.25x_2 - 1.5)^2} + 10e^{-(7.25x_1 + 1.5)^2 - (7.25x_2 - 1.5)^2}$, cf. Figure 1 (left). The trajectory of the diffusion process (1.3) was simulated via the Euler-Maruyama scheme, generating the sequence of ‘continuous-time’ states $(x_r, r \geq 0) \subset \mathcal{O}$ by the iteration

$$x_{r+1} = \nabla f_0(x_r) \delta_t + \sqrt{2f_0(x_r)} \delta_t W_r, \quad W_r \stackrel{\text{iid}}{\sim} N(0, 1),$$

suitably modified to incorporate (elastic) reflections at the boundary; see Figure 1 (centre). We set the initial condition x_0 at the origin, specified the time stepsize by $\delta_t = 5 \times 10^{-6}$,

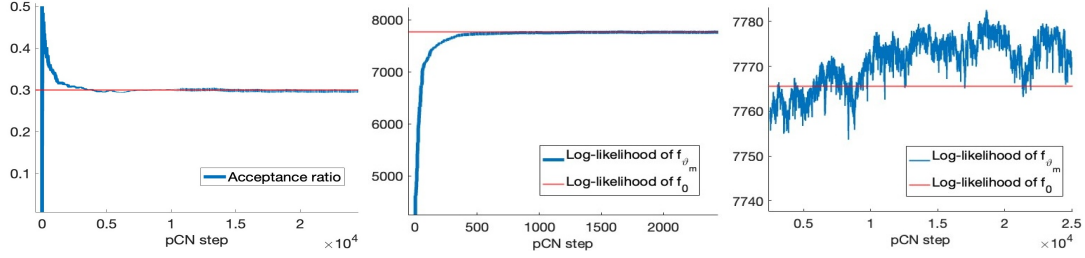


FIG 4. Left: the acceptance ratio along the 25000 iterations of the pCN algorithm, for the case $n = 50000$. Centre and right, respectively: the log-likelihood $\log(L_n(f_{\vartheta_m}))$ for the first 2500 chain steps, and for the steps from the 2500th to the 25000th, again for $n = 50000$.

and repeated the scheme for 5×10^8 times, giving the overall time horizon $T = 5 \times 10^8 \times \delta_t = 2500$. From the simulated trajectory, discrete observations $X^{(n)} = (X_0, X_D, \dots, X_{nD})$ were then sampled with time lags $D = .05$ according to $X_{iD} := x_{iD/\delta_t}$, cf. Figure 1 (right). Note that $D/\delta_t = 10^4 \gg 1$, resulting in a realistic representation of the scenario with low-frequency data.

4.2. *Parameterisation and prior specification.* Across the experiments, we used the truncated Gaussian series priors from (3.3), with the same truncation level $K = 68$, regularity $\alpha = 1$ and variability $\sigma^2 = 500$. Moreover, we used the parameterisation of conductivities f given by (3.1)-(3.2), with link function $\phi(\cdot) = f_{\min} + \exp(\cdot)$ and $f_{\min} = .1$. The L^2 -norm of the reparameterised ground truth $F_0 = \log(f_0 - f_{\min})$ is $\|F_0\|_2 = .8727$, while the L^2 -approximation error resulting from ‘projecting’ F_0 onto the linear space spanned by the eigenfunction $\{1, e_1, \dots, e_K\}$ equals .0848, leading to a ‘benchmark’ relative error of 9.72%.

4.3. *Results for the pCN algorithm.* We begin by presenting the results for the pCN algorithm from Section 3.2. The Monte Carlo approximations $F_{\bar{\vartheta}_M}$ for the posterior mean estimators \bar{F}_n of $F = \log(f - f_{\min})$ are plotted in Figure 3, with increasing sample sizes $n = 500, 2500, 50000$. As expected from the posterior consistency result of [53], they show a progressive improvement in the quality of reconstruction. Table 1 reports the obtained L^2 -estimation errors for the posterior mean estimates.

The stepsize in the pCN algorithm was chosen (depending on the sample size) amongst $\delta \in \{.01, .005, .005, .001, .001, .0001\}$ to achieve acceptance probabilities of around 30% after the burnin phase, cf. Figure 4 (left). Each run of the posterior sampler was initialised at the ‘cold start’ $\vartheta_0 = 0$ and was terminated after $M = 25000$ iterations, discarding the first 2500 ones as the burnin. During such burnin phases, the generated chains were observed to effectively move from their starting points towards the region where the posterior concentrates. This is visualised, for $n = 50000$, in Figure 4 (centre and right) via the trace-plot of the associated log-likelihood values, which rapidly increase towards and then oscillate around the log-likelihood of the ground truth.

For each pCN step, the evaluation of the likelihood ratios to compute the acceptance probabilities (3.8) was carried out via the routine (2.13). The truncation level J for the series in (2.13) was chosen adaptively across the iterations so to include all the approximate eigenvalues $0 < \lambda_1^{(\varepsilon)} \leq \dots \leq \lambda_J^{(\varepsilon)} \leq 250$, after which the exponentially decaying coefficients in (2.13) satisfy $e^{-D\lambda_j^{(\varepsilon)}} \leq e^{-.05 \times 250} = 3.7267 \times 10^{-6}$ for all $j > J$. For the run with sample size $n = 50000$, the $M = 25000$ chain steps took approximately 56 minutes, with an average computation time of .13 seconds per iteration.

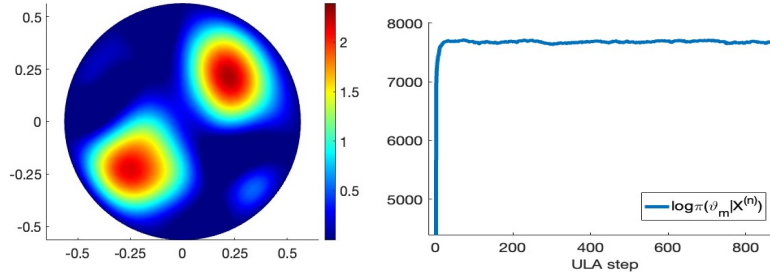


FIG 5. Left: the posterior mean estimate \bar{F}_n , for $n = 50000$, obtained via the ULA, to be compared to the ground truth F_0 shown in Figure 1 (left). The overall computational time was 90 minutes. Right: the log-posterior density $\log \pi(\vartheta_m | X^{(n)})$ for the first 1000 chain steps.

Further details on the results obtained via the pCN algorithm are provided in Appendix C, including chain trace-plots and the resulting approximate marginal posterior distributions of the Fourier coefficients $\theta_0, \dots, \theta_K$. Additional numerical experiments will also be discussed, investigating the role of the initialisation point, the implementation of other classes of Gaussian priors, and the recovery of different ground truths.

4.4. *Results for the ULA.* Based on the same domain, ground truth, synthetic data set $X^{(n)}$, with $n = 50000$, and prior specification used in Section 4.3, we next considered posterior sampling via the ULA, cf. Section 3.3. Figure 5 (left) shows the resulting (Monte Carlo approximations to the) posterior mean estimate \bar{F}_n of the reparametrised conductivity function F . The corresponding L^2 -estimation error was .20327, yielding a relative error of 23.28%.

A total of $M = 10000$ iterations of the ULA were used, with stepsize $\delta = .000025$ and initialisation point $\vartheta_0 = 0$. Compared to the pCN method, through the incorporation of the gradient, the ULA chain was observed to move very efficiently towards the regions of higher posterior probability, which is visualised in Figure 5 (right) by the rapid increase and subsequent stabilisation of the log-posterior density. Accordingly, a shorter burnin of 250 samples was employed. Within each iteration of the ULA, the required gradient evaluation was performed through the routine (3.7). The computational parameters (including the choice of the truncation level J) for the finite element method were specified exactly as for the pCN method in the previous section. The runtime of the ULA was around 90 minutes, with an average computation time of .54 seconds per iteration.

4.5. *Results for the MAP estimator (via gradient descent).* We conclude by presenting the numerical recovery results for the optimisation methods described in Section 3.4. The MAP estimate arising from the same prior (and dataset) employed in Sections 4.3 and 4.4 is shown in Figure 6 (left), with associated L^2 -estimation error equal to .2622 (and relative error of 30%).

The MAP estimate was computed via the gradient descent algorithm, initialised at $\vartheta_0 = 0$ and run, with stepsize $\delta = .00001$, until the verification of the convergence criterion $|\vartheta_{m+1} - \vartheta_m| < .001$. In total, $M = 116$ iterations were necessary to achieve convergence; see Figure 6 (centre). See Figure 6 (right) for the trace-plot of the log-posterior density along the steps of the scheme, which exhibits a rapid increase over the initial iterations, similarly to the ULA. The required evaluation of the log-posterior density gradient was performed exactly as outlined in Section 4.4, resulting in an overall computation time of around 1 minute.

Interestingly, the obtained MAP estimate appears to be visually close in shape to the posterior means calculated via the pCN algorithm and the ULA, with a relatively comparable

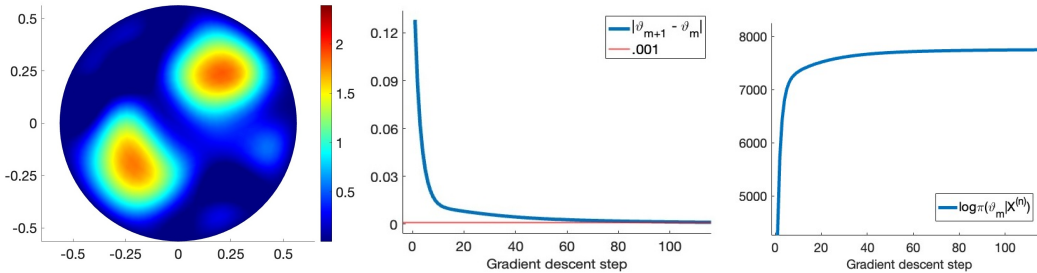


FIG 6. Left: the MAP estimate, with $n = 50000$, computed by the gradient descent, to be compared to the ground truth F_0 shown in Figure 1 (left). The overall computational time was 1 minute. Centre: the distances $|\vartheta_{m+1} - \vartheta_m|$ between consecutive gradient descent iterates. Right: the log-posterior density $\log \pi(\vartheta_m | X^{(n)})$ along the gradient descent steps.

estimation error. This is despite the multimodality of the posterior and the consequent convergence of the gradient descent towards a local maximum; further see Appendix C.

5. Summary and further discussion. In this article, we have developed novel approaches to statistical inference with discrete observations from a class of stochastic diffusion models. Using the PDE characterisation of the transition density functions as fundamental solutions of certain divergence-form heat equations, we have employed abstract parabolic PDE arguments to derive a novel closed-form expression for gradients of likelihoods. Leveraging spectral theory for the elliptic generators, we have then derived powerful series representations for the likelihood and its gradient. Computationally, we have argued (and demonstrated through simulation studies) that these developments lead to reliable and efficient numerical routines based on finite element methods for elliptic eigenvalue problems, that can be used as the basis for the construction of gradient-free and gradient-based statistical methods. This has been illustrated through the implementation and empirical investigation of some commonly used MCMC algorithms and optimisation techniques for nonparametric Bayesian inference with Gaussian priors.

While our work provides novel theoretical and methodological contributions to the challenging problem of inference with low-frequency diffusion data, it also raises several interesting open research questions. Let us conclude by expanding upon two important ones.

5.1. Extensions to models with a potential energy field. The scope of the present investigation has been focused on diffusion processes in isolated media, governed by eq. (1.2) and (1.3). Extensions to models beyond these is of primary interest and a natural avenue for future research. In particular, many of the ideas developed here can be generalised to the important case where the diffusing particles are immersed within a (spatially-varying) ‘potential energy’ field $U : \mathcal{O} \rightarrow \mathbb{R}$ and thus are subject to a ‘displacement force’ directed towards the local minima of U , identified by the gradient vector field ∇U . This results in an SDE with additional drift component,

$$(5.1) \quad dX_t = f(X_t)\nabla U(X_t)dt + \nabla f(X_t)dt + \sqrt{2f(X_t)}dW_t + \nu(X_t)dL_t, \quad t \geq 0,$$

with associated (Gibbs-type) invariant probability density function and infinitesimal generator

$$(5.2) \quad \mu(x) \propto e^{-U(x)}, \quad x \in \mathcal{O}; \quad \mathcal{L}_{f,\mu}\phi := \frac{1}{\mu} \nabla \cdot (\mu f \nabla \phi).$$

As the latter is again in divergence form, and hence self-adjoint with respect to the inner product of $L^2(\mathcal{O})$, conditional inference on the conductivity function f given any U may then be pursued with minimal modifications to the approach developed in Section 2. In fact, in the realistic scenario of U being also unknown, we envision decomposing the problem by obtaining a preliminary estimate $\hat{\mu}_n$ of the invariant probability density function μ (for instance via standard linear kernel density estimators; see e.g. [24, 29, 38, 39, 56]). Based on $\hat{\mu}_n$, the statistical analysis on f can then be performed by replacing the generator $\mathcal{L}_{f,\mu}$ in (5.2) with a plug-in estimate $\mathcal{L}_{f,\hat{\mu}_n}$. Alternatively, a joint Bayesian model can be considered by endowing the additional drift component ∇U in (5.1) with a prior distribution (such as those employed in [38]), which would then require to modify our MCMC algorithms to be of ‘Gibbs’ type. These generalisations are, however, beyond the scope of the present work.

5.2. Bounds on the computational complexity via gradient stability. Another important issue concerns the computational complexity of the employed posterior sampling and optimisation algorithms, going beyond the qualitative invariance properties discussed in Sections 3.2 and 3.3. A recent line of work initiated by Nickl and Wang in [58] has shown that polynomial-time bounds on the iteration complexity of MCMC methods may be obtained under ‘local convexity’ properties for the (negative) log-likelihood near the ground truth, quantified via a stability estimate for the log-likelihood gradient (i.e. a lower bound for its minimal eigenvalue), jointly with regularity properties of the associated Hessian matrix.

In the present setting, this program can indeed be pursued, albeit under a considerable amount of technical work. In particular, one may approach the verification of the key gradient stability condition using the characterisation of the Frechét derivatives in (2.5) and (2.11). Similarly, our ‘bootstrap’ PDE arguments also provide a blueprint for deriving the required higher-order regularity properties for the log-likelihood.

6. Proofs of Theorem 2.2, Corollary 2.3 and Proposition 3.2. In order to achieve a self-contained exposition, we deferred the proof of our main result, Theorem 2.1, to Appendix A. We here present the proofs of Theorem 2.2, Corollary 2.3 and Proposition 3.2.

6.1. Proof of Theorem 2.2. We will use throughout notation and facts from the proof of Theorem 2.1, which can be found in Appendix A. Let $R > 0$, and let $g, h \in C^{1+\kappa}(\mathcal{O})$ with $\|g\|, \|h\|_{C^{1+\kappa}} \leq R$. For some regularisation parameter $\delta > 0$ which will be chosen below in dependence on $\|g\|_{C^1}$, let $D\Phi_{f+g}^\delta$ and $D\Phi_f^\delta$ be ‘regularised Frechét derivatives’ defined as in (A.16) below, and make the decomposition

$$\begin{aligned} & \|D\Phi_{f+g}[h] - D\Phi_f[h]\|_{L^\infty} \\ & \leq \|D\Phi_{f+g}[h] - D\Phi_{f+g}^\delta[h]\|_{L^\infty} \\ & \quad + \|D\Phi_f[h] - D\Phi_f^\delta[h]\|_{L^\infty} + \|D\Phi_{f+g}^\delta[h] - D\Phi_f^\delta[h]\|_{L^\infty} \\ & =: \|I\|_{L^\infty} + \|II\|_{L^\infty} + \|III\|_{L^\infty}. \end{aligned}$$

We estimate each of the terms separately. Our goal is to show that for some $\zeta > 0$,

$$\|I\|_{L^\infty} + \|II\|_{L^\infty} + \|III\|_{L^\infty} = O(\|h\|_{C^1} \|g\|_{C^1}^\zeta).$$

Arguing like in the estimates for term *IV* in the proof of Theorem 2.1, there exists some constant $\eta > 0$ (specifically, chosen as in (A.17) below) such that

$$\|I\|_{L^\infty} + \|II\|_{L^\infty} = O(\|h\|\delta^\eta).$$

It remains to estimate term *III*. To this end, we define the function $w : [0, T] \rightarrow L^2(\mathcal{O})$ by

$$w := (\partial_t - \mathcal{L}_{f+g})^{-1}[\mathcal{L}_h u_{f+g}^\delta] - (\partial_t - \mathcal{L}_f)^{-1}[\mathcal{L}_h u_f^\delta],$$

where we have used the previous notation $\mathcal{L}_h[\cdot] = \nabla \cdot (h\nabla[\cdot])$ (despite h potentially taking nonpositive values). By inspection of the definition of $D\Phi^\delta$, we have that $III = w(D)$. The function w satisfies the PDE

$$\begin{aligned} (\partial_t - \mathcal{L}_f)w &= \mathcal{L}_h u_{f+g}^\delta + (\mathcal{L}_{f+g} - \mathcal{L}_f)(\partial_t - \mathcal{L}_{f+g})^{-1}[\mathcal{L}_h u_{f+g}^\delta] - \mathcal{L}_h u_f^\delta \\ &= \mathcal{L}_h(u_{f+g}^\delta - u_f^\delta) + \mathcal{L}_g(\partial_t - \mathcal{L}_{f+g})^{-1}[\mathcal{L}_h u_{f+g}^\delta]. \end{aligned}$$

Using Theorem A.1 and the Sobolev embedding $H^2(\mathcal{O}) \subset C(\bar{\mathcal{O}})$ (holding since $d \leq 3$), we obtain that for any $\alpha \in (0, 1)$,

$$\begin{aligned} \|III\|_{L^\infty} &= \|w(D)\|_{L^\infty} \\ &\lesssim \|w\|_{C_{\alpha+\mu}^\alpha((0,T]; H_N^2(\mathcal{O}))} \\ &\lesssim \|\mathcal{L}_h(u_{f+g}^\delta - u_f^\delta) + \mathcal{L}_g(\partial_t - \mathcal{L}_{f+g})^{-1}[\mathcal{L}_h u_{f+g}^\delta]\|_{C_{\alpha+\mu}^\alpha((0,T]; L^2(\mathcal{O}))} \\ &\leq \|\mathcal{L}_h(u_{f+g}^\delta - u_f^\delta)\|_{C_{\alpha+\mu}^\alpha((0,T]; L^2(\mathcal{O}))} \\ &\quad + \|\mathcal{L}_g(\partial_t - \mathcal{L}_{f+g})^{-1}[\mathcal{L}_h u_{f+g}^\delta]\|_{C_{\alpha+\mu}^\alpha((0,T]; L^2(\mathcal{O}))} \\ &=: III_a + III_b, \end{aligned}$$

where the spaces $C_{\alpha+\mu}^\alpha((0,T]; L^2(\mathcal{O}))$ and $C_{\alpha+\mu}^\alpha((0,T]; H_N^2(\mathcal{O}))$ are defined in (A.7) below. Noting that the difference $u_{f+g}^\delta - u_f^\delta$ equals the term $R_0^\delta[g]$ defined in (A.14), we now choose $\alpha > 0$ small enough – like in the Lemmas A.2 and A.3 below – to obtain that

$$\begin{aligned} \|\mathcal{L}_h(u_{f+g}^\delta - u_f^\delta)\|_{C_{\alpha+\mu}^\alpha((0,T]; L^2(\mathcal{O}))} &\lesssim \|h\|_{C^1} \|u_{f+g}^\delta - u_f^\delta\|_{C_{\alpha+\mu}^\alpha((0,T]; H_N^2(\mathcal{O}))} \\ &= \|h\|_{C^1} \|R_0^\delta[g]\|_{C_{\alpha+\mu}^\alpha((0,T]; H_N^2(\mathcal{O}))} \\ &\lesssim \|h\|_{C^1} \|g\|_{C^1} \delta^{-\gamma}, \end{aligned}$$

where $\gamma \equiv \gamma(\alpha) = \alpha(d/2 + 2) + (1 - \alpha)d/4$. By our choice of $\alpha > 0$ it is ensured that $\gamma(\alpha) < 1$.

The term III_b can be treated similarly. Using Theorem B.1,

$$\begin{aligned} \|\mathcal{L}_g(\partial_t - \mathcal{L}_{f+g})^{-1}[\mathcal{L}_h u_{f+g}^\delta]\|_{C_{\alpha+\mu}^\alpha((0,T]; L^2(\mathcal{O}))} &\lesssim \|g\|_{C^1} \|(\partial_t - \mathcal{L}_{f+g})^{-1}[\mathcal{L}_h u_{f+g}^\delta]\|_{C_{\alpha+\mu}^\alpha((0,T]; H_N^2(\mathcal{O}))} \\ &\lesssim \|g\|_{C^1} \|\mathcal{L}_h u_{f+g}^\delta\|_{C_{\alpha+\mu}^\alpha((0,T]; L^2(\mathcal{O}))}. \end{aligned}$$

The last expression is almost identical to the right hand side of the PDE (A.3) satisfied by $R_0^\delta[h]$, except with u_{f+g} in place of u_{f+h} . Following the exact same argument as in the proof of Lemma A.2, it can be shown that $\|\mathcal{L}_h u_{f+g}^\delta\|_{C_{\alpha+\mu}^\alpha((0,T]; L^2(\mathcal{O}))} = O(\|h\|_{C^1} \delta^{-\gamma})$. Overall, we have obtained that $III = O(\|h\|_{C^1} \|g\|_{C^1} \delta^{-\gamma})$.

Finally, choose $\delta := \|g\|_{C^1}$; upon combining all the preceding estimates, this yields

$$\|I\|_{L^\infty} + \|II\|_{L^\infty} + \|III\|_{L^\infty} \lesssim \|h\|_{C^1} (\|g\|_{C^1}^\eta + \|g\|_{C^1}^{1-\gamma}),$$

which concludes the proof upon choosing $\zeta = \min\{\eta, 1 - \gamma\}$. \square

6.2. *Proof of Corollary 2.3.* For f and h satisfying the assumptions of Corollary 2.3, recall the expression of the Frechét derivative from Theorem 2.1,

$$D\Phi_f[h] = \int_0^D P_{D-s,f} [\nabla \cdot (h \nabla p_{s,f}(x, \cdot))] (y) ds.$$

By the spectral representations (2.8) and (2.9) for the transition operators and density functions, we can then write the above integrand as, for any fixed $x, y \in \mathcal{O}$ and $s \in (0, D]$, recalling that $e_{f,0} = 1$ (independently of f),

$$\begin{aligned} & P_{D-s,f} [\nabla \cdot (h \nabla p_{s,f}(x, \cdot))] (y) \\ (6.1) \quad &= \sum_{j=0}^{\infty} e^{-(D-s)\lambda_{f,j}} \langle \nabla \cdot (h \nabla p_{s,f}(x, \cdot)), e_{f,j} \rangle_{L^2} e_{f,j}(y) \\ &= \sum_{j=0}^{\infty} \sum_{j'=1}^{\infty} e^{-D\lambda_{f,j}} e^{s(\lambda_{f,j} - \lambda_{f,j'})} \langle \nabla \cdot (h \nabla e_{f,j'}), e_{f,j} \rangle_{L^2} e_{f,j'}(x) e_{f,j}(y). \end{aligned}$$

Now,

$$\langle \nabla \cdot (h \nabla e_{f,j'}), e_{f,j} \rangle_{L^2} = \langle h \Delta e_{f,j'}, e_{f,j} \rangle_{L^2} + \langle \nabla h \cdot \nabla e_{f,j'}, e_{f,j} \rangle_{L^2},$$

and since by Green's first identity (e.g. [34, Section C.2]), recalling that $\partial_\nu e_{f,j'} = \nabla e_{f,j'} \cdot \nu = 0$,

$$\begin{aligned} \langle h \Delta e_{f,j'}, e_{f,j} \rangle_{L^2} &= \int_{\partial \mathcal{O}} h e_{f,j} \nabla e_{f,j'} \cdot \nu d\sigma - \int_{\mathcal{O}} \nabla (h e_{f,j}) \cdot \nabla e_{f,j'} dx \\ &= - \int_{\mathcal{O}} h \nabla e_{f,j} \cdot \nabla e_{f,j'} dx - \int_{\mathcal{O}} e_{f,j} \nabla h \cdot \nabla e_{f,j'} dx \\ &= - \langle h, \nabla e_{f,j} \cdot \nabla e_{f,j'} \rangle_{L^2} - \langle \nabla h \cdot \nabla e_{f,j'}, e_{f,j} \rangle_{L^2}, \end{aligned}$$

we have

$$\langle \nabla \cdot (h \nabla e_{f,j'}), e_{f,j} \rangle_{L^2} = - \langle h, \nabla e_{f,j} \cdot \nabla e_{f,j'} \rangle_{L^2}.$$

Replaced into (6.1), this gives

$$\begin{aligned} & P_{D-s,f} [\nabla \cdot (h \nabla p_{s,f}(x, \cdot))] (y) \\ &= - \sum_{j,j'=1}^{\infty} e^{-D\lambda_{f,j}} e^{s(\lambda_{f,j} - \lambda_{f,j'})} \langle h, \nabla e_{f,j} \cdot \nabla e_{f,j'} \rangle_{L^2} e_{f,j'}(x) e_{f,j}(y), \end{aligned}$$

and finally

$$\begin{aligned} D\Phi_f[h] &= - \sum_{j,j'=1}^{\infty} e^{-D\lambda_{f,j}} \left(\int_0^D e^{s(\lambda_{f,j} - \lambda_{f,j'})} ds \right) \langle h, \nabla e_{f,j} \cdot \nabla e_{f,j'} \rangle_{L^2} e_{f,j'}(x) e_{f,j}(y) \\ &= \sum_{j,j'=1}^{\infty} C_{f,j,j'} \langle h, \nabla e_{f,j} \cdot \nabla e_{f,j'} \rangle_{L^2} e_{f,j'}(x) e_{f,j}(y), \end{aligned}$$

where

$$C_{f,j,j'} := \begin{cases} -D e^{-\lambda_{f,j} D}, & \lambda_{f,j} = \lambda_{f,j'} \\ (e^{-\lambda_{f,j} D} - e^{-\lambda_{f,j'} D}) / (\lambda_{f,j} - \lambda_{f,j'}), & \text{otherwise.} \end{cases}$$

□

6.3. *Proof of Proposition 3.2.* For fixed $x, y \in \mathcal{O}$, denote for convenience

$$(6.2) \quad l: \mathbb{R}^{K+1} \rightarrow \mathbb{R}, \quad l(\theta) = \log p_{D, f_\theta}(x, y).$$

The proof then clearly follows if we show that l is continuously differentiable and that for $k = 0, \dots, K$,

$$(6.3) \quad \partial_{\theta_k} l(\theta) = \frac{D\Phi_{f_\theta}[(\phi' \circ F_\theta)e_k]}{p_{D, f_\theta}(x, y)},$$

where $D\Phi_{f_\theta}$ is the linear operator defined as in (2.5) with $f = f_\theta$. Recalling the notation $\Phi(f) \equiv \Phi_{D, x, y}(f) = p_{D, f}(x, y)$, $f \in \mathcal{F}$, the map l in (6.2) is seen to be the result of the composition

$$l = \log \circ \Phi \circ \Lambda \circ \Theta,$$

where

$$\Lambda: C^2(\bar{\mathcal{O}}) \rightarrow \mathcal{F}, \quad F_\theta \mapsto f_\theta = \phi \circ F_\theta; \quad \Theta: \mathbb{R}^{K+1} \rightarrow C^2(\bar{\mathcal{O}}), \quad \theta \mapsto F_\theta.$$

The linear function Θ is smooth (in the Frechét sense), with $D\Theta_\theta = \Theta$ for all $\theta \in \mathbb{R}^{K+1}$. Further, it is easy to see that in view of the regularity of ϕ , the function Λ also is smooth, with Frechét derivative given by the linear operator

$$D\Lambda: C^2(\bar{\mathcal{O}}) \rightarrow C^2(\bar{\mathcal{O}}), \quad D\Lambda_F[h] = (\phi' \circ F)h.$$

Theorem 2.1 and Theorem 2.2 together imply that Φ is continuously differentiable. The differentiability of l is then obtained the chain rule, e.g. [34, Section E.4]. In particular, with ξ_k the k^{th} element of the standard basis of \mathbb{R}^{K+1} ,

$$\begin{aligned} \partial_{\theta_k} l(\theta) &= Dl_\theta[\xi_k] \\ &= \left(D \log_{[\Phi \circ \Lambda \circ \Theta](\theta)} \circ D\Phi_{[\Lambda \circ \Theta](\theta)} \circ D\Lambda_{\Theta(\theta)} \circ D\Theta_\theta \right) [\xi_k] \\ &= \frac{(D\Phi_{[\Lambda \circ \Theta](\theta)} \circ D\Lambda_{\Theta(\theta)} \circ \Theta)[\xi_k]}{[\Phi \circ \Lambda \circ \Theta](\theta)} \\ &= \frac{(D\Phi_{f_\theta} \circ D\Lambda_{F_\theta})[e_k]}{p_{D, f_\theta}(x, y)} = \frac{D\Phi_{f_\theta}[(\phi' \circ F_\theta)e_k]}{p_{D, f_\theta}(x, y)}. \end{aligned}$$

This concludes the derivation of (6.3) and the proof of the proposition.

Acknowledgments. The authors would like to thank Richard Nickl and Markus Reiß for several helpful discussions.

Funding. M. G. gratefully acknowledges the support of MUR - Prin 2022 - Grant no. 2022CLTYP4, funded by the European Union – Next Generation EU, and the affiliation to the "de Castro" Statistics Initiative, Collegio Carlo Alberto, Torino. S. W. gratefully acknowledges the support of the Air Force Office of Scientific Research Multidisciplinary University Research Initiative (MURI) project ANSRE.

REFERENCES

- [1] ABRAHAM, K. and NICKL, R. (2019). On statistical Caldéron problems. *Mathematical Statistics and Learning* **2** 165–216.
- [2] AGMON, S., DOUGLIS, A. and NIRENBERG, L. (1964). Estimates near the boundary for solutions of elliptic partial differential equations satisfying general boundary conditions II. *Communications on Pure and Applied Mathematics* **17** 35–92.
- [3] AÏT-SAHALIA, Y. (2002). Maximum likelihood estimation of discretely sampled diffusions: a closed-form approximation approach. *Econometrica* **70** 223–262.
- [4] AÏT-SAHALIA, Y. (2008). Closed-form likelihood expansions for multivariate diffusions. *The Annals of Statistics* **36** 906–937.
- [5] ALLEN, E. (2007). Modeling with Itô stochastic differential equations. *Mathematical Modelling: Theory and Applications* **22**. Springer, Dordrecht.
- [6] ALTMAYER, R. (2022). Polynomial time guarantees for sampling based posterior inference in high-dimensional generalised linear models. *arXiv preprint arXiv:2208.13296*.
- [7] BABUŠKA, I. and OSBORN, J. E. (1989). Finite element-Galerkin approximation of the eigenvalues and eigenvectors of selfadjoint problems. *Mathematics of computation* **52** 275–297.
- [8] BABUŠKA, I. and OSBORN, J. (1991). Eigenvalue problems. In *Finite Element Methods (Part 1). Handbook of Numerical Analysis* **2** 641–787. Elsevier.
- [9] BAEHR, H. D. and STEPHAN, K. (1998). *Heat conduction and mass diffusion* In *Heat and Mass Transfer* 105–250. Springer Berlin Heidelberg, Berlin, Heidelberg.
- [10] BAKRY, D., GENTIL, I. and LEDOUX, M. (2014). *Analysis and geometry of Markov diffusion operators* **348**. Springer, Cham.
- [11] BANDEIRA, A. S., MAILLARD, A., NICKL, R. and WANG, S. (2023). On free energy barriers in Gaussian priors and failure of cold start MCMC for high-dimensional unimodal distributions. *Philosophical Transactions of the Royal Society A* **381** 20220150.
- [12] BESKOS, A., GIROLAMI, M., LAN, S., FARRELL, P. E. and STUART, A. M. (2017). Geometric MCMC for infinite-dimensional inverse problems. *Journal of Computational Physics* **335** 327–351.
- [13] BESKOS, A., PAPASPILIOPOULOS, O. and ROBERTS, G. (2009). Monte carlo maximum likelihood estimation for discretely observed diffusion processes. *Annals of statistics* **37** 223–245.
- [14] BESKOS, A., PAPASPILIOPOULOS, O., ROBERTS, G. O. and FEARNHEAD, P. (2006). Exact and computationally efficient likelihood-based estimation for discretely observed diffusion processes (with discussion). *Journal of the Royal Statistical Society Series B: Statistical Methodology* **68** 333–382.
- [15] BLADT, M., FINCH, S. and SØRENSEN, M. (2016). Simulation of multivariate diffusion bridges. *Journal of the Royal Statistical Society Series B: Statistical Methodology* **78** 343–369.
- [16] BOFFI, D. (2010). Finite element approximation of eigenvalue problems. *Acta numerica* **19** 1–120.
- [17] BOHR, J. and NICKL, R. (2021). On log-concave approximations of high-dimensional posterior measures and stability properties in non-linear inverse problems. *arXiv e-prints arXiv:2105.07835*.
- [18] BRAMBLE, J. H. and OSBORN, J. (1973). Rate of convergence estimates for nonselfadjoint eigenvalue approximations. *Mathematics of computation* **27** 525–549.
- [19] BRIANE, V., VIMOND, M. and KERVANN, C. (2020). An overview of diffusion models for intracellular dynamics analysis. *Briefings in Bioinformatics* **21** 1136–1150.
- [20] CALDERÓN, A.-P. (1980). On an inverse boundary value problem. In *Seminar on Numerical Analysis and its Applications to Continuum Physics (Rio de Janeiro, 1980)* 65–73. Soc. Brasil. Mat., Rio de Janeiro.
- [21] CHATELIN, F. (1973). Convergence of approximation methods to compute eigenlements of linear operations. *SIAM Journal on Numerical Analysis* **10** 939–948.
- [22] COTTER, S. L., ROBERTS, G. O., STUART, A. M. and WHITE, D. (2013). MCMC Methods for Functions: Modifying Old Algorithms to Make Them Faster. *Statistical Science* **28** 424–446.
- [23] CUI, T., LAW, K. J. H. and MARZOUK, Y. M. (2016). Dimension-independent likelihood-informed MCMC. *J. Comput. Phys.* **304** 109–137.
- [24] DALALYAN, A. and REISS, M. (2007). Asymptotic statistical equivalence for ergodic diffusions: the multi-dimensional case. *Probability theory and related fields* **137** 25–47.
- [25] DANERS, D. (2000). Heat kernel estimates for operators with boundary conditions. *Mathematische Nachrichten* **217** 13–41.
- [26] DAVIES, E. B. (1995). *Spectral theory and differential operators* **42**. Cambridge University Press.
- [27] DELYON, B. and HU, Y. (2006). Simulation of conditioned diffusion and application to parameter estimation. *Stochastic Processes and their Applications* **116** 1660–1675.
- [28] DESCLOUX, J., NASSIF, N. and RAPPAZ, J. (1978). On spectral approximation. Part 1. The problem of convergence. *RAIRO. Analyse numérique* **12** 97–112.

- [29] DEXHEIMER, N., STRAUCH, C. and TROTTNER, L. (2022). Adaptive invariant density estimation for continuous-time mixing Markov processes under sup-norm risk. In *Annales de l'Institut Henri Poincaré (B) Probabilités et statistiques* **58** 2029–2064. Institut Henri Poincaré.
- [30] DURHAM, G. B. and GALLANT, A. R. (2002). Numerical techniques for maximum likelihood estimation of continuous-time diffusion processes. *Journal of Business & Economic Statistics* **20** 297–338.
- [31] ELERIAN, O., CHIB, S. and SHEPHARD, N. (2001). Likelihood inference for discretely observed nonlinear diffusions. *Econometrica* **69** 959–993.
- [32] ENGL, H. W., HANKE, M. and NEUBAUER, A. (1996). *Regularization of inverse problems. Mathematics and its Applications* **375**. Kluwer, Dordrecht.
- [33] ERAKER, B. (2001). MCMC analysis of diffusion models with application to finance. *Journal of Business & Economic Statistics* **19** 177–191.
- [34] EVANS, L. C. (2010). *Partial differential equations*, Second ed. American Math. Soc.
- [35] GHOSAL, S. and VAN DER VAART, A. W. (2017). *Fundamentals of Nonparametric Bayesian Inference*. Cambridge University Press, New York.
- [36] GINÉ, E. and NICKL, R. (2016). *Mathematical foundations of infinite-dimensional statistical models*. Cambridge University Press, New York.
- [37] GIORDANO, M. and NICKL, R. (2020). Consistency of Bayesian inference with Gaussian process priors in an elliptic inverse problem. *Inverse Problems, to appear*.
- [38] GIORDANO, M. and RAY, K. (2022). Nonparametric Bayesian inference for reversible multidimensional diffusions. *The Annals of Statistics* **50** 2872–2898.
- [39] GOBET, E., HOFFMANN, M. and REISS, M. (2004). Nonparametric estimation of scalar diffusions based on low frequency data. *The Annals of Statistics* **32** 2223 – 2253.
- [40] GOLIGHTLY, A. and WILKINSON, D. J. (2008). Bayesian inference for nonlinear multivariate diffusion models observed with error. *Computational Statistics & Data Analysis* **52** 1674–1693.
- [41] GRAHAM, I. G., KUO, F. Y., NICHOLS, J. A., SCHEICHL, R., SCHWAB, C. and SLOAN, I. H. (2015). Quasi-Monte Carlo finite element methods for elliptic PDEs with lognormal random coefficients. *Numerische Mathematik* **131** 329–368.
- [42] HECKERT, A., DAHAL, L., TJIAN, R. and DARZACQ, X. (2022). Recovering mixtures of fast-diffusing states from short single-particle trajectories. *Elife* **11** e70169.
- [43] HOFFMANN, M. and RAY, K. (2022). Bayesian estimation in a multidimensional diffusion model with high frequency data. *arXiv preprint arXiv:2211.12267*.
- [44] KESSLER, M. and SØRENSEN, M. (1999). Estimating equations based on eigenfunctions for a discretely observed diffusion process. *Bernoulli* 299–314.
- [45] KNYAZEV, A. V. and OSBORN, J. E. (2006). New a priori FEM error estimates for eigenvalues. *SIAM journal on numerical analysis* **43** 2647–2667.
- [46] KOHN, R. and VOGELIUS, M. (1984). Determining conductivity by boundary measurements. *Communications on pure and applied mathematics* **37** 289–298.
- [47] LIN, M., CHEN, R. and MYKLAND, P. (2010). On generating Monte Carlo samples of continuous diffusion bridges. *Journal of the American Statistical Association* **105** 820–838.
- [48] LIONS, J.-L. and MAGENES, E. (1972). *Non-homogeneous boundary value problems and applications. Vol. I*. Springer-Verlag, New York-Heidelberg.
- [49] LUNARDI, A. (1995). *Analytic Semigroups and Optimal Regularity for Parabolic Problems*. Birkhäuser.
- [50] MAJDA, A. J. and HARLIM, J. (2012). *Filtering complex turbulent systems*. Cambridge University Press.
- [51] NACHMAN, A. I. (1988). Reconstructions from boundary measurements. *Annals of Mathematics* **128** 531–576.
- [52] NICKL, R. (2023). *Bayesian Non-linear Statistical Inverse Problems. Zurich Lectures in Advanced Mathematics*. EMS Press.
- [53] NICKL, R. (to appear). Inference for diffusions from low frequency measurements. *The Annals of Statistics*.
- [54] NICKL, R. and PATERNAIN, G. P. (2022). On some information-theoretic aspects of non-linear statistical inverse problems. In *Proc. Int. Cong. Math* **7** 5516–5538.
- [55] NICKL, R. and RAY, K. (2020). Nonparametric statistical inference for drift vector fields of multidimensional diffusions. *Ann. Statist.* **48** 1383–1408.
- [56] NICKL, R. and SÖHL, J. (2017). Nonparametric Bayesian posterior contraction rates for discretely observed scalar diffusions. *Ann. Statist.* **45** 1664–1693.
- [57] NICKL, R., VAN DE GEER, S. and WANG, S. (2020). Convergence rates for penalized least squares estimators in PDE constrained regression problems. *SIAM/ASA Journal on Uncertainty Quantification* **8** 374–413.
- [58] NICKL, R. and WANG, S. (2024). On polynomial-time computation of high-dimensional posterior measures by Langevin-type algorithms. *Journal of the European Mathematical Society* **26** 1031–1112.

- [59] PAPASPILIOPOULOS, O., ROBERTS, G. O. and STRAMER, O. (2013). Data augmentation for diffusions. *Journal of Computational and Graphical Statistics* **22** 665–688.
- [60] PEDERSEN, A. R. (1995). Consistency and asymptotic normality of an approximate maximum likelihood estimator for discretely observed diffusion processes. *Bernoulli* **257**–279.
- [61] PELETIER, M. A., SAVARÉ, G. and VENERONI, M. (2012). Chemical Reactions as Γ -Limit of Diffusion. *SIAM Review* **54** 327–352.
- [62] POKERN, Y., STUART, A. M. and VAN ZANTEN, J. H. (2013). Posterior consistency via precision operators for Bayesian nonparametric drift estimation in SDEs. *Stochastic Process. Appl.* **123** 603–628.
- [63] RASMUSSEN, C. E. and WILLIAMS, C. (2006). *Gaussian processes for machine learning* **2**. MIT press Cambridge, MA.
- [64] RICHTER, G. R. (1981). An inverse problem for the steady state diffusion equation. *SIAM J. Appl. Math.* **41** 210–221.
- [65] ROBERTS, G. O. and STRAMER, O. (2001). On inference for partially observed nonlinear diffusion models using the Metropolis–Hastings algorithm. *Biometrika* **88** 603–621.
- [66] ROBERTS, G. O. and TWEEDIE, R. L. (1996). Exponential convergence of Langevin distributions and their discrete approximations. *Bernoulli* **2** 341–363.
- [67] SCHAUER, M., VAN DER MEULEN, F. and VAN ZANTEN, H. (2017). Guided proposals for simulating multi-dimensional diffusion bridges. *Bernoulli* **23** 2917–2950.
- [68] SHREVE, S. E. (2004). *Stochastic calculus for finance. II. Springer Finance*. Springer-Verlag, New York Continuous-time models.
- [69] SPRUNGK, B., WEISSMANN, S. and ZECH, J. (2023). Metropolis-adjusted interacting particle sampling. *arXiv preprint arXiv:2312.13889*.
- [70] STUART, A. M. (2010). Inverse problems: a Bayesian perspective. *Acta Numer.* **19** 451–559.
- [71] TANAKA, H. (1979). Stochastic differential equations with reflecting boundary condition in convex regions. *Hiroshima Math. J.* **9** 163–177.
- [72] TAYLOR, M. E. (2011). *Partial differential equations I. Basic theory*. Springer, New York.
- [73] TIERNEY, L. (1998). A note on Metropolis-Hastings kernels for general state spaces. *Annals of applied probability* 1–9.
- [74] TRIEBEL, H. (1978). *Interpolation theory, function spaces, differential operators. North-Holland Mathematical Library* **18**. North-Holland, New York.
- [75] UHLMANN, G. (2009). Electrical impedance tomography and Calderón’s problem. *Inverse problems* **25** 123011.
- [76] VAINIKKO, G. M. (1964). Asymptotic error bounds for projection methods in the eigenvalue problem. *Ž. Vyčisl. Mat i Mat. Fiz.* **4** 405–425.
- [77] VAN DER MEULEN, F. and SCHAUER, M. (2017). Bayesian estimation of discretely observed multi-dimensional diffusion processes using guided proposals. *Electronic Journal of Statistics* **11** 2358–2396.
- [78] VAN DER MEULEN, F., VAN DER VAART, A. W. and VAN ZANTEN, J. (2006). Convergence rates of posterior distributions for Brownian semimartingale models. *Bernoulli* **12** 863–888.
- [79] VAN DER VAART, A. *Asymptotic statistics*. Cambridge University Press, Cambridge.
- [80] VAN WAAIJ, J. and VAN ZANTEN, H. (2016). Gaussian process methods for one-dimensional diffusions: Optimal rates and adaptation. *Electronic Journal of Statistics* **10** 628–645.
- [81] WANG, S. (2019). The nonparametric LAN expansion for discretely observed diffusions. *Electron. J. Stat.* **13** 1329–1358.

APPENDIX A: PROOF OF THEOREM 2.1

Given some fixed constant $f_{\min} > 0$, recall the definition of the parameter space \mathcal{F} in (2.1), and the notation $\mathcal{L}_f[\cdot] = \nabla \cdot (f \nabla[\cdot])$ for the infinitesimal generator of $(X_t, t \geq 0)$, with domain

$$\mathcal{D}(\mathcal{L}_f) = H_N^2(\mathcal{O}) = \left\{ u \in H^2(\mathcal{O}) : \partial_\nu u = 0 \text{ on } \partial\mathcal{O} \right\},$$

equipped with the $H^2(\mathcal{O})$ -norm. Moreover, let $\varphi_t(x, y)$, $x, y \in \mathcal{O}$, and $(P_{t,0}, t \geq 0)$ respectively denote the transition densities and the transition semigroup of the reflected Brownian motion on \mathcal{O} ,

$$(A.1) \quad dY_t = \sqrt{2}dW_t + \nu(Y_t)dL_t, \quad t \geq 0.$$

A.1. Proof strategy. In order to prove the gradient characterisation stated in Theorem 2.1, we first introduce a sequence of regularised transition densities $p_{t,f}^\delta$ that are shown to satisfy certain parabolic PDEs whose initial conditions become singular as $\delta \rightarrow 0$ (Section A.2). For each fixed $\delta > 0$, we then use the regularity theory for parabolic PDEs (reviewed in Section A.3) to estimate the differences between the regularised transition densities (Section A.4). Using a recursive argument, higher order differences can also be controlled (Section A.5). Finally, the result is obtained by employing a careful limiting argument to let the regularisation parameter $\delta \rightarrow 0$ (Section A.6).

A.2. Regularised transition densities. For any conductivity function $f \in \mathcal{F}$, we define a regularised version of the transition density $p_{t,f}$ by

$$p_{t,f}^\delta(x, y) := P_{t,f}[\varphi_\delta(\cdot, y)](x) = P_{\delta,0}[p_{t,f}(x, \cdot)](y), \quad t, \delta > 0, \quad x, y \in \mathcal{O}.$$

It will be helpful to regard these as functions from $[0, T]$ to $L^2(\mathcal{O})$ for some $T > 0$, where y is fixed and the space variable is x . To this end, we introduce the notation

$$u_f^\delta(t) := p_{t,f}^\delta(\cdot, y), \quad u_f^\delta : [0, T] \rightarrow L^2(\mathcal{O}).$$

By standard parabolic PDE theory (see [49, Proposition 4.1.2]), it is clear that u_f^δ uniquely solves the initial value problem

$$(A.2) \quad \begin{cases} (\partial_t - \mathcal{L}_f)u_f^\delta(t) = 0, & \text{for } t > 0, \\ u_f^\delta(0) = \varphi_\delta(\cdot, y). \end{cases}$$

Now suppose that h is a ‘small perturbation’ such that $f + h \in \mathcal{F}$. Then, using (A.2) and the corresponding PDE with \mathcal{L}_{f+h} in place of \mathcal{L}_f , we see that the difference $u_{f+h}^\delta - u_f^\delta$ constitutes the (unique) solution to

$$(A.3) \quad \begin{cases} (\partial_t - \mathcal{L}_f)w(t) = \nabla \cdot (h \nabla u_{f+h}^\delta(t)), & \text{for } t > 0, \\ w(0) = 0. \end{cases}$$

A.3. A key parabolic regularity result. We will crucially use the PDE characterisation (A.3) to derive a norm bound for $u_{f+h}^\delta - u_f^\delta$ (in a suitable function space). To do so, we will make extensive use of the optimal regularity theory of parabolic PDEs, e.g. [49]. For the convenience of the reader, we shall summarise some key results below – details are left to Appendix B.1.

It is well-known that $\mathcal{L}_f : H_N^2(\mathcal{O}) \rightarrow L^2(\mathcal{O})$ is a ‘sectorial operator’ in the sense that its ‘resolvent set’ contains a large enough sector in the complex plane \mathbb{C} , and that the resolvents satisfy a suitable norm estimate; see Appendix B.1 for the precise definition. Consequently,

the transition semigroup $e^{t\mathcal{L}_f}$ can be interpreted using the holomorphic functional calculus. For any bounded and continuous function $g : [0, T] \rightarrow L^2(\mathcal{O})$ and any initial condition $u_0 \in H_N^2(\mathcal{O})$, consider the initial value problem

$$(A.4) \quad \begin{cases} (\partial_t - \mathcal{L}_f)u(t) = g(t), & t \in (0, T), \\ u(0) = u_0. \end{cases}$$

Then, by standard theory, laid out e.g. in Chapter 4.1. of [49], the unique solution to (A.4) is given by the variation-of-constants formula¹

$$(A.5) \quad u(t) = e^{t\mathcal{L}_f}u_0 + \int_0^t e^{(t-s)\mathcal{L}_f}g(s)ds, \quad t \in [0, T].$$

Thus, the regularity theory for the solutions to (A.4) reduces to the study of the above representation formula. We will also use the notation $(\partial_t - \mathcal{L}_f)^{-1}$ to denote the solution operator mapping (suitably smooth and integrable) functions $g : [0, T] \rightarrow L^2(\mathcal{O})$ to the solution of (A.5) with $u_0 = 0$,

$$(A.6) \quad [(\partial_t - \mathcal{L}_f)^{-1}g](t) = \int_0^t e^{(t-s)\mathcal{L}_f}g(s)ds, \quad t \in [0, T].$$

For $\alpha \in (0, 1)$, let $C^\alpha([0, T]; L^2(\mathcal{O}))$ denote the space of α -Hölder continuous functions from $[0, T]$ to $L^2(\mathcal{O})$. For $0 < \alpha < 1$, $\beta > 0$ and $X \in \{L^2(\mathcal{O}), H_N^2(\mathcal{O})\}$, we introduce the spaces

$$(A.7) \quad \begin{aligned} C_\beta^\alpha((0, T]; X) &:= \bigcap_{0 < \varepsilon \leq T} C^\alpha([\varepsilon, T]; X) \cap \left\{ u : \sup_{0 < t \leq T} t^{\beta-\alpha} \|u(t)\|_X < \infty \right\} \\ &\cap \left\{ u : \sup_{0 < \varepsilon < T} \varepsilon^\beta \|u\|_{C^\alpha([\varepsilon, T], X)} < \infty \right\}, \end{aligned}$$

normed by

$$\|u\|_{C_\beta^\alpha((0, T]; X)} := \sup_{0 < t \leq T} t^{\beta-\alpha} \|u(t)\|_X + \sup_{0 < \varepsilon < T} \varepsilon^\beta \|u\|_{C^\alpha([\varepsilon, T], X)}.$$

Note that if $\beta > \alpha$ the above norm allows for $\|u(t)\|_X$ to blow up at polynomial rate when $t \rightarrow 0$.

The following ‘optimal regularity’ estimate for the solution u given by the variation-of-constants formula (A.5) is a version of Theorem 4.3.7 in [49], and is used repeatedly throughout our proofs. A more general version can be found in Theorem B.1 below. We shall only need the case $u_0 = 0$.

THEOREM A.1. *For some $\alpha, \mu \in (0, 1)$, assume that $g \in C_{\alpha+\mu}^\alpha((0, T]; L^2(\mathcal{O}))$, and let $u : [0, T] \rightarrow L^2(\mathcal{O})$ be given by (A.5). Then, $u \in C_{\alpha+\mu}^\alpha((0, T]; H_N^2(\mathcal{O}))$ and $\partial_t u \in C_{\alpha+\mu}^\alpha((0, T]; L^2(\mathcal{O}))$. Moreover, there exists a constant $C > 0$ (independent of g) such that*

$$\|u\|_{C_{\alpha+\mu}^\alpha((0, T]; H_N^2(\mathcal{O}))} + \|\partial_t u\|_{C_{\alpha+\mu}^\alpha((0, T]; L^2(\mathcal{O}))} \leq C \|g\|_{C_{\alpha+\mu}^\alpha((0, T]; L^2(\mathcal{O}))}.$$

Informally speaking, the theorem asserts that the solution (A.5) satisfies two types of ‘parabolic regularity’. Firstly, the regularity *in space* of u is of order $H_N^2(\mathcal{O})$ whenever the spatial smoothness of g is of $L^2(\mathcal{O})$ type. Secondly, u also possesses regularity *in time*, in that the smoothness of $\partial_t u$ matches that of g .

¹This should be interpreted as a Bochner integral of $L^2(\mathcal{O})$ -valued functions. We shall not be concerned with distinguishing different notions of solution to (A.4), since all solutions considered here will constitute ‘strict’ solutions. This is the strongest notion of those considered in the abstract parabolic theory; see, e.g. [49].

A.4. Estimates for differences of regularised transition densities. We are now ready to use the PDE (A.3) to derive bounds for differences between regularised transition densities.

LEMMA A.2. *Suppose that $d \leq 3$ and that $f, h : \mathcal{O} \rightarrow \mathbb{R}$ are such that $f, f + h \in \mathcal{F}$, where \mathcal{F} is given by (2.1). Let*

$$w_{f,h} := u_{f+h}^\delta - u_f^\delta, \quad w_{f,h} : [0, T] \rightarrow L^2(\mathcal{O}).$$

Then, there exist some constants $\alpha \in (0, 1)$ (sufficiently small), $\mu \in (0, 1)$ (sufficiently large), $\gamma \in (0, 1)$ as well as $C > 0$ only depending on $f_{\min}, \|f\|_{C^1}, \|h\|_{C^1}, \mu$ and γ such that

$$\|w_{f,h}\|_{C_{\alpha+\mu}^\alpha((0,T];H_N^2(\mathcal{O}))} + \|\partial_t w_{f,h}\|_{C_{\alpha+\mu}^\alpha((0,T];L^2(\mathcal{O}))} \leq C \|h\|_{C^1} \delta^{-\gamma}.$$

The preceding bound is the main technical result of this section. It will be the key for us to employ a bootstrap argument to also control ‘higher order approximations’ of the transition densities; see Section A.5 below.

PROOF. Since $w_{f,h}$ satisfies the parabolic PDE (A.3), in light of Theorem A.1, it suffices to derive a regularity estimate for the inhomogeneity term in (A.3), which we shall denote by

$$g(t) \equiv g_{f,h}^\delta(t) := \nabla \cdot (h \nabla u_{f+h}^\delta(t)), \quad g : [0, T] \rightarrow L^2(\mathcal{O}).$$

Our goal is to bound the $C_{\alpha+\mu}^\alpha((0, T]; L^2(\mathcal{O}))$ -norm of g for α and μ to be suitably chosen later in the proof. This is achieved in four steps; Steps 1-3 deal with estimating

$$\sup_{\varepsilon \in (0, T]} \varepsilon^{\alpha+\mu} \|g\|_{C^\alpha([\varepsilon, T]; L^2(\mathcal{O}))},$$

while Step 4 deals with bounding

$$\sup_{t \in (0, T]} t^\mu \|g(t)\|_{L^2}.$$

Step 1. Fix any $\varepsilon \in (0, T)$, as well as any $\varepsilon < t' < t \leq T$. Then, we have that

$$\begin{aligned} \|g(t) - g(t')\|_{L^2} &= \left\| \nabla \cdot (h \nabla (u_{f+h}^\delta(t) - u_{f+h}^\delta(t'))) \right\|_{L^2} \\ &\lesssim \|h\|_{C^1} \|u_{f+h}^\delta(t) - u_{f+h}^\delta(t')\|_{H^2}. \end{aligned}$$

In order to further bound the right hand side, we use the norm equivalence

$$(A.8) \quad C^{-1} (\|\mathcal{L}_{f+h} u\|_{L^2} + \|u\|_{L^2}) \leq \|u\|_{H^2} \leq C (\|\mathcal{L}_{f+h} u\|_{L^2} + \|u\|_{L^2})$$

from Lemma B.2, holding for all $u \in H_N^2(\mathcal{O})$ and for some C that only depends on f_{\min} and $\|f + h\|_{C^1}$. It follows that

$$(A.9) \quad \begin{aligned} &\|u_{f+h}^\delta(t) - u_{f+h}^\delta(t')\|_{H^2} \\ &\simeq \|\mathcal{L}_{f+h} [u_{f+h}^\delta(t) - u_{f+h}^\delta(t')]\|_{L^2} + \|u_{f+h}^\delta(t) - u_{f+h}^\delta(t')\|_{L^2} \\ &=: I + II. \end{aligned}$$

Step 2: Term I. Term I is the most difficult to bound among the two, and we treat it first. Denoting by Id the identity operator, and using the semigroup property of $(P_{t,f+h}, t \geq 0)$, the definition of u_{f+h}^δ as well as the fact that \mathcal{L}_{f+h} and $P_{t,f+h}$ commute, we have that

$$\begin{aligned} \|\mathcal{L}_{f+h} [u_{f+h}^\delta(t) - u_{f+h}^\delta(t')]\|_{L^2} &= \|\mathcal{L}_{f+h} (P_{t-t',f+h} - Id) [P_{t',f+h} [\varphi_\delta(\cdot, y)]]\|_{L^2} \\ &= \|(P_{t-t',f+h} - Id) [\mathcal{L}_{f+h} P_{t',f+h} [\varphi_\delta(\cdot, y)]]\|_{L^2}. \end{aligned}$$

Moreover, standard analytic semigroup theory implies that for some $M < \infty$ it holds that

$$(A.10) \quad \sup_{0 < t \leq T} t \|\mathcal{L}_{f+h} P_{t,f+h}\|_{L^2 \rightarrow L^2} \leq M; \quad \sup_{0 < t \leq T} t \|\mathcal{L}_{f+h} P_{t,f+h}\|_{H_N^2 \rightarrow H_N^2} \leq M,$$

see e.g. the estimates (2.1.1) in [49]. Above, for $X \in \{L^2(\mathcal{O}), H_N^2(\mathcal{O})\}$, we have denoted by $\|\cdot\|_{X \rightarrow X}$ the usual operator norm. Next, for $\alpha \in (0, 1)$ we denote by \mathcal{D}_α a suitable interpolation space between $L^2(\mathcal{O})$ and $H_N^2(\mathcal{O})$ defined in (B.4) below. This space has norm

$$\|u\|_{\mathcal{D}_\alpha} := \|u\|_{L^2} + \sup_{t \in (0,1)} t^{-\alpha} \|P_{t,f} u - u\|_{L^2};$$

see (B.5). Using the interpolation inequality

$$\|u\|_{\mathcal{D}_\alpha} \lesssim \|u\|_{L^2}^{1-\alpha} \|u\|_{H^2}^\alpha, \quad u \in \mathcal{D}_\alpha,$$

as well (A.10), we may therefore estimate

$$\begin{aligned} & \|(P_{t-t',f+h} - Id)[\mathcal{L}_{f+h} P_{t',f+h}[\varphi_\delta(\cdot, y)]]\|_{L^2} \\ & \lesssim (t-t')^\alpha \|\mathcal{L}_{f+h} P_{t',f+h}[\varphi_\delta(\cdot, y)]\|_{\mathcal{D}_\alpha} \\ & \lesssim (t-t')^\alpha \|\mathcal{L}_{f+h} P_{t',f+h}[\varphi_\delta(\cdot, y)]\|_{L^2}^{1-\alpha} \|\mathcal{L}_{f+h} P_{t',f+h}[\varphi_\delta(\cdot, y)]\|_{H^2}^\alpha \\ & \lesssim (t-t')^\alpha (t')^{-1} \|\varphi_\delta(\cdot, y)\|_{L^2}^{1-\alpha} \|\varphi_\delta(\cdot, y)\|_{H^2}^\alpha \\ & \lesssim (t-t')^\alpha \varepsilon^{-1} \|\varphi_\delta(\cdot, y)\|_{L^2}^{1-\alpha} \|\varphi_\delta(\cdot, y)\|_{H^2}^\alpha. \end{aligned}$$

Next, we use the heat kernel estimates from Lemma B.6 below to obtain the bound

$$(A.11) \quad \begin{aligned} & (t-t')^\alpha \varepsilon^{-1} \|\varphi_\delta(\cdot, y)\|_{L^2}^{1-\alpha} \|\varphi_\delta(\cdot, y)\|_{H^2}^\alpha \\ & \lesssim (t-t')^\alpha \varepsilon^{-1} \delta^{-(1-\alpha)d/4} \delta^{-\alpha(d/2+2)} = (t-t')^\alpha \varepsilon^{-1} \delta^{-\gamma}, \end{aligned}$$

where we have set

$$(A.12) \quad \gamma \equiv \gamma(\alpha) := (1-\alpha)d/4 + \alpha(d/2+2) = d/4 + \alpha(2+d/4).$$

Since $d \leq 3$, we can (and will) choose a sufficiently small value for $\alpha > 0$ to guarantee that $\gamma < 1$, as required in the statement of the lemma.

Step 3: Term II; combining the estimates. Term II can be estimated similarly. Indeed, it holds that for some $M > 0$,

$$\sup_{0 < t \leq T} \|\mathcal{L}_{f+h} P_{t,f+h}\|_{L^2 \rightarrow L^2} \leq M; \quad \sup_{0 < t \leq T} \|\mathcal{L}_{f+h} P_{t,f+h}\|_{H_N^2 \rightarrow H_N^2} \leq M.$$

Then, arguing as above, we obtain that

$$(A.13) \quad \begin{aligned} & \|(P_{t-t',f+h} - Id)[P_{t',f+h}[\varphi_\delta(\cdot, y)]]\|_{L^2} \lesssim (t-t')^\alpha \|\varphi_\delta(\cdot, y)\|_{L^2}^{1-\alpha} \|\varphi_\delta(\cdot, y)\|_{H^2}^\alpha \\ & \lesssim (t-t')^\alpha \delta^{-(1-\alpha)d/4} \delta^{-\alpha(d/2+2)} \\ & = (t-t')^\alpha \delta^{-\gamma}. \end{aligned}$$

Combining (A.9), (A.11) and (A.13) then implies that $\|g\|_{C^\alpha([\varepsilon, T]; L^2(\mathcal{O}))} \lesssim \|h\|_{C^1} \varepsilon^{-1} \delta^{-\gamma}$. Now choose any $\mu \in (1-\alpha, 1)$. For such μ , we have proven that

$$\sup_{\varepsilon \in (0, T]} \varepsilon^{\alpha+\mu} \|g\|_{C^\alpha([\varepsilon, T]; L^2(\mathcal{O}))} < \delta^{-\gamma} \|h\|_{C^1}.$$

Step 4. There remains to bound $\sup_{0 < t \leq 1} t^\mu \|g(t)\|_{L^2}$. Arguing as before and using again the norm equivalence (A.8),

$$\begin{aligned} \|g(t)\|_{L^2} &\lesssim \|h\|_{C^1} \|P_{t,f+h}[\varphi_\delta(\cdot, y)]\|_{H^2} \\ &\simeq \|P_{t,f+h} \mathcal{L}_{f+h}[\varphi_\delta(\cdot, y)]\|_{L^2} + \|P_{t,f+h}[\varphi_\delta(\cdot, y)]\|_{L^2}. \end{aligned}$$

Just like in Steps I and II, we focus on the first term, as the second one is easier to control. By another application of the standard properties of analytic semigroups, it holds that for some $M < \infty$,

$$\sup_{0 < t \leq 1} \|P_{t,f+h} \mathcal{L}_{f+h}\|_{L^2 \rightarrow L^2} \leq t^{-1} M; \quad \sup_{0 < t \leq 1} \|P_{t,f+h} \mathcal{L}_{f+h}\|_{H^2 \rightarrow L^2} \leq M;$$

cf. eq. (2.1.1) in [49]. Using interpolation theory, e.g. Theorem 1.2.6 in [49], and by possibly changing the constant M , we then obtain that

$$\sup_{0 < t \leq 1} \|P_{t,f+h} \mathcal{L}_{f+h}\|_{\mathcal{D}_\alpha \rightarrow L^2} \leq t^{\alpha-1} M.$$

It follows that

$$\|P_{t,f+h} \mathcal{L}_{f+h}[\varphi_\delta(\cdot, y)]\|_{L^2} \lesssim t^{\alpha-1} \|\varphi_\delta(\cdot, y)\|_{L^2}^{1-\alpha} \|\varphi_\delta(\cdot, y)\|_{H^2}^\alpha.$$

We now may follow the same arguments as in (A.11) and (A.13) to derive the estimate,

$$\|g(t)\|_{L^2} \lesssim t^{\alpha-1} \delta^{-\gamma}.$$

Choosing α and γ as in (A.12), arguing as in (A.11) and using that $\mu > 1 - \alpha$, we then obtain that

$$\sup_{0 < t \leq T} t^\mu \|g(t)\|_{L^2} \leq \sup_{0 < t \leq T} t^{\mu-(1-\alpha)} \|g(t)\|_{L^2} \lesssim T^{\mu-(1-\alpha)} \|h\|_{C^1} \delta^{-\gamma}.$$

This completes the proof of the lemma. \square

A.5. Higher-order approximations. One can interpret the difference $w_{f,h} = u_{f+h}^\delta - u_f^\delta$ as the remainder term of a ‘zeroth order’ (i.e. constant) approximation of the operator $\tilde{f} \mapsto u_{\tilde{f}}^\delta$ at some fixed point $f \in \mathcal{F}$. In light of this interpretation, fixing some $f \in \mathcal{F}$, we introduce the notation

$$M_0^\delta[h](t) := u_f^\delta(t), \quad M_0^\delta[h] : [0, T] \rightarrow L^2(\mathcal{O}),$$

for the zeroth order approximation, and define the remainder term by

$$(A.14) \quad R_0^\delta[h](t) := u_{f+h}^\delta(t) - u_f^\delta(t), \quad R_0^\delta : [0, T] \rightarrow L^2(\mathcal{O}).$$

While this notation may at first seem artificial, it will prove very convenient for generalisations to higher order local polynomial approximations in directions h around some $f \in \mathcal{F}$, which we now define recursively. The following construction is adapted from [81].

For any $k \geq 1$ and f, h as above, and recalling the solution operator (A.6), we define the k^{th} order ‘monomial’ approximation term as

$$M_k^\delta[h](t) := (\partial_t - \mathcal{L}_f)^{-1} [\nabla \cdot (h \nabla M_{k-1}^\delta[h])](t).$$

Naturally, since we are mostly interested in the characterisation of the first-order derivative, the most important term will be the linear one, $M_1^\delta[h]$; see Corollary A.4. The above definitions should at first be understood to be formal expressions – in the next lemma, it will be recursively shown that the terms $M_{k-1}^\delta[h]$ are suitably regular such that the action of the solution operator $(\partial_t - \mathcal{L}_f)^{-1}$ upon them is well-defined.

Before doing so, we note that it is clear from the recursive definition that, for all $k \geq 1$, $M_k^\delta[h]$ is homogeneous of degree k in h . Indeed, the sum $\sum_{l=0}^k M_l^\delta[h]$ will serve as our ‘candidate’ k^{th} order local polynomial approximation to the transition densities around f . We denote the associated remainder term by

$$R_k^\delta[h] := u_{f+h}^\delta - \sum_{l=0}^k M_l^\delta[h].$$

In order to show that the approximation by $\sum_{l=0}^k M_l^\delta[h]$ is the correct one, we will prove that the size of $R_k^\delta[h]$ is of order at most $o(\|h\|_{C^1}^k)$. Indeed, from the definition, it is easily seen that, for each $k \geq 1$, $R_k^\delta[h]$ also satisfies a recursive relationship, which reads

$$(A.15) \quad \begin{cases} (\partial_t - \mathcal{L}_f)R_{k-1}^\delta[h](t) = [\nabla \cdot (h \nabla R_{k-1}^\delta[h])](t), & \text{for } t > 0, \\ R_k^\delta[h](0) = 0. \end{cases}$$

Using this characterisation, we will now extend Lemma A.2 (which established an upper bound for $R_0^\delta[h]$) to all $R_k^\delta[h]$, $k \geq 1$, by induction (again, we note that the case $k = 1$ will be the most important for us, but proving the estimate for all $k \geq 1$ is no more complicated than the argument for $k = 1$).

LEMMA A.3. *Suppose that $d \leq 3$ and that $f, h : \mathcal{O} \rightarrow \mathbb{R}$ are such that $f, f + h \in \mathcal{F}$. Then, for any $k \geq 0$, there exists a sufficiently small constant $\alpha > 0$, some $\gamma \in (0, 1)$ and some $C > 0$ such that*

$$\|R_k^\delta[h]\|_{C_{\alpha+\mu}^{\alpha+\mu}((0,T];H_N^2(\mathcal{O}))} + \|\partial_t R_k^\delta[h]\|_{C_{\alpha+\mu}^{\alpha+\mu}((0,T];L^2(\mathcal{O}))} \leq C \|h\|_{C^1}^{k+1} \delta^{-\gamma}.$$

The key implication of the preceding lemma is that it identifies the directional derivatives of the regularised transition densities. Using the lemma with $k = 1$, we immediately obtain that the Fréchet derivative of the regularised maps $f \mapsto u_f^\delta$ must be given by the operator $h \mapsto M_\delta^1[h]$. In light of this, we introduce the notation

$$(A.16) \quad D\Phi_f^\delta[h] := M_1^\delta[h](D).$$

COROLLARY A.4. *Suppose that $d \leq 3$. Then, with $\alpha, \mu, \gamma \in (0, 1)$ as in Lemma A.3, we have that*

$$\|u_{f+h}^\delta - u_f^\delta - D\Phi_f^\delta[h]\|_{C_{\alpha+\mu}^{\alpha+\mu}((0,T];H_N^2(\mathcal{O}))} = \|R_\delta^1[h]\|_{C_{\alpha+\mu}^{\alpha+\mu}((0,T];H_N^2(\mathcal{O}))} = O(\delta^{-\gamma} \|h\|_{C^1}^2),$$

as $h \rightarrow 0$. In particular, using the Sobolev embedding $H^2(\mathcal{O}) \subset C(\mathcal{O})$, it follows that for any fixed and positive $D > 0$,

$$\|u_{f+h}^\delta(D) - u_f^\delta(D) - D\Phi_f^\delta[h]\|_{L^\infty} = O(\delta^{-\gamma} \|h\|_{C^1}^2).$$

In fact, following the arguments of [81], one could also prove that the regularised transition densities are direction-wise analytic. However, this is not needed for the algorithmic purposes of this article, and we shall omit this generalisation in order to avoid additional technicalities.

We conclude this section with the proof of Lemma A.3.

PROOF OF LEMMA A.3. We proceed by induction on the order k . **Induction start** $k = 0$. This is shown in Lemma A.2.

Induction step $(k - 1) \rightarrow k$. Suppose now that $k \geq 1$, and that the claim holds for some $k - 1$. In view of the PDE characterisation (A.15) of $R_k^\delta[h]$ and by the regularity estimate from

Theorem A.1, our proof strategy is to derive a bound for $\|\nabla \cdot (h \nabla R_{k-1}^\delta[h])\|_{C_{\alpha+\mu}^\alpha((0,T];L^2(\mathcal{O}))}$. To this end, for each $t \in (0, T]$, we estimate

$$\begin{aligned} t^\mu \|\nabla \cdot (h \nabla R_{k-1}^\delta[h])(t)\|_{L^2} &\lesssim t^\mu \|h\|_{C^1} \|R_{k-1}^\delta[h](t)\|_{H^2} \\ &\lesssim \|h\|_{C^1} \|R_{k-1}^\delta[h]\|_{C_{\alpha+\mu}^\alpha((0,T];H_N^2(\mathcal{O}))}. \end{aligned}$$

Similarly, it holds that for any $t > t' \geq \varepsilon > 0$,

$$\begin{aligned} \varepsilon^{\alpha+\mu} \|\nabla \cdot (h \nabla [R_{k-1}^\delta[h]](t) - \nabla \cdot (h \nabla R_{k-1}^\delta[h])(t'))\|_{L^2} \\ \leq \varepsilon^{\alpha+\mu} \|h\|_{C^1} \|R_{k-1}^\delta[h](t) - R_{k-1}^\delta[h](t')\|_{H^2} \\ \leq \varepsilon^{\alpha+\mu} \|h\|_{C^1} (t-t')^\alpha \|R_{k-1}^\delta[h](t)\|_{C^\alpha([\varepsilon,T];H_N^2(\mathcal{O}))} \\ \leq \|h\|_{C^1} (t-t')^\alpha \|R_{k-1}^\delta[h]\|_{C_{\alpha+\mu}^\alpha([0,T];H_N^2(\mathcal{O}))}. \end{aligned}$$

Thus, using the above two displays together with the PDE (A.15), the regularity estimate (B.1) and the induction hypothesis, we obtain

$$\begin{aligned} \|R_k^\delta[h]\|_{C_{\alpha+\mu}^\alpha((0,T];H_N^2(\mathcal{O}))} + \|\partial_t R_k^\delta[h]\|_{C_{\alpha+\mu}^\alpha((0,T];L^2(\mathcal{O}))} \\ \leq \|\nabla \cdot (h \nabla R_{k-1}^\delta[h])\|_{C_{\alpha+\mu}^\alpha((0,T];L^2(\mathcal{O}))} \\ \lesssim \|h\|_{C^1} \|R_{k-1}^\delta[h]\|_{C_{\alpha+\mu}^\alpha((0,T];H_N^2(\mathcal{O}))} \leq C \|h\|_{C^1} \|h\|_{C^1}^k \delta^{-\gamma}, \end{aligned}$$

which proves the claim. \square

A.6. Taking the limit $\delta \rightarrow 0$. Corollary A.4 characterises the linearisation of the regularised transition densities for fixed $\delta > 0$. To prove Theorem 2.1, we need to take the limit $\delta \rightarrow 0$. Since the regularity estimates obtained in the previous section depend in a specific manner on δ , this requires some care; in particular, δ will be chosen according to the size of the perturbation h .

PROOF OF THEOREM 2.1. Fix $x, y \in \mathcal{O}$, and f and h as in the hypotheses. Our goal to show that the (unregularised) transition densities satisfy

$$\left| p_{D,f+h}(x, y) - p_{D,f}(x, y) - D\Phi_f[h](x) \right| = o(\|h\|_{C^1}).$$

To mirror the preceding notation, we write $u_f(t) := p_{t,f}(\cdot, y)$, $t \geq 0$. Then, it suffices to show that

$$\|u_{f+h}(D) - u_f(D) - D\Phi_f[h]\|_{L^\infty} = o(\|h\|_{C^1}).$$

We take the ‘intuitive’ approach of approximating each of the above three terms with their δ -regularised version, obtaining the decomposition

$$\begin{aligned} \|u_{f+h}(D) - u_f(D) - D\Phi_f[h]\|_{L^\infty} &\leq \|u_{f+h}^\delta(D) - u_{f+h}^\delta(D) - D\Phi_f^\delta[h]\|_{L^\infty} \\ &\quad + \|u_{f+h}^\delta(D) - u_{f+h}(D)\|_{L^\infty} \\ &\quad + \|u_f^\delta(D) - u_f(D)\|_{L^\infty} + \|D\Phi_f^\delta[h] - D\Phi_f[h]\|_{L^2} \\ &=: I + II + III + IV. \end{aligned}$$

Choice of δ . We now make the crucial choice for the regularisation parameter δ in dependence of h . Let $\gamma \in (0, 1)$ be the constant from Lemma A.3. Then, we fix some $\beta \in (1, \gamma^{-1})$,

and set $\delta := \|h\|_{C^1}^\beta$. For this choice of δ , we will be able to show that all four terms in the preceding decomposition are of order $o(\|h\|_{C^1})$.

Term I. The first term is exactly equal to $\|R_1^\delta[h](D)\|_{L^\infty}$. Thus, using Lemma A.3 as well as the Sobolev embedding $H^2(\mathcal{O}) \subset C(\mathcal{O})$ (since $d \leq 3$), we see that for some $\alpha > 0$,

$$\begin{aligned} I &= \|R_1^\delta[h](D)\|_{L^\infty} \\ &\lesssim \|R_1^\delta[h](D)\|_{H^2} \lesssim \|R_1^\delta[h]\|_{C_{\alpha+\mu}^\alpha((0,T];H_N^2(\mathcal{O}))} \lesssim \|h\|_{C^1}^2 \delta^{-\gamma} = \|h\|_{C^1}^{2-\gamma\beta} = o(\|h\|_{C^1}). \end{aligned}$$

For the last identity, we used that $\beta\gamma < 1$.

Term II. Let us denote the transition operators of the reflected Brownian motion by $(P_t, t > 0)$. Since $(P_t, t > 0)$ constitutes an analytic semigroup generated by the Laplace operator acting on $C(\mathcal{O})$ with domain $C_N^2(\mathcal{O}) := \{u \in C^2(\mathcal{O}) : \partial_\nu u = 0\}$ (see Section B.1.3 below for details), we can use the inequality (B.7) together with the assumption that $\|h\|_{C^2} \leq 1$ to obtain

$$II = \|(P_\delta - Id)u_{f+h}(D)\|_{C(\mathcal{O})} \lesssim \delta \|u_{f+h}(D)\|_{C_N^2(\mathcal{O})} \lesssim \delta \|u_{f+h}(D)\|_{C^{2+\eta}} = o(\|h\|_{C^1}).$$

Here, we also used the fact that

$$\sup_{h \in C^2: \|h\|_{C^{1+\eta}} \leq 1} \|u_{f+h}\|_{C^{2+\eta}} < \infty,$$

which follows from Lemma B.7 below.

Term III. The third term can be treated in the same way as Term II, with u_{f+h} replaced by u_f .

Term IV. We further decompose

$$\begin{aligned} IV &= \|D\Phi_f^\delta[h] - D\Phi_f[h]\|_{L^\infty} \\ &= \left\| \int_0^D P_{D-s,f} [\mathcal{L}_h(p_{s,f}^\delta(x, \cdot) - p_{s,f}(x, \cdot))] ds \right\|_{L^\infty} \\ &= \left\| \int_0^{D/2} P_{D-s,f} [\mathcal{L}_h(p_{s,f}^\delta(x, \cdot) - p_{s,f}(x, \cdot))] ds \right\|_{L^\infty} \\ &\quad + \left\| \int_{D/2}^D P_{D-s,f} [\mathcal{L}_h(p_{s,f}^\delta(x, \cdot) - p_{s,f}(x, \cdot))] ds \right\|_{L^\infty} \\ &=: IV_a + IV_b. \end{aligned}$$

Term IV_a. The main difficulty is to deal with the singularity of $p_{s,f}$ for $s \rightarrow 0$. Using Lemma B.8, we obtain that for some $C > 0$ and any $t > D/2$,

$$\begin{aligned} \|P_{t,f} [\mathcal{L}_h(p_{s,f}^\delta(x, \cdot) - p_{s,f}(x, \cdot))]\|_{L^\infty} &\leq \|\nabla \cdot (h \nabla (p_{s,f}^\delta(x, \cdot) - p_{s,f}(x, \cdot)))\|_{(H_N^2)^*} \\ &= \sup_{\varphi \in H_N^2: \|\varphi\|_{H^2} \leq 1} \left| \int_{\mathcal{O}} [\nabla \cdot (h \nabla (p_{s,f}^\delta(x, \cdot) - p_{s,f}(x, \cdot)))](z) \varphi(z) dz \right|. \end{aligned}$$

Using the self-adjointness of the differential operator $\nabla \cdot (h \nabla [\cdot])$, the dual characterisation of $\|\cdot\|_{L^2}$, (B.6) as well as Lemma B.6, for any $\eta \in (0, 1/2)$ we can further estimate the right hand side, up to a multiplicative constant, by

$$\begin{aligned} &\sup_{\varphi \in H_N^2: \|\varphi\|_{H^2} \leq 1} \left| \int_{\mathcal{O}} (p_{s,f}^\delta(x, z) - p_{s,f}(x, z)) [\nabla \cdot (h \nabla \varphi)](z) dz \right| \\ &\lesssim \|h\|_{C^1} \|p_{s,f}^\delta(x, \cdot) - p_{s,f}(x, \cdot)\|_{L^2} \end{aligned}$$

$$\begin{aligned}
&= \|h\|_{C^1} \|(P_{\delta,0} - Id)p_{s,f}(x, \cdot)\|_{L^2} \\
&\lesssim \|h\|_{C^1} \delta^\eta \|p_{s,f}(x, \cdot)\|_{H^{2\eta}} \\
&\lesssim \|h\|_{C^1} \delta^\eta \|p_{s,f}(x, \cdot)\|_{L^2}^{1-\eta} \|p_{s,f}(x, \cdot)\|_{H^2}^\eta \lesssim \|h\|_{C^1} \delta^\eta s^{-d(1-\eta)/4} s^{-\eta(d/2+2)}.
\end{aligned}$$

Now let

$$(A.17) \quad \gamma \equiv \gamma(\eta) := d(1-\eta)/4 + \eta(d/2 + 2).$$

Note that this corresponds to the exponent defined in (A.12). By choosing $\eta > 0$ small enough and using the fact that $d \leq 3$, we can ensure that $\gamma < 1$, so that the previous expression is integrable at $s = 0$. As a consequence, for any such η , we have

$$IV_a \lesssim \|h\|_{C^1} \delta^\eta = o(\|h\|_{C^1}).$$

Term IV_b . We now turn to term IV_b . Here, we fix some $y \in \mathcal{O}$. Then, using the self-adjointness of \mathcal{L}_h as well as of $P_{\delta,0} - Id$, we obtain

$$\begin{aligned}
&\int_{D/2}^D P_{D-s,f} [\mathcal{L}_h(p_{s,f}^\delta(x, \cdot) - p_{s,f}(x, \cdot))](y) ds \\
&= \int_{D/2}^D \langle P_{D-s,f}(y, \cdot), \mathcal{L}_h(p_{s,f}^\delta(x, \cdot) - p_{s,f}(x, \cdot)) \rangle_{L^2} ds \\
&= \int_{D/2}^D \langle (P_{\delta,0} - Id) \mathcal{L}_h(P_{D-s,f}(y, \cdot)), p_{s,f}(x, \cdot) \rangle_{L^2} ds \\
&= \int_{D/2}^D P_{s,f} [(P_{\delta,0} - Id) \mathcal{L}_h(P_{D-s,f}(y, \cdot))](x) ds \\
&= \int_0^{D/2} P_{D-s,f} [(P_{\delta,0} - Id) \mathcal{L}_h(p_{s,f}(y, \cdot))](x) ds \\
&\leq \int_0^{D/2} \|P_{D-s,f} [(P_{\delta,0} - Id) \mathcal{L}_h(p_{s,f}(y, \cdot))]\|_{L^\infty} ds.
\end{aligned}$$

Now, we can employ a similar chain of estimates (albeit slightly more complicated) as we did for term IV_a . Another type of interpolation space between $L^2(\mathcal{O})$ and $H_N^2(\mathcal{O})$, different from the previously used ones, will be useful here. We follow Chapter 1, Section 2.1 of [48]. We denote by $[H_N^2(\mathcal{O}), L^2(\mathcal{O})]_\eta$, $\eta \in [0, 1]$, the interpolation spaces obtained through the construction there, defined as the domain of fractional powers Δ^η of the Neumann-Laplacian, satisfying $H_N^2(\mathcal{O}) \subseteq [H_N^2(\mathcal{O}), L^2(\mathcal{O})]_\eta \subseteq L^2(\mathcal{O})$. By the duality result is Theorem 6.2 of Chapter 1 in [48] and identifying $(L^2(\mathcal{O}))^* = (L^2(\mathcal{O}))^*$, it holds that for all $\eta \in [0, 1]$,

$$(A.18) \quad ([H_N^2(\mathcal{O}), L^2(\mathcal{O})]_{1-\eta})^* = [L^2(\mathcal{O}), (H_N^2(\mathcal{O}))^*]_\eta.$$

For any $s \in [0, D]$, using Lemma B.8, we can then estimate the integrand as follows, for any $\eta \in (0, 1)$,

$$\begin{aligned}
&\|P_{D-s,f} [(P_{\delta,0} - Id) \mathcal{L}_h(p_{s,f}(y, \cdot))]\|_{L^\infty} \\
&\lesssim \|(P_{\delta,0} - Id) \mathcal{L}_h(p_{s,f}(y, \cdot))\|_{(H_N^2)^*} \\
&\lesssim \sup_{\varphi \in H_N^2(\mathcal{O}): \|\varphi\|_{H^2} \leq 1} \left| \langle (P_{\delta,0} - Id) \mathcal{L}_h(p_{s,f}(y, \cdot)), \varphi \rangle_{L^2} \right|
\end{aligned}$$

$$\begin{aligned}
&\lesssim \sup_{\varphi \in H_N^2(\mathcal{O}): \|\varphi\|_{H^2} \leq 1} \left| \langle p_{s,f}(y, \cdot), \mathcal{L}_h(P_{\delta,0} - Id)\varphi \rangle_{L^2} \right| \\
&\lesssim \|p_{s,f}(y, \cdot)\|_{[H_N^2, L^2]_\eta} \sup_{\varphi \in H_N^2(\mathcal{O}): \|\varphi\|_{H^2} \leq 1} \|\mathcal{L}_h(P_{\delta,0} - Id)\varphi\|_{([H_N^2, L^2]_\eta)^*} \\
&\lesssim \|p_{s,f}(y, \cdot)\|_{H^2}^\eta \|p_{s,f}(y, \cdot)\|_{L^2}^{1-\eta} \sup_{\varphi \in H_N^2(\mathcal{O}): \|\varphi\|_{H^2} \leq 1} \|\mathcal{L}_h(P_{\delta,0} - Id)\varphi\|_{[L^2, (H_N^2)^*]_{1-\eta}},
\end{aligned}$$

the last step holding since $([L^2(\mathcal{O}), H_N^2(\mathcal{O})]_\eta)^* = [L^2(\mathcal{O}), (H_N^2(\mathcal{O}))^*]_{1-\eta}$ (see Theorem 6.2 in [48]). Then, using Lemma A.5 below, as well as the boundedness of $P_{\delta,0} - Id$ as an operator from $H_N^2(\mathcal{O})$ to itself, we see that

$$\begin{aligned}
\|\mathcal{L}_h(P_{\delta,0} - Id)\varphi\|_{([L^2, H_N^2]_\eta)^*} &\lesssim \|h\|_{C^1} \|(P_{\delta,0} - Id)\varphi\|_{[L^2, H_N^2]_{1-\eta}} \\
&\lesssim \|h\|_{C^1} \|(P_{\delta,0} - Id)\varphi\|_{L^2}^\eta \|(P_{\delta,0} - Id)\varphi\|_{H^2}^{1-\eta} \\
&\lesssim \|h\|_{C^1} \delta^\eta \|\varphi\|_{H^2}.
\end{aligned}$$

Now, we can choose $\eta > 0$ small enough, just as after (A.17), such that $\gamma(\eta) < 1$. Combining the preceding estimates, we obtain that

$$\|P_{D-s,f}[(P_{\delta,0} - Id)\mathcal{L}_h(p_{s,f}(y, \cdot))]\|_{L^\infty} \lesssim \|h\|_{C^1} \delta^\eta s^{-\gamma},$$

which is integrable on $s \in (0, D/2)$. Upon integration, we have $IV_b = O(\|h\|_{C^1} \delta^\eta) = o(\|h\|_{C^1})$, and the proof is complete. \square

LEMMA A.5. *Let $\eta \in [0, 1]$. Then, there exists some $C > 0$ such that for all $h \in C^1(\mathcal{O})$ and all $u \in H_N^2(\mathcal{O})$,*

$$\|\mathcal{L}_h u\|_{[L^2, (H_N^2)^*]_{1-\eta}} \leq C \|h\|_{C^1} \|u\|_{[H_N^2, L^2]_\eta}.$$

PROOF. Clearly, $\mathcal{L}_h : H_N^2(\mathcal{O}) \rightarrow L^2(\mathcal{O})$ is bounded and satisfies, for any $u \in H_N^2(\mathcal{O})$,

$$\|\mathcal{L}_h u\|_{L^2} = \|\nabla \cdot (h \nabla u)\|_{L^2} \lesssim \|h\|_{C^1} \|u\|_{H^2}.$$

Using a standard duality argument, we then obtain that for some $C > 0$, for any $u \in H_N^2(\mathcal{O})$,

$$\begin{aligned}
\|\mathcal{L}_h u\|_{(H_N^2)^*} &= \sup_{\varphi \in H_N^2(\mathcal{O}): \|\varphi\|_{H^2} \leq 1} \left| \int_{\mathcal{O}} \varphi(x) \mathcal{L}_h u(x) dx \right| \\
&= \sup_{\varphi \in H_N^2(\mathcal{O}): \|\varphi\|_{H^2} \leq 1} \left| \int_{\mathcal{O}} u(x) \mathcal{L}_h \varphi(x) dx \right| \\
&\leq C \sup_{\varphi \in L^2(\mathcal{O}): \|\varphi\|_{L^2} \leq 1} \left| \int_{\mathcal{O}} u(x) \varphi(x) dx \right| = C \|u\|_{L^2}.
\end{aligned}$$

Following the argument of the Theorem 5.1 in [48], we then see that for all $u \in H_N^2(\mathcal{O})$,

$$\|\mathcal{L}_h u\|_{[L^2, (H_N^2)^*]_\eta} \lesssim \|u\|_{[H_N^2, L^2]_\eta}.$$

But at the same time, by (A.18), we have that $[L^2(\mathcal{O}), (H_N^2(\mathcal{O}))^*]_\eta = [H_N^2(\mathcal{O}), L^2(\mathcal{O})]_{1-\eta}$, completing the proof. \square

APPENDIX B: AUXILIARY TECHNICAL RESULTS ON PARABOLIC EQUATIONS AND HEAT KERNELS

We review some basic definitions and facts about analytic semigroups, which constitute some crucial technical tools in the proofs of our main results.

B.1. Background on parabolic PDEs. A key idea underpinning the analysis to follow is to interpret a collection of transition operators $(P_t, t \geq 0)$ as an analytic semigroup generated by a so-called ‘sectorial’ operator \mathcal{L} . This allows to study the regularity properties of the solutions to abstract Cauchy problems of the form

$$(B.1) \quad \begin{cases} \partial_t u(t) = \mathcal{L}u(t) + g(t), & t \in (0, T), \\ u(0) = u_0. \end{cases}$$

Naturally, in our setting, the relevant operator is given by the infinitesimal generator \mathcal{L}_f of the diffusion process (1.3).

B.1.1. Sectorial operators and analytic semigroups. We follow the presentation in the monograph by Lunardi [49]. Let X be a complex Banach space, and suppose that $\mathcal{L} : \mathcal{D}(\mathcal{L}) \rightarrow X$ is a linear operator with domain $\mathcal{D}(\mathcal{L}) \subseteq X$, constituting a (not necessarily densely defined) subspace of X . Heuristically, \mathcal{L} is called a *sectorial operator* if its resolvent set $\rho(\mathcal{L}) \subseteq \mathbb{C}$ contains a ‘sector’, and if the resolvents $R(\lambda, \mathcal{L})$, $\lambda \in \rho(\mathcal{L})$, satisfy a certain decay. In particular, \mathcal{L} is sectorial if there exist constants $\omega \in \mathbb{R}$, $\theta \in (\pi/2, \pi)$, and $M > 0$ such that

$$\rho(\mathcal{L}) \supset S_{\theta, \omega} := \{\lambda \in \mathbb{C} : \lambda \neq \omega, |\arg(\lambda - \omega)| < \theta\},$$

and, denoting by $\|\cdot\|_{X \rightarrow X}$ the usual operator norm,

$$(B.2) \quad \|R(\lambda, \mathcal{L})\|_{X \rightarrow X} \leq \frac{M}{|\lambda - \omega|}, \quad \forall \lambda \in S_{\theta, \omega}.$$

It turns out that sectoriality is sufficient to that the operator exponentials $(e^{t\mathcal{L}}, t > 0)$ are well-defined via functional calculus. They then form the analytic semigroup

$$(P_t, t \geq 0), \quad P_t := e^{t\mathcal{L}},$$

in the sense that the map $t \mapsto P_t$ is analytic.

B.1.2. Characterisation of $\mathcal{D}(\mathcal{L})$ and interpolation spaces. The domain $\mathcal{D}(\mathcal{L})$ of the sectorial operator \mathcal{L} is naturally equipped with the graph norm

$$\|u\|_{\mathcal{D}(\mathcal{L})} := \|u\|_X + \|\mathcal{L}u\|_X, \quad u \in \mathcal{D}(\mathcal{L}).$$

Moreover, the behaviour of the map $t \mapsto e^{t\mathcal{L}}u$ at $t = 0$ characterises the domain $\mathcal{D}(\mathcal{L})$. Namely, it holds that $\lim_{t \rightarrow 0} (e^{t\mathcal{L}}u - u)/t$ exists (as a limit in X) and equals $\mathcal{L}u$ if and only if $u \in \mathcal{D}(\mathcal{L})$ and $\mathcal{L}u \in \overline{\mathcal{D}(\mathcal{L})}$. As an consequence, for every $u \in \mathcal{D}(\mathcal{L})$ with $\mathcal{L}u \in \overline{\mathcal{D}(\mathcal{L})}$, an alternative characterisation of the graph norm of u is

$$(B.3) \quad \|u\|_{\mathcal{D}(\mathcal{L})} \simeq \|u\|_X + \sup_{0 < t \leq 1} t^{-1} \|e^{t\mathcal{L}}u - u\|_X.$$

One can similarly define certain interpolation spaces \mathcal{D}_α , for $\alpha \in (0, 1)$, between X and $\mathcal{D}(\mathcal{L})$, which are of importance in the proofs. Specifically, set

$$(B.4) \quad \mathcal{D}_\alpha := \left\{ u \in X : \sup_{t \in (0, 1]} t^{-\alpha} \|e^{t\mathcal{L}}u - u\|_X < \infty \right\},$$

which is equipped with norm

$$(B.5) \quad \|u\|_{\mathcal{D}_\alpha} := \|u\|_X + \sup_{t \in (0, 1]} t^{-\alpha} \|e^{t\mathcal{L}}u - u\|_X.$$

We refer to Section 2.2.1 and Proposition 2.2.4 in [49] for further details on the interpretation of these spaces – note that our spaces \mathcal{D}_α correspond to the spaces $D_{\mathcal{L}}(\alpha) = (X, \mathcal{D}(\mathcal{L}))_\alpha$ from [49]. The above interpolation can be defined for instance via the ‘K-method’; see the display (1.2.4) in [49].

B.1.3. *The case $\mathcal{L} = \mathcal{L}_f$.* For our purposes, the relevant instance is the transition semi-group $(P_{t,f}, t \geq 0)$ of the reflected diffusion process (1.3), with associated (elliptic) infinitesimal generator $\mathcal{L}_f[\cdot] = \nabla \cdot (f \nabla[\cdot])$ equipped with zero Neumann boundary conditions. Two different realisations of the operator \mathcal{L}_f will play a role, firstly viewed as an operator on the Hilbert space $X = L^2(\mathcal{O})$ with domain

$$H_N^2(\bar{\mathcal{O}}) = \{u \in H^2(\mathcal{O}) : \partial_\nu u = 0 \text{ on } \partial\mathcal{O}\},$$

and secondly as an operator on the Banach space $X = C(\bar{\mathcal{O}})$ with domain $C_N^2(\bar{\mathcal{O}})$ defined similarly to $H_N^2(\mathcal{O})$. It is well-known that \mathcal{L}_f forms a sectorial operator on both spaces. Indeed, on $L^2(\mathcal{O})$, this follows from Theorems 3.1.2 and 3.1.3 in [49], where the main tool for the verification of the resolvent bounds (B.2) are the a-priori estimates by Agmon-Douglis-Nirenberg [2]. On $C(\bar{\mathcal{O}})$, similar resolvent bounds can be verified; see Section 3.1.5, and especially Corollary 3.1.24 (ii), in [49]. We also note that the zero Neumann boundary conditions imposed here satisfy the non-tangentiality condition (3.1.3) in [49], since

$$\inf_{x \in \partial\mathcal{O}} \left| \sum_{i=1}^n \nu_i^2(x) \right| = \inf_{x \in \partial\mathcal{O}} |\nu(x)| = 1 > 0.$$

The equations (B.3) and (B.5) then directly yield useful characterisations of Sobolev- and Hölder-type norms in terms of the behaviour of $P_{t,f}u - u$, which we use throughout. Specifically, we note that for any $u \in H_N^2(\mathcal{O})$, $f \in \mathcal{F}$ and $\alpha \in [0, 1]$, it holds that

$$(B.6) \quad \|P_{t,f}u - u\|_{L^2} \lesssim t^\alpha \|u\|_{H^{2\alpha}}, \quad t \in (0, 1).$$

Similarly, for $u \in C_N^2(\mathcal{O})$,

$$(B.7) \quad \|P_{t,f}u - u\|_{L^\infty} \lesssim t \|u\|_{C^2}, \quad t \in (0, 1).$$

B.1.4. *Regularity estimates for parabolic PDEs.* We now provide an overview on some key regularity results for the parabolic PDE (B.1). A variety of notions of solutions to such equations exists in the literature. Since, via the regularisation argument developed in Section A, we only need to consider a sequence of parabolic PDEs with regularised initial conditions, the strongest of these notions will suffice for our purposes: thus, when we speak of a solution to the Cauchy problem (B.1), we mean a *strict solution* in the sense that for all $t \in [0, T]$, $\partial_t u(t) = \mathcal{L}u(t) + g(t)$ and $u(0) = u_0$.

When $g : [0, T] \rightarrow X$ is continuous, one then shows that any (strict) solution to (B.1) must necessarily be given by the variation-of-constants formula

$$u(t) = e^{t\mathcal{L}}u_0(t) + \int_0^t e^{(t-s)\mathcal{L}}g(s)ds, \quad 0 \leq t \leq T,$$

where the integral on the right hand side is in the Bochner sense; see Proposition 4.1.2 in [49]. For our purposes, this property is always fulfilled.

Turning to the regularity of the solutions to the Cauchy problem (B.1), the following (scales of) function spaces are needed: firstly, for $\alpha \in (0, 1)$, let $C^\alpha([0, T]; X)$ be the set of α -Hölder continuous functions from $[0, T]$ to X . Secondly, we introduce spaces that allow for certain singularities at $t = 0$ – this is central for the proofs in Section A, as it enables to derive regularity estimates that are uniform with respect to the regularisation parameter introduced there. For $0 < \alpha < 1$ and $\beta > 0$, set

$$C_\beta^\alpha((0, T]; X) := \bigcap_{0 < \varepsilon \leq T} C^\alpha([\varepsilon, T]; X) \cap \left\{ u : \sup_{0 < t \leq T} t^{\beta-\alpha} \|u(t)\|_X < \infty \right\} \\ \cap \left\{ u : \sup_{0 < \varepsilon < T} \varepsilon^\beta \|u\|_{C^\alpha([\varepsilon, T], X)} < \infty \right\}.$$

The following result is deduced from Theorem 4.3.1 (iii) and Theorem 4.3.7 in [49]. Since we shall only deal with the case $u_0 = 0$, let

$$(B.8) \quad u(t) = \int_0^t e^{(t-s)\mathcal{L}} g(s) ds.$$

THEOREM B.1. (i) Suppose that $g \in C^\alpha([0, T]; X)$ for some $\alpha \in (0, 1)$, and let $g(0) \in \mathcal{D}(\mathcal{L})$. Then, u in (B.8) constitutes a strict solution to the Cauchy problem (B.1). Furthermore, $u \in C^\alpha([0, T]; \mathcal{D}(\mathcal{L})) \cap C^{1+\alpha}([0, T]; X)$.

(ii) Suppose additionally that $g \in C_{\alpha+\mu}^\alpha((0, T]; X)$ for some $\alpha, \mu \in (0, 1)$. Then, there exists $C > 0$ (independent of g) such that

$$\|u\|_{C_{\alpha+\mu}^\alpha((0, T]; \mathcal{D}(\mathcal{L}))} + \|\partial_t u\|_{C_{\alpha+\mu}^\alpha((0, T]; X)} \leq C \|g\|_{C_{\alpha+\mu}^\alpha((0, T]; X)}.$$

B.2. Estimates for elliptic second order differential operators. The proofs in Section A also require a number of estimates for the solutions of elliptic PDEs, both in L^2 -type norms and in uniform norms. We begin providing the estimates for the former. The first result is a basic lemma concerning the equivalence of the graph norm of \mathcal{L}_f , for f belonging to the parameter space \mathcal{F} from (2.1), and the $H^2(\mathcal{O})$ -norm.

LEMMA B.2. Let $R > 0$. There exists a constant $C > 0$ only depending on f_{\min} , R and \mathcal{O} such that for all $f \in \mathcal{F}$ with $\|f\|_{C^1} \leq R$, and all $u \in H_N^2(\mathcal{O})$,

$$C^{-1} \|u\|_{H^2} \leq \|u\|_{L^2} + \|\mathcal{L}_f u\|_{L^2} \leq C \|u\|_{H^2}.$$

PROOF. To prove the second inequality, we estimate

$$\|\mathcal{L}_f u\|_{L^2} = \|f \Delta u + \nabla f \cdot \nabla u\|_{L^2} \lesssim \|f\|_{L^\infty} \|\Delta u\|_{L^2} + \|f\|_{C^1} \|\nabla u\|_{L^2} \lesssim R \|u\|_{H^2}.$$

Thus, it remains to show the first inequality. For that, it suffices to prove that $\|\Delta u\|_{L^2} \leq C(\|u\|_{L^2} + \|\mathcal{L}_f u\|_{L^2})$ for some $C > 0$ only depending on f_{\min} , R and \mathcal{O} . To this end, we use the definition of \mathcal{L}_f , the interpolation inequality

$$\|\nabla u\|_{L^2} \lesssim \|u\|_{L^2}^{1/2} \|u\|_{H^2}^{1/2} \lesssim \|u\|_{L^2} + \|u\|_{L^2}^{1/2} \|\Delta u\|_{L^2}^{1/2},$$

as well as Cauchy's inequality with $\varepsilon > 0$, to obtain that for some universal constants $c, c' > 0$, and for $\varepsilon \in (0, 1]$,

$$(B.9) \quad \begin{aligned} \|\Delta u\|_{L^2} &= \|f^{-1}(\mathcal{L}_f u - \nabla f \cdot \nabla u)\|_{L^2} \\ &\leq f_{\min}^{-1} \|\mathcal{L}_f u\|_{L^2} + f_{\min}^{-1} \|\nabla f \cdot \nabla u\|_{L^2} \\ &\leq f_{\min}^{-1} \|\mathcal{L}_f u\|_{L^2} + c f_{\min}^{-1} \|f\|_{C^1} (\|u\|_{L^2} + \|u\|_{L^2}^{1/2} \|\Delta u\|_{L^2}^{1/2}) \\ &\leq f_{\min}^{-1} \|\mathcal{L}_f u\|_{L^2} + c' f_{\min}^{-1} \|f\|_{C^1} \left(\frac{\|u\|_{L^2}}{2\varepsilon} + \frac{\varepsilon \|\Delta u\|_{L^2}}{2} \right). \end{aligned}$$

Now, choosing $\varepsilon > 0$ small enough and subtracting the term containing Δu on the right hand side, we obtain that for some $C > 0$ only depending on f_{\min} , R and \mathcal{O} ,

$$\frac{1}{2} \|\Delta u\|_{L^2} \leq C (\|\mathcal{L}_f u\|_{L^2} + \|u\|_{L^2}),$$

as desired. This concludes the proof of the lemma. \square

Next, we study the analogous mapping properties of \mathcal{L}_f with respect to the Hölder spaces $C^{2+\eta}(\mathcal{O})$ and $C^\eta(\mathcal{O})$ for $\eta \in (0, 1)$. Define

$$C_N^{2+\eta}(\mathcal{O}) := \{u \in C^{2+\eta}(\mathcal{O}) : \partial_\nu u = 0 \text{ on } \partial\mathcal{O}\}.$$

LEMMA B.3. *Suppose that $f \in \mathcal{F}$. For any $\eta \in (0, 1)$, there exists $C > 0$ only depending on $\|f\|_{C^{1+\eta}}$, f_{\min} and \mathcal{O} such that for all $u \in C_N^{2+\eta}(\mathcal{O})$,*

$$C^{-1}\|u\|_{C^{2+\eta}} \leq \|u\|_{C^\eta} + \|\mathcal{L}_f u\|_{C^\eta} \leq C\|u\|_{C^{2+\eta}}.$$

PROOF. Throughout, we will use the fact that for $\eta \in (0, 1)$, the spaces $C^\eta(\mathcal{O})$ and $C^{2+\eta}(\mathcal{O})$ equal the Hölder-Zygmund spaces $\mathcal{C}^\eta(\mathcal{O})$ and $\mathcal{C}^{2+\eta}(\mathcal{O})$, with equivalent norms (see e.g. [74] for definitions). For these, we have the classical multiplication inequalities

$$\|uv\|_{C^\alpha} \lesssim \|u\|_{C^\alpha} \|v\|_{C^\alpha}, \quad u, v \in C^\alpha(\mathcal{O}), \quad \alpha \geq 0.$$

The second inequality in the statement of the lemma then follows from the estimate

$$\begin{aligned} \|\mathcal{L}_f u\|_{C^\eta} &= \|f\Delta u + \nabla f \cdot \nabla u\|_{C^\eta} \\ &\lesssim \|f\|_{C^\eta} \|\Delta u\|_{C^{2+\eta}} + \|f\|_{C^{1+\eta}} \|\nabla u\|_{C^{1+\eta}} \lesssim \|f\|_{C^{1+\eta}} \|u\|_{C^{2+\eta}}. \end{aligned}$$

For the first inequality, we use the fact that the Laplace operator establishes (jointly with the trace operator $\text{Tr}[\cdot]$) a topological isomorphism

$$u \mapsto (\Delta u, \text{Tr}[u]), \quad (\Delta, \text{Tr}) : C_N^{\alpha+2}(\mathcal{O}) \rightarrow C^\alpha(\mathcal{O}) \times C^{\alpha+2}(\partial\mathcal{O}),$$

for any $\alpha \geq 0$; see, for instance, Theorem 4.3.4 in [74] or also display (5.6) in [57]. Moreover, we note that by the chain rule, for any $f \in \mathcal{F}$, since $f \geq f_{\min}$, it holds that

$$\|f^{-1}\|_{C^1} \lesssim \|f\|_{C^1},$$

where the multiplicative constant only depends on f_{\min} . Using this, we obtain

$$\begin{aligned} \|u\|_{C^{2+\eta}} &\lesssim \|\Delta u\|_{C^\eta} + \|u\|_{C^\eta} \\ &= \|f^{-1}(\mathcal{L}_f u - \nabla f \cdot \nabla u)\|_{C^\eta} + \|u\|_{C^\eta} \\ &\lesssim \|f^{-1}\|_{C^1} (\|\mathcal{L}_f u\|_{C^\eta} + \|f\|_{C^{1+\eta}} \|u\|_{C^{1+\eta}}) + \|u\|_{C^\eta} \\ &\lesssim \|f\|_{C^1} \|\mathcal{L}_f u\|_{C^\eta} + \|f\|_{C^1} \|f\|_{C^{1+\eta}} \|u\|_{C^\eta}^{1/2} \|u\|_{C^{2+\eta}}^{1/2} + \|u\|_{C^\eta} \\ &\leq \|f\|_{C^1} \|\mathcal{L}_f u\|_{C^\eta} + \|f\|_{C^1} \|f\|_{C^{1+\eta}} \left(\frac{1}{2\varepsilon} \|u\|_{C^\eta} + \frac{\varepsilon}{2} \|u\|_{C^{2+\eta}} \right) + \|u\|_{C^\eta}, \end{aligned}$$

for any $\varepsilon > 0$, where we used in the last step that $ab \leq a^2/(2\varepsilon) + \varepsilon b^2/2$ for any $a, b \in \mathbb{R}$. Thus, choosing $\varepsilon > 0$ large enough (only depending on f_{\min} , $\|f\|_{C^{1+\eta}}$ and \mathcal{O}) and subsequently subtracting the term in the right hand side containing $\|u\|_{C^{2+\eta}}$, we have proved as desired that

$$\|u\|_{C^{2+\eta}} \lesssim \|\mathcal{L}_f u\|_{C^\eta} + \|u\|_{C^\eta}.$$

□

Next, we state and prove the following lemma which entails that the constants in Weyl's asymptotics for the eigenvalues of \mathcal{L}_f can be controlled by terms that only depends on upper and lower bounds for the conductivity function f .

LEMMA B.4. *There exists a constant $C > 0$ only depending f_{\min} , $\|f\|_{L^\infty}$ and \mathcal{O} such that the eigenvalues $(\lambda_{f,j}, j \geq 0)$ of the operator $-\mathcal{L}_f$ with domain $\mathcal{D}(\mathcal{L}_f) = H_N^2(\mathcal{O})$, ordered increasingly, satisfy*

$$C^{-1}j^{2/d} \leq \lambda_{f,j} \leq Cj^{2/d}.$$

PROOF. Let the action of the quadratic form associated to $-\mathcal{L}_f$ on functions $u \in H^1(\mathcal{O})$ be denoted by

$$Q_f(u) = -\langle u, \mathcal{L}_f u \rangle = \int_{\mathcal{O}} f(x) |\nabla u(x)|^2 dx.$$

For any finite-dimensional subspace $L \subseteq \mathcal{D}(\mathcal{L}_f)$, define

$$\lambda_{f,j}(L) := \sup_{u \in L: \|u\|_{L^2} \leq 1} Q_f(u).$$

We use the standard ‘minimax’ characterisation of the eigenvalues via minimising the above quantity over all subspaces of dimension j :

$$\lambda_{f,j} = \inf_{L \subseteq \mathcal{D}(\mathcal{L}_f): \dim(L)=j} \lambda_{f,j}(L).$$

Now let us denote the eigenvalues of the Neumann-Laplace operator $-\Delta = \mathcal{L}_1$ by $\lambda_j = \lambda_{1,j}$, with associated quadratic form $Q_{\Delta}(u) = \int_{\mathcal{O}} |u(x)|^2 dx$. Using Weyl’s law, it holds that for some constant $c \equiv c(\mathcal{O}) \geq 1$, we have $\lambda_j \in [c^{-1}j^{2/d}, cj^{2/d}]$. It then follows immediately from the above ‘variational’ characterisation of the eigenvalues that there is a further constant $c' \equiv c'(f_{\min}, \|f\|_{L^\infty}) > 0$ for which

$$\lambda_{f,j} \in [(c')^{-1}\lambda_j, c'\lambda_j] = [C^{-1}j^{2/d}, Cj^{2/d}],$$

with $C \equiv C(f_{\min}, \|f\|_{L^\infty}, \mathcal{O}) > 0$, concluding the proof. \square

We conclude this section with a lemma on the growth of Sobolev- and Hölder norms of the eigenfunctions $e_{f,j}$, which follow straightforwardly from the previous lemmas in this section.

LEMMA B.5. *Let $d \leq 3$, $R > 0$ and $\eta \in (0, 1)$. There exists a constant $C > 0$ only depending on f_{\min} , R , \mathcal{O} and η such that the following holds true.*

i) *For all $f \in \mathcal{F}$ with $\|f\|_{C^1} \leq R$ and all $j \geq 0$, $\|e_{f,j}\|_{H^2} \leq C(1 + j^{2/d})$.*

ii) *For all $f \in \mathcal{F}$ with $\|f\|_{C^{1+\eta}} \leq R$ and all $j \geq 0$, $\|e_{f,j}\|_{C^{2+\eta}} \leq C(1 + j^{5/d})$.*

PROOF. Part i) follows from an application of Lemma B.2 and B.4, which together imply

$$\|e_{f,j}\|_{H^2} \simeq \|e_{f,j}\|_{L^2} + \|\mathcal{L}_f e_{f,j}\|_{L^2} \lesssim 1 + j^{2/d}.$$

Note that the implicit constants, by Lemmas B.2 and B.4, only depend on the relevant quantities in the statement.

To prove part ii), we use Lemma B.3, the classical interpolation inequality for Hölder spaces (see, e.g., Corollary 1.2.19 from [49]), the Sobolev embedding, Lemma B.4 as well as the first part of this lemma, to estimate

$$\begin{aligned} \|e_{f,j}\|_{C^{2+\eta}} &\simeq \|e_{f,j}\|_{C^\eta} + \|\mathcal{L}_f e_{f,j}\|_{C^\eta} \\ &\lesssim (1 + \lambda_{f,j}) \|e_{f,j}\|_{C^\eta} \\ (B.10) \quad &\lesssim (1 + \lambda_{f,j}) \|e_{f,j}\|_{L^\infty}^{2/(2+\eta)} \|e_{f,j}\|_{C^{2+\eta}}^{\eta/(2+\eta)} \\ &\lesssim (1 + j^{2/d}) \|e_{f,j}\|_{H^2}^{2/(2+\eta)} \|e_{f,j}\|_{C^{2+\eta}}^{\eta/(2+\eta)} \\ &\lesssim (1 + j^{2/d})^{1+2/(2+\eta)} \|e_{f,j}\|_{C^{2+\eta}}^{\eta/(2+\eta)}. \end{aligned}$$

The statement follows from dividing both sides by $\|e_{f,j}\|_{C^{2+\eta}}^{\eta/(2+\eta)}$ and noting that $\eta < 1$. \square

B.3. Estimates for the Neumann heat kernel. We now turn to deriving estimates for the Neumann heat kernels $p_{t,f}$. Again, we start with L^2 -type bounds.

LEMMA B.6. *Let $p_{t,f}$ denote the heat kernel (i.e. the transition density function) of the reflected diffusion process (1.3). For all $f \in \mathcal{F}$, there exists a constant $C > 0$ only depending on f_{\min} , $\|f\|_{L^\infty}$ and \mathcal{O} , such that*

$$\sup_{y \in \mathcal{O}} \|p_{t,f}(\cdot, y)\|_{L^2} \leq Ct^{-d/4}, \quad t > 0.$$

Moreover, for $d \leq 3$ we also have that for some constant $C \equiv C(\mathcal{O}) > 0$,

$$\sup_{y \in \mathcal{O}} \|p_{t,f}(\cdot, y)\|_{H^2} \leq Ct^{-d/2-2}, \quad t > 0.$$

In particular, the heat kernel φ_δ of the reflected standard Brownian motion on \mathcal{O} (corresponding to the case $f = 1$) satisfies

$$\sup_{y \in \mathcal{O}} \|\varphi_\delta(\cdot, y)\|_{L^2} \leq C\delta^{-d/4}, \quad \delta > 0.$$

PROOF. We first note that by the classical Gaussian estimates for the Neumann heat kernel (e.g. [25])

$$p_{t,f}(x, y) \leq Ct^{-d/2} \exp\left(-\frac{\|x-y\|^2}{Ct}\right),$$

for some C only depending on f_{\min} and $\|f\|_{L^\infty}$. Then,

$$\begin{aligned} \|p_{t,f}(\cdot, y)\|_{L^2}^2 &\lesssim \int_{\mathcal{O}} t^{-d} \exp\left(-\frac{2\|x-y\|^2}{Ct}\right) dx \\ &\leq t^{-d/2} \int_{\mathcal{O}} t^{-d/2} \exp\left(-\frac{2\|x-y\|^2}{Ct}\right) dx \lesssim t^{-d/2}, \end{aligned}$$

proving the first claim. For the estimate in $H^2(\mathcal{O})$, assume that $d \leq 3$. Using the spectral decomposition

$$p_{t,f}(x, y) = \sum_{j=0}^{\infty} e^{-\lambda_{f,j}t} e_{f,j}(x) e_{f,j}(y), \quad t > 0, \quad x, y \in \mathcal{O},$$

Then, using the Sobolev embedding and Lemmas B.4 and B.5, it follows that for some $c > 0$,

$$\begin{aligned} \|p_{t,f}(\cdot, y)\|_{H^2} &\leq \sum_{j=0}^{\infty} e^{-\lambda_{f,j}t} \|e_{f,j}\|_{H^2} |e_{f,j}(y)| \\ &\lesssim \sum_{j=0}^{\infty} e^{-cj^{-2/d}t} \|e_{f,j}\|_{H^2}^2 \simeq \sum_{j=0}^{\infty} e^{-cj^{-2/d}t} (1 + j^{4/d}), \end{aligned}$$

which is further upper bounded by

$$\begin{aligned} \int_0^\infty e^{-cj^{2/d}t} (1 + j^{4/d}) dj &= \int_0^\infty e^{-cx^2} (1 + x^d t^{-d/2})^{4/d} x^{d-1} t^{-d/2} dx \\ &\lesssim t^{-d/2} + t^{-d/2-2}, \end{aligned}$$

which proves the second claim. \square

Next, we derive the following uniform estimate.

LEMMA B.7. *Let $\eta \in (0, 1)$, $D > 0$ and $R > 0$. Then, there exists $C \equiv C(D, R, f_{\min}) > 0$ such that for every $f \in \mathcal{F}$ with $\|f\|_{C^{1+\eta}} \leq R$ and for every $y \in \mathcal{O}$,*

$$\|p_{D,f}(\cdot, y)\|_{C^{2+\eta}} \leq C.$$

PROOF. Let us fix $y \in \mathcal{O}$ and f as in the statement. Recall the notation $u_f(D) = p_{D,f}(\cdot, y)$. Then, using the spectral decomposition, the preceding estimates as well as Lemmas B.4 and B.5, we see that for some constants $c, C > 0$ (only depending on D, R, f_{\min}, η and \mathcal{O})

$$\begin{aligned} \|u_f(D)\|_{C^{2+\eta}} &\leq \sup_{y \in \mathcal{O}} \sum_{j=0}^{\infty} e^{-D\lambda_{f,j}} \|e_{f,j}\|_{C^{2+\eta}} |e_{f,j}(y)| \\ &\leq \sum_{j=0}^{\infty} e^{-D\lambda_{f,j}} \|e_{f,j}\|_{C^{2+\eta}} \|e_{f,j}\|_{L^\infty} \\ &\lesssim \sum_{j=0}^{\infty} e^{-D\lambda_{f,j}} \|e_{f,j}\|_{C^{2+\eta}} \|e_{f,j}\|_{H^2} \lesssim \sum_{j=0}^{\infty} e^{-cDj^{2/d}} (1 + j^{5/d})(1 + j^{2/d}) \lesssim C. \end{aligned}$$

□

Alongside the above upper bounds, we record the following lower bound for the Neumann heat kernel, holding uniformly over balls of Hölder spaces – see Proposition 4 in [53]. In particular, if $\|f\|_{C^\alpha} \leq B$ for some even integer $\alpha > d/2 - 1$ and some $B > 0$, then for every $t > 0$

$$\inf_{x, y \in \mathcal{O}} p_{t,f}(x, y) \geq C,$$

for a constant $C \equiv C(t, \mathcal{O}, d, f_{\min}, B, \alpha) > 0$.

Finally, we conclude with a uniform estimate for the action of the transition operator $P_{t,f}$ over functions in $L^2(\mathcal{O})$.

LEMMA B.8. *Suppose that $d \leq 3$. Then, for any $D_0 > 0$ and $R > 0$ there exist constants $C, C' > 0$ only depending on D_0, R, f_{\min} , and \mathcal{O} such that for all $t \geq D_0$ and all $f \in \mathcal{F}$ with $\|f\|_{C^1} \leq R$, $P_t : L^2(\mathcal{O}) \rightarrow L^\infty(\mathcal{O})$ is a bounded linear operator satisfying*

$$(B.11) \quad \|P_{t,f}\varphi\|_{L^\infty} \leq C \|P_{t,f}\varphi\|_{H^2} \leq C' \|\varphi\|_{(H_N^2)^*}, \quad \forall \varphi \in L^2(\mathcal{O}).$$

PROOF. The first inequality is simply an application of the Sobolev embedding. To prove the second, we first note that $P_{t,f} : L^2(\mathcal{O}) \rightarrow \mathcal{D}(\mathcal{L}_f) = H_N^2(\mathcal{O})$ is linear and bounded, with operator norm only depending on D_0, R, f_{\min} , and \mathcal{O} . This is seen by applying the previous lemmas in this section, and by using Parseval's identity (twice), to the effect that

$$\begin{aligned} \|P_{t,f}\varphi\|_{H^2}^2 &\simeq \|P_{t,f}\varphi\|_{L^2}^2 + \|\mathcal{L}_f P_{t,f}\varphi\|_{L^2}^2 \\ &\leq \|\varphi\|_{L^2}^2 + \sum_{j=0}^{\infty} |\langle e_{f,j}, \varphi \rangle_{L^2}|^2 \lambda_{f,j}^2 e^{-2t\lambda_{f,j}} \lesssim \|\varphi\|_{L^2}^2. \end{aligned}$$

Now, applying this twice with $t/2$ (which is still lower bounded by $D_0/2$) instead of t , and using the self-adjointness of $P_{f,t/2}$, we obtain that

$$\begin{aligned}
\|P_{t,f}\varphi\|_{H^2} &\leq \|P_{f,t/2}\varphi\|_{L^2} \\
&= \sup_{\phi \in L^2(\mathcal{O}): \|\phi\|_{L^2} \leq 1} \left| \int_{\mathcal{O}} \phi(x) P_{f,t/2}\varphi(x) dx \right| \\
&= \sup_{\phi \in L^2(\mathcal{O}): \|\phi\|_{L^2} \leq 1} \left| \int_{\mathcal{O}} \varphi(x) P_{f,t/2}\phi(x) dx \right| \\
&\lesssim \sup_{\phi \in H_N^2(\mathcal{O}): \|\phi\|_{H^2} \leq 1} \left| \int_{\mathcal{O}} \phi(x)\varphi(x) dx \right| = \|\varphi\|_{(H_N^2)^*}.
\end{aligned}$$

□

APPENDIX C: FURTHER NUMERICAL RESULTS

In this appendix we provide additional simulation studies and expand the investigation of the numerical results presented in Sections 4.

C.1. Initialisation of the algorithms. The choice of the starting points for iterative schemes such as the ones considered in the present article, cf. (3.8), (3.11) and (3.13), is known to be a delicate issue that, in high-dimensional and non-convex settings, may have a profound impact on the overall recovery performance; see e.g. [11], where a discussion and further references can be found. To investigate the influence of the initialisation on the employed pCN algorithm, ULA and gradient descent method, we performed a set of numerical experiments based on the same synthetic data set $X^{(n)}$, with $n = 50000$, and the same Gaussian prior $\Pi(\cdot)$ used in Section 4, each consisting in a run of the three schemes with a differently specified starting point ϑ_0 . In particular, alongside the cold start $\vartheta_0 = 0$ under which the results in Sections 4 were obtained, we considered the ‘warm start’ $\vartheta_0 = \theta_0$, where $\theta_0 \in \mathbb{R}^{K+1}$ is the vector of Fourier coefficients of the true (reparametrised) conductivity function F_0 , the ‘random start’ $\vartheta_0 \sim \Pi(\cdot)$, and the ‘challenging start’ $\vartheta_0 = -\theta_0$. The results are summarised in the comparative Tables 2 - 4, with each row corresponding to a different starting point.

C.1.1. Initialisation of sampling-based methods. As revealed by Tables 2 and 3 respectively, the performances of the pCN algorithm and the ULA were only slightly impacted in our numerical experiments by the choice of the initialiser, in terms of both the magnitude of the estimation error associated to the resulting posterior mean estimates, and the number of iterations required by the generated chains to move from the starting points to the regions containing higher posterior probability. Indeed, the same burnin times were deemed adequate across the runs of each method (except for the ones with warm start, for which no burnin was necessary).

C.1.2. Initialisation of gradient descent and the implications of multimodality. A significantly stronger dependence on the initialisation step was instead observed for the computation of the MAP estimator via the gradient descent method. As reported in Table 4, the runs with cold and random starts (first and third row) required a similar number of iterations to converge (according to the criterion established in Section 4.5), and resulted in comparable estimation errors, which are both larger than the ones attained by the posterior mean estimates corresponding to the same initialisation. On the other hand, for the warm start (second

TABLE 2
Performance of the pCN algorithm under different starting points

pCN	$\ell_n(f_{\vartheta_0})$	n. iterations	burnin	stepsize	acceptance ratio	$\ F_0 - \bar{F}_n\ _2$
$\vartheta_0 = 0$	4254.7336	25000	2500	.0001	29.53%	.2097
$\vartheta_0 = \theta_0$	7707.9226	25000	0	.0001	29.49%	.1812
$\vartheta_0 \sim \Pi(\cdot)$	809.0839	25000	2500	.0001	30.76%	.1995
$\vartheta_0 = -\theta_0$	-11193.9608	25000	2500	.0001	32.01%	.2094

TABLE 3
Performance of the ULA under different starting points

ULA	$\log \pi(\vartheta_0 X^{(n)})$	n. iterations	burnin	stepsize	$\ F_0 - \bar{F}_n\ _2$
$\vartheta_0 = 0$	425.4734	10000	250	.000025	.2033
$\vartheta_0 = \theta_0$	7702.2889	10000	0	.000025	.2024
$\vartheta_0 \sim \Pi(\cdot)$	806.9926	10000	250	.000025	.2035
$\vartheta_0 = -\theta_0$	-11199.5945	10000	250	.000025	.2056

TABLE 4
Performance of the gradient descent method under different starting points

MAP	$\log \pi(\vartheta_0 X^{(n)})$	n. iterations	stepsize	$\ F_0 - \hat{F}_n\ _2$
$\vartheta_0 = 0$	425.4734	135	.00001	.2507
$\vartheta_0 = \theta_0$	7702.2889	35	.00001	.0912
$\vartheta_0 \sim \Pi(\cdot)$	2856.6789	140	.00001	.2852
$\vartheta_0 = -\theta_0$	-11199.5945	372	.00001	.5928

row), a greatly reduced number of iterations were sufficient, and the obtained estimation error is by a wide margin the lowest across all the methods and all the experiments (and in fact it is close to the lower bound given by the approximation error from projecting the ground truth on the linear space spanned by the employed basis functions, which is equal to .08477). Finally, the challenging start $\vartheta_0 = -\theta_0$ (fourth row) was observed to produce the opposite effect, heavily slowing down the convergence of the scheme and yielding a sharp deterioration in the reconstruction quality.

The observed influence of the initialisation in this context furnishes a strong indication that the posterior distribution is multimodal, whence different starting points imply the convergence of the gradient descent method to a potentially different local optimum. The numerical results for the (computationally more intensive) pCN algorithm and the ULA are then aligned with the heuristics that sampling-based methods may generally be more robust in non-convex settings. These observations will be further corroborated by an examination of the one-dimensional marginal posterior distributions in Appendix C.2 below.

C.2. One-dimensional marginal posterior distributions. Figure 7 (left column) shows the trace-plots ($\vartheta_{m,k}$, $m = 0, 1, \dots, M$), with $M = 25000$, for some representative individual components (specifically, for $k = 2, 6, 14, 15, 16$) of the approximate posterior samples obtained via the pCN algorithm in the context of the simulation study discussed in Appendix C.1 above, based on low-frequency observations $X^{(n)}$ with $n = 50000$. Trace-plots of different colours corresponds to the four different considered starting points. For the cold start $\vartheta_0 = 0$ (marked in blue), under which the results in Section 4.3 were obtained, the associated Monte Carlo approximations (after the burnin) to the marginal posterior probability density functions of $\theta_k|X^{(n)}$, where $\theta_k = \langle F, e_k \rangle_{L^2}$, are shown in the right column, alongside the

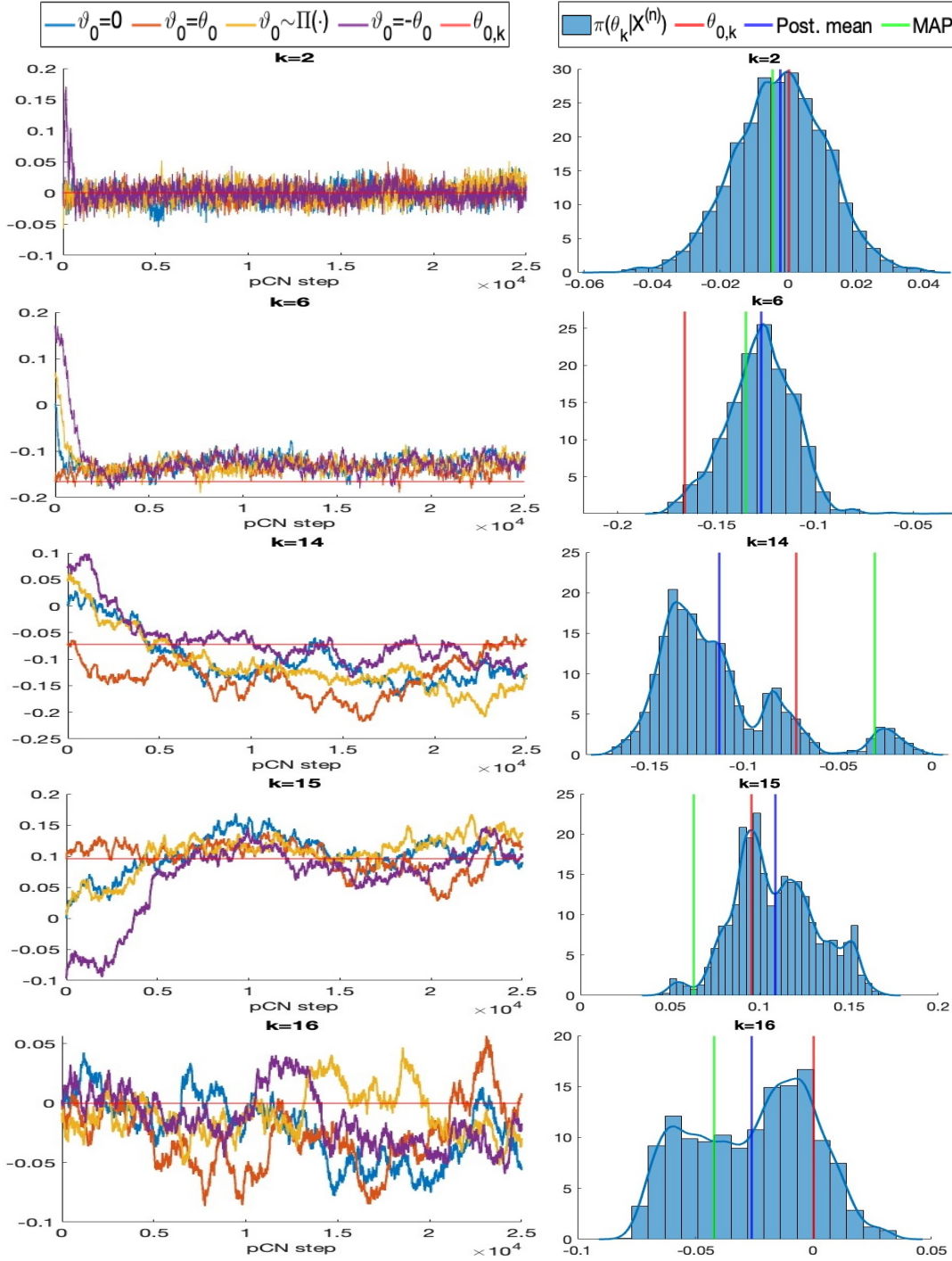


FIG 7. Left column: trace-plots for some individual components of 25000 approximate samples from the posterior distribution of $\theta|X^{(n)}$ obtained via the pCN algorithm with different starting points. Right column: resulting approximations to the marginal posterior probability density functions.

value of the corresponding true Fourier coefficients $\theta_{0,k}$ (vertical red lines) and the approximate posterior mean estimates $\bar{\vartheta}_{M,k}$ (vertical blue lines). The corresponding components of the MAP estimates calculated in Section 4.5 via the gradient descent algorithm are also reported (vertical green lines).

C.2.1. Unimodality and Gaussian approximations for the lower frequencies. An inspection of the plots showcases some interesting features for the statistical task at hand: in particular, for the lower frequencies, including for the first two displayed cases $k = 2$ and $k = 6$, the obtained marginal posterior distributions of the Fourier coefficients appear to be unimodal and approximately of Gaussian shape. This lead to a substantial agreement between the posterior mean and the MAP estimates.

We also note that the marginal posterior distribution of $\theta_6|X^{(n)}$ displays a visible shrinkage towards the origin, which arises from the regularisation induced by the employed Gaussian prior. Such remaining finite sample effects are a possible indication of the potential severely ill-posedness of the problem and the resulting logarithmic rate of convergence, cf. [53].

C.2.2. Multimodality for the higher frequencies. For the higher frequencies (corresponding to the cases $k = 13, 14, 15$ in Figure 7), the marginal posterior distributions instead exhibit multiple local modes, as may be expected from the nonlinearity of the likelihood. In turn, this can be seen to impact the performance of the MAP estimators for which, through the gradient descent algorithm, we can generally only compute local optimisers. In line with the results in Appendix C.1, the sampling-based posterior mean estimators appear to be overall more robust to such non-convex settings.

A comparison of the shapes of the obtained marginal posterior distributions for the lower and higher frequencies further raises the question of the validity, in the considered statistical model, of the ‘Bernstein-von Mises’ phenomenon and of a global Gaussian limit for the posterior distribution $\Pi(\cdot|X^{(n)})$ as $n \rightarrow \infty$. In related parameter identification problems for the conductivity function in steady-state elliptic PDEs, an impossibility result was established in [54]. For the problem at hand, the results for the higher frequencies seem to provide some negative evidence.

C.3. Stationary Gaussian process priors. Alongside the random series expansions on orthonormal bases considered in the previous sections, a popular alternative approach to construct Gaussian priors on function spaces defined on d -dimensional domains, $d \in \mathbb{N}$, is through the specification of a stationary covariance kernel, namely a symmetric and positive semidefinite function $C : \mathbb{R}^d \times \mathbb{R}^d \rightarrow \mathbb{R}$ such that $C(x, y) = C(x + z, y + z)$ for all $x, y, z \in \mathbb{R}^d$; see Chapter 4 in [63]. A widely used choice is the Matérn kernel,

$$(C.1) \quad C_{\text{MAT}}(x, y) := \frac{2^{1-\alpha}}{\Gamma(\alpha)} \left(\frac{|x - y|\sqrt{2\alpha}}{\ell} \right)^\alpha B_\alpha \left(\frac{|x - y|\sqrt{2\alpha}}{\ell} \right),$$

where Γ is the Gamma function, B_α denotes a modified Bessel function of the second kind, and $\alpha, \ell > 0$ are hyper-parameters governing the regularity and the length-scale, respectively (cf. Figure 8). A second example of interest is the squared exponential kernel,

$$(C.2) \quad C_{\text{SE}}(x, y) := e^{-|x-y|^2/(2\ell^2)},$$

corresponding to the limit of the Matérn one when $\alpha \rightarrow \infty$.

C.3.1. Posterior inference with stationary Gaussian process priors. For the considered diffusion domain $\mathcal{O} \subset \mathbb{R}^d$ and given any stationary covariance kernel C , let $G = (G(x), x \in \mathcal{O})$ be the associated centred and stationary Gaussian process indexed by \mathcal{O} , identified by the relation

$$(C.3) \quad E[G(x)G(y)] = C(x, y), \quad x, y \in \mathcal{O}.$$

In particular, if C is either taken to be equal to the Matérn kernel (C.1) with $\alpha > 2 + d/2$ (and any $\ell > 0$) or the squared exponential kernel (C.2) then, arguing as in p. 330f in [35],

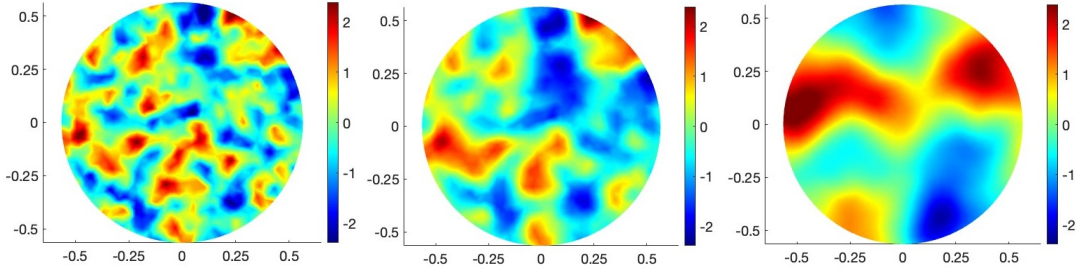


FIG 8. *Left to right: samples from the Matérn process priors with regularity $\alpha = 2.5$ and with length scales $\ell = .05, .1, .25$, respectively.*

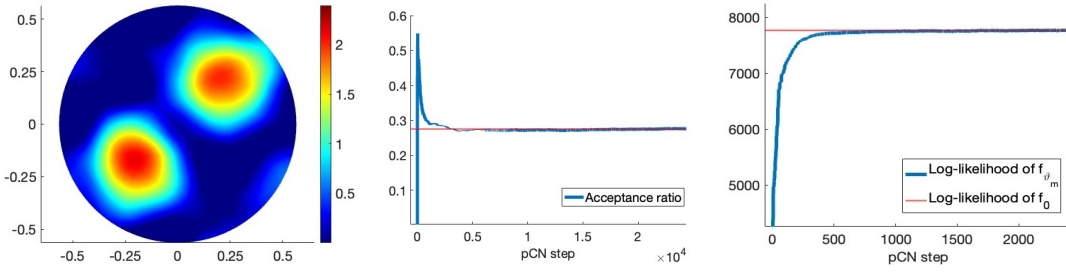


FIG 9. *Left: the posterior mean estimate \bar{F}_n arising from a Matérn process prior with hyper-parameters $\alpha = 2.5$ and $\ell = .25$, obtained via the pCN algorithm, to be compared to the ground truth F_0 shown in Figure 1 (left). The overall computational time was 58 minutes. Centre: the acceptance ratio along the iterations of the pCN algorithm. Right: the log-likelihood for the first 2500 chain steps.*

the (cylindrically defined) law $\Pi(\cdot)$ of the random function G can be shown to be supported on $C^2(\mathcal{O})$ (in fact, on $C^\infty(\mathcal{O})$ in the latter case), and thus may serve as an appropriate prior model for the (reparametrised) conductivity function F in (3.1). Prior distributions of this kind can be implemented in practice by discretising the parameter space according to the expansion

$$(C.4) \quad F(x) \equiv F_\theta(x) := \sum_{k=0}^K \theta_k \eta_k(x), \quad K \in \mathbb{N}, \quad \theta_0, \dots, \theta_K \in \mathbb{R}, \quad x \in \mathcal{O},$$

where now η_0, \dots, η_K are piece-wise linear functions associated to a grid of points $y_0, \dots, y_K \in \mathcal{O}$ (e.g. the ones resulting from a triangulation of the domain), completely determined by the identity $\eta_k(y_{k'}) = 1_{\{k=k'\}}$. As a consequence, the function F_θ in (C.4) satisfies $F_\theta(y_k) = \theta_k$ for all $k = 0, \dots, K$, and for any $x \in \mathcal{O}$ the value $F_\theta(x)$ is found by linearly interpolating the pairs $\{(y_k, \theta_k), k = 0, \dots, K\}$. Accordingly, modelling F via the stationary Gaussian process prior $\Pi(\cdot)$ with covariance structure (C.3) corresponds to assigning to the vector of function evaluations $\theta := (\theta_0, \dots, \theta_K) \in \mathbb{R}^{K+1}$ the multivariate Gaussian prior

$$(C.5) \quad \theta \sim N(0, \Lambda), \quad \Lambda := (C(y_k, y_{k'}))_{k, k'=0}^K \in \mathbb{R}^{K+1, K+1}.$$

With such set-up, inference based on the posterior distribution of $\theta | X^{(n)}$ can be implemented by readily adapting the gradient-free and gradient-based methods outlined in Section 3, replacing the discretisation scheme (3.2) with (C.4) and formally substituting in all the relevant equations the Neumann-Laplacian eigenfunctions $\{1, e_1, \dots, e_K\}$ used in the former

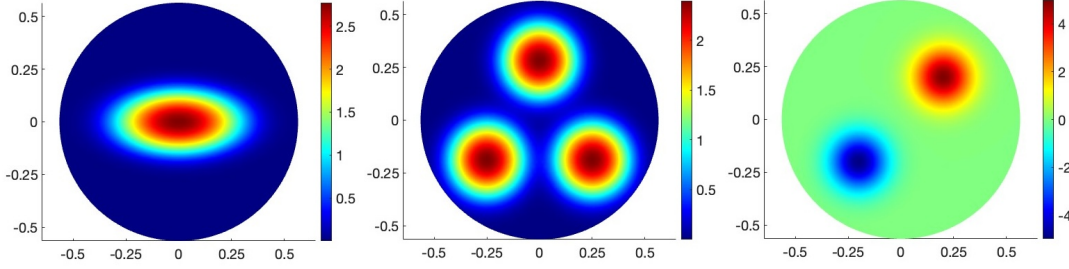


FIG 10. Left to right: the (reparametrised) conductivity functions $F_0^{(1)}$, $F_0^{(2)}$ and $F_0^{(3)}$.

TABLE 5
Recovery performances for the posterior mean \bar{F}_n and the MAP estimate \hat{F}_n , for different ground truths

	$\ F_0\ _2$	proj. error	$\ F_0 - \bar{F}_n\ _2$, pCN	$\ F_0 - \bar{F}_n\ _2$, ULA	$\ F_0 - \hat{F}_n\ _2$
$F_0^{(1)}$.7627	.0759	.1671	.20548	.1815
$F_0^{(2)}$.9623	.0834	.2295	.3461	.3306
$F_0^{(3)}$	1.2275	.1212	.3751	.30848	.2972

with the linear interpolation functions $\{\eta_0, \dots, \eta_K\}$, and the diagonal multivariate Gaussian prior (3.3) with the discretised stationary Gaussian one defined by (C.5). The numerical routines (2.13) and (3.7) for the evaluation of the likelihood and the gradient of the log-posterior density require no further modifications.

C.3.2. Numerical experiments. Based on the same data set $X^{(n)}$, with $n = 50000$, underlying the simulation studies presented in Section 4 and in Appendices C.1 and C.2, we implemented posterior inference with the Matérn process prior. For brevity, let us focus on the results obtained via the pCN algorithm.

We set the hyper-parameters for the covariance kernel (C.1) to $\alpha = 2.5$ and $\ell = .25$, and employed the discretisation scheme (C.4) with $K = 881$ linear interpolation functions defined over an unstructured triangular mesh covering the domain. Figure 9 (left) shows the obtained posterior mean estimate of the reparametrised conductivity function, computed through the ergodic average of $M = 25000$ samples from the pCN algorithm, initialised at the cold start $\vartheta_0 = 0$. The stepsize was tuned to $\delta = .000375$, with which a final acceptance ratio of 27.58% was obtained; see Figure 9 (centre). A burnin phase comprising the first 2500 iterates was identified, which we visualise in Figure 9 (right) via the trace-plot of the log-likelihood. The obtained L^2 -estimation error is equal to .1872, yielding a relative error of 22.42%. The procedure required an overall computational time of 58 minutes on a MacBook Pro with M1 processor, with an average of .14 seconds per iterate.

C.4. Additional simulation studies. We conclude this section presenting some further empirical investigations in which we considered the recovery of three additional true conductivity functions, respectively specified, under the reparametrisation $F = \log(f - f_{\min})$, with $f_{\min} = .1$, by

$$F_0^{(1)}(x_1, x_2) = \log(1 + 15e^{-(5x_1)^2 - (10x_2)^2});$$

$$F_0^{(2)}(x_1, x_2) = \log(1 + 10e^{-(8x_1)^2 - (8x_2 - 2.25)^2} + 10e^{-(8x_1 + 2)^2 - (8x_2 + 1.5)^2})$$

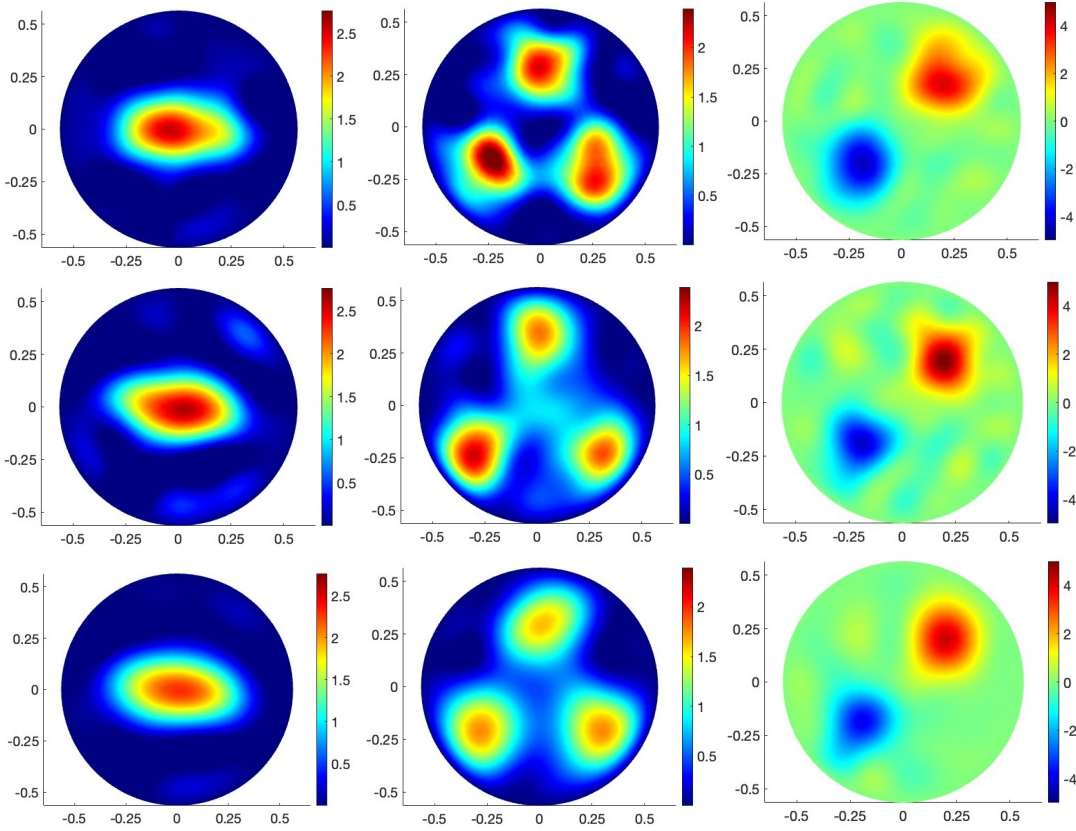


FIG 11. Left column, top to bottom, respectively: the posterior means (computed via the pCN algorithm and the ULA) and the MAP estimate for the ground truth $F_0^{(1)}$ shown in Figure 10 (left). Prior variability: $\sigma^2 = 100$. For pCN, the stepsize was set to $\delta = .00025$, the burnin to 2500, and the acceptance ratio was 42.85%. For ULA, $\delta = .000025$, burnin: 250. For gradient descent, $\delta = .00001$, and 99 iterations were necessary for convergence. Central column: estimates for $F_0^{(2)}$, shown in Figure 10 (centre). Prior variability: $\sigma^2 = 500$. For pCN, $\delta = .0001$, burnin: 2500, acceptance ratio: 32.19%. For ULA, $\delta = .000025$, burnin: 250. For gradient descent, $\delta = .00005$, number of iterations: 249. Right column: estimates for $F_0^{(3)}$, shown in Figure 10 (right). Prior variability: $\sigma^2 = 500$. For pCN, $\delta = .0001$, burnin: 5000, acceptance ratio: 27.75%. For ULA, $\delta = .000025$, burnin: 250. For gradient descent, $\delta = .00005$, number of iterations: 152.

$$+ 10e^{-(8x_1-2)^2-(8x_2+1.5)^2};$$

$$F_0^{(3)}(x_1, x_2) = 5e^{-(7.5x_1-1.5)^2-(7.5x_2-1.5)^2} - 5e^{-(7.5x_1+1.5)^2-(7.5x_2+1.5)^2},$$

for $(x_1, x_2) \in \mathcal{O}$; see Figure 10. For each of these, we generated synthetic data sets of discrete observations $X^{(n)}$, with $n = 50000$, as described in Section 4.1, sampling from the Euler-Maruyama approximations of the corresponding continuous trajectories at low ‘frequency’ $\delta_t/D = .0001$. Next, for each set of observations, we implemented posterior inference with a truncated Gaussian series priors based on the Neumann-Laplacian eigenpairs, defined as in (3.3), numerically computing the associated posterior mean estimates via the pCN algorithm and the ULA, and the MAP estimates through the gradient descent method. Across the three collections of experiments, the same truncation level $K = 68$ and the same regularity parameter $\alpha = 1$ for the prior were used. Each run of the pCN algorithm and of the ULA comprised 25000 and 10000 steps respectively, while each instance of the gradient descent method was iterated until the fulfilment of the convergence criterion laid out in Section 4.5.

All the schemes were initialised with cold starts. The obtained results are summarised in Table 5 and visualised in Figure 11. The computation times were in line with those of the experiments presented in the previous sections.